

Dissertation

Quantitative Magnetic Resonance Imaging of Brain Iron

Christian Langkammer

presented to the Faculty of Electrical Engineering  
of Graz University of Technology



Graz University of Technology  
Institute of Medical Engineering  
Kronesgasse 2, 8010 Graz, Austria

Graz, 2012

## Statutory declaration

I declare that I have authored this thesis independently, that I have not used other than the declared sources/resources and that I have explicitly marked all material which has been quoted either literally or by content from the used sources.

Graz, 2012

## ABSTRACT

Iron as the most abundant trace element in the human brain is essential to biochemical processes as oxygen transportation, myelin production, and neurotransmitter synthesis. However, it can become toxic when available in excessive amounts. Abnormal high iron concentrations have been linked to neurodegenerative and inflammatory processes occurring in prevalent neurological disorders such as Alzheimer's disease, Parkinson's disease and multiple sclerosis. Therefore investigations of the involvement of iron in the etiology and disease progression rely on its exact measurement. Magnetic Resonance Imaging (MRI) seems a potential candidate for assessing iron concentration in vivo, because of its sensitivity to paramagnetic effects and non-invasiveness.

The potential of MRI relaxation rate mapping, phase imaging, and quantitative susceptibility mapping for assessing iron concentration in the human brain was studied in this work. Because it is unclear which parameters represent valid and sensitive measures for iron, postmortem studies of the human brain chemically validated the theoretical considerations. Iron concentrations were determined for a variety of anatomical brain regions using several MRI techniques and, additionally, using inductively coupled plasma mass spectroscopy. Based on these measurements a model of the biophysical mechanisms underlying MRI contrast generation in the human brain was developed and subsequently applied in clinical studies of multiple sclerosis and amyotrophic lateral sclerosis.

In conclusion, iron concentrations in the human brain can be assessed in vivo by using MRI. While iron is the determinant source of contrast in gray matter, the counteracting diamagnetism of myelin reduces the sensitivity of MRI based iron measurements in white matter. Patients suffering from multiple sclerosis and amyotrophic lateral sclerosis showed regionally increased iron accumulation, which was associated with the clinical severity and type of the disease.

Keywords: quantitative MRI, brain iron, myelin, contrast generation, postmortem, relaxation rate mapping, phase imaging, quantitative susceptibility mapping

## KURZFASSUNG

Eisen ist das häufigste Spurenelement im menschlichen Gehirn und erfüllt nicht nur beim Sauerstofftransport sondern auch bei der Produktion von Myelin und der Synthese von Neurotransmittern eine wichtige Rolle. In übermäßigen Mengen hat freies Eisen allerdings eine toxische Wirkung. Abnormal hohe Eisenkonzentrationen werden mit degenerativen und entzündlichen Vorgängen bei vielen neurologischen Erkrankungen wie Alzheimer, Parkinson und Multipler Sklerose in Verbindung gebracht. Weitere Untersuchungen zur Ätiologie und Progression dieser Erkrankungen im Zusammenhang mit Eiseneinlagerungen erfordern jedoch deren exakte Bestimmung *in vivo*. In diesem Zusammenhang erweist sich die Magnetresonanztomographie (MRT) als attraktives Verfahren, welches als nicht-invasives, bildgebendes Verfahren die Charakterisierung von paramagnetischen Effekten und damit potentiell auch die Bestimmung der Eisenkonzentration ermöglicht.

In der vorliegenden Arbeit wurde das Potential der MR-Relaxometrie, der Phasenbildgebung und der Suszeptibilitätsbestimmung für die Quantifizierung von Eisen im Gehirn untersucht. Besonderer Fokus wurde auf die Sensitivität dieser Methoden zur Bestimmung der Eisenkonzentration gelegt. Dazu wurden postmortale Studien mit massenspektroskopischer Bestimmung von regionalen Eisenkonzentrationen in definierten anatomischen Regionen durchgeführt. Basierend auf diesen Ergebnissen wurde ein Modell für den biophysikalischen Kontrastmechanismus von Eisen im menschlichen Gehirn entwickelt, welches schließlich im Rahmen von klinischen Studien angewandt wurde.

Anhand der durchgeführten Studien konnte nachgewiesen werden, dass regionale Eisenkonzentrationen mittels MRT im menschlichen Gehirn gemessen werden können. Während Eisen in der grauen Substanz bestimmt werden kann, verringert der diamagnetische Anteil von Myelin jedoch die Sensitivität der Messungen in der weißen Substanz. Patienten mit Multipler Sklerose und amyotropher Lateralsklerose zeigten erhöhte fokale Eisenakkumulationen, welche mit dem Phänotyp und der Krankheitsausprägung assoziiert sind.

Schlagwörter: Magnetresonanztomographie (MRT), Eisen, Myelin, Kontrastmechanismen, Postmortem, MR-Relaxometrie, Phasenbildgebung, Suszeptibilitätsbestimmung

## ACKNOWLEDGEMENTS

I have the great pleasure of acknowledging the help and support of a number of individuals who have contributed in the completion of this thesis.

I offer my sincerest gratitude to my supervisor Stefan, who has supported me throughout my thesis with his guidance and dedication, whilst providing me the opportunity to work in my own “special” way. He supported me with unflinching encouragement combined with foresight and drive, but always stayed rational, problem-oriented and focused as it was absolutely necessary.

Moreover, I would like to thank my official supervisor of the Institute of Medical Engineering, Rudi, for his support and especially for the organization of the MRI-Club, which brings the people from all institutions together as it was also essential to my work.

My sincere thanks go in particular to Niki for his endless motivation to recruit the cases for our study and subsequently spending very long nights at the scanner, followed by even longer days on duty. I deeply acknowledge his commitment and hope besides working we can extend our fly fishing skills as the salmons are still waiting.

Very special thanks also go to my long-term lab mate, Michi. Not solely for sharing the office and the ideas with me, but also for all those funny occasions, which might have been only funny to us. I really wish her all the best!

I would like to thank Christian for his guidance and encouraging advices. I am much indebted to him for his valuable assistance and his broad knowledge and comprehension when putting technical features into a clinical context. When talking about clinics I am especially grateful to Professor Fazekas, who did not only set new standards regarding response time of emails and for commenting manuscripts beside running the clinic, but also supported this work by encouraging talented people to work on brain iron. I am very proud to be a part of this great team.

I am heartily thankful to my wonderful colleagues in the Department of Neurology – Dani, Katja, Marisa, Margit, Marghe, Naira, Patricia, Sonja, Michael, Lukas and Thomas for their constructive cooperation, lunch time talks and especially for enriching the knowledge about fMRI ;). Furthermore, Alex, Karin and Martin helped me incredibly by “organizing” scan time between other people’s slots, which I do highly appreciate. I would like to thank my great colleagues from the Ludwig Boltzmann Institute for Clinical-Forensic Imaging: Eva,

Belin, Eva-Maria, Evi and Professor Yen. Also, I would like to thank my very amusing colleagues from the Department of Radiology: Gernot, Fritz and Karl – may the coffee never end and we might gain the control over the entire computer network! Additionally I would like to express my gratitude to my talented colleagues of the Institute of Medical Engineering: Andi, Bernhard, Clemens, Florian, Doga, Manuel, Mike, and Peter – we have learned a lot about MRI during our weekly meetings at the Tick-Tack.

Moreover, I gratefully thank the very best analytical chemist, Walter, for his outstanding dedication and interest in our project.

There have been several wonderful individuals I luckily have met on conferences. It is always a great pleasure to see Claudia, Monika, Xeni and Francesco from Basel. I am very grateful to Andreas and Ferdinand from Jena for our fruitful cooperation and want to thank in particular Ferdinand for his persistency concerning details and the long and enlightening discussions. I am happy that one of my dearest friends had also the brilliant idea to do “something with MRI”. Daniel, this was an absolutely bright turn, which is providing us now with extra time for conferences and after-conference discussions.

I appreciate the help of all the above mentioned people very much. The last years would not have been such an awesome time without my friends. Thank you!

Finally, I would like to thank Lydia and my brother Patrik for their love and most especially I thank my parents for their unconditional support.

*I dedicate this thesis is to my grandparents.*



## CONTENT

<i>Abstract</i>	3
<i>Kurzfassung</i>	4
<i>Acknowledgements</i>	5
<i>Content</i>	8
<i>Introduction</i>	9
<i>Methods for MRI of brain iron</i>	15
<i>Study 1: Quantitative MR imaging of brain iron: A postmortem validation study</i>	36
<i>Study 2: Susceptibility induced gray-white matter MRI contrast in the human brain</i>	51
<i>Study 3: Quantitative susceptibility mapping as a means to measure brain iron? A postmortem validation study</i>	68
<i>Study 4: Mapping of iron deposition in conjunction with assessment of nerve fiber tract integrity in amyotrophic lateral sclerosis</i>	82
<i>Study 5: Determinants of brain iron in multiple sclerosis: a quantitative 3T MRI study</i>	95
<i>Study 6: Quantitative susceptibility mapping in multiple sclerosis</i>	108
<i>Summary and outlook</i>	122
<i>References</i>	129
<i>Curriculum vitae</i>	147
<i>List of publications</i>	148



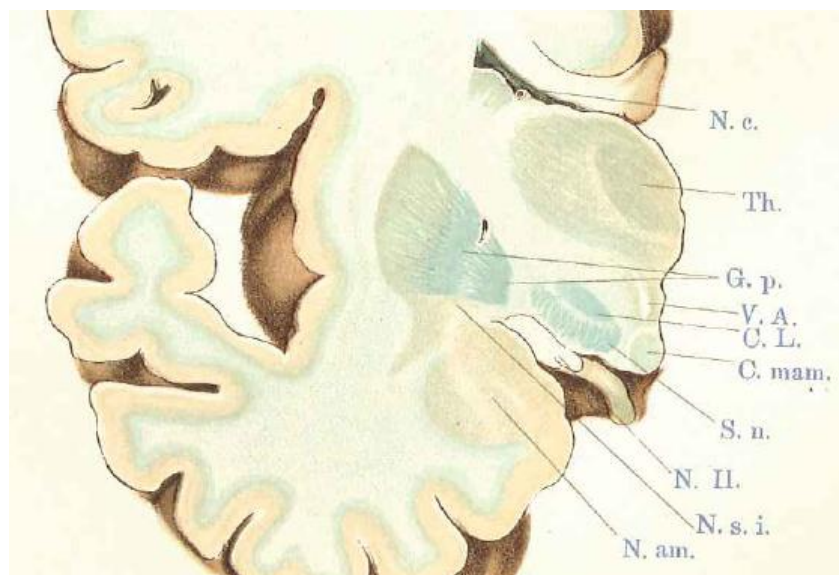
## INTRODUCTION

### IRON IN THE HUMAN BRAIN

Research on brain iron started in the 19<sup>th</sup> century, when Max Perls discovered that a mixture of potassium ferrocyanide and hydrochloric acid can be used to detect iron oxides in brain tissue (Perls, 1867). This histochemical technique, called *Perls' or Prussian Blue* staining, is widely applied, however, because of its low sensitivity several chemical methods have been proposed which allow a improved visualization especially in fixed tissue (Koeppen, 2003). In 1886, Zaleski found that iron bound to hemoglobin is not reacting to the staining and therefore separated it according to the form of binding into hem bound and non-hem bound iron (Zaleski, 1886).

The distribution of non-hem bound iron in the human brain was investigated histochemical (Spatz, 1922) and were later confirmed by quantitative studies (Stein, 1923). Spatz grouped anatomical regions according to their iron concentration. Highest iron concentrations were observed in the globus pallidus and substantia nigra, followed by nucleus ruber, nucleus dentatus, corpus subthalamicum, putamen and nucleus caudatus (Figure 1)

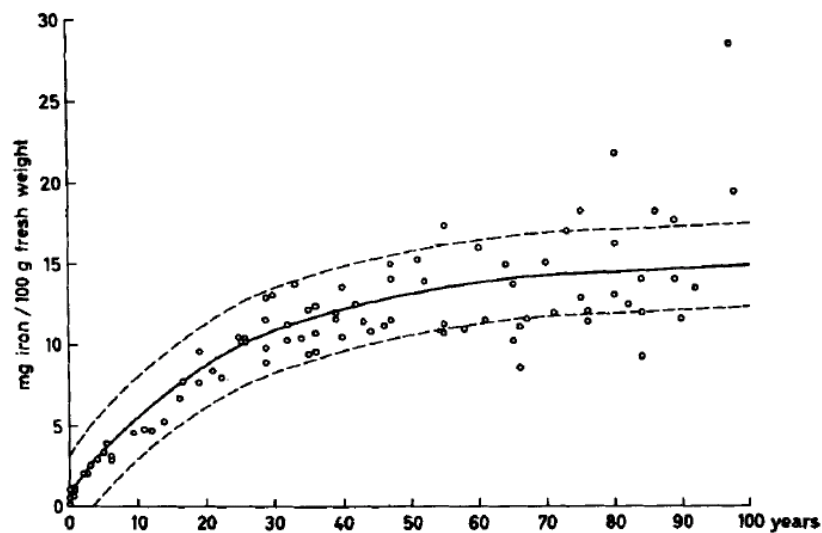
Figure 1



Distribution of non-heme bound iron in the human brain visualized by Perls' staining. Non-hem bound iron is colored in blue and the brain was sliced in coronal orientation. Figure taken from (Spatz, 1922).

Additionally to the regional distribution of brain iron, in the milestone paper of Hallgren and Sourander they found that ferritin bound iron is accumulating in the brain until the 4<sup>th</sup> decade of life during the course of normal aging (Figure 2) (Hallgren and Sourander, 1958). Thereafter, the iron levels remain fairly constant with the exception of the thalamus, where a decline after an age of about 35 years has been reported. Hallgren's work, including the iron concentrations of 81 subjects, has been used as a lookup table for estimating putative regional brain iron concentrations. However, when considering the standard deviation of the regression curves it is evident that it can only serve as a rough estimate, but not for estimating iron levels reliably in individual subjects.

Figure 2

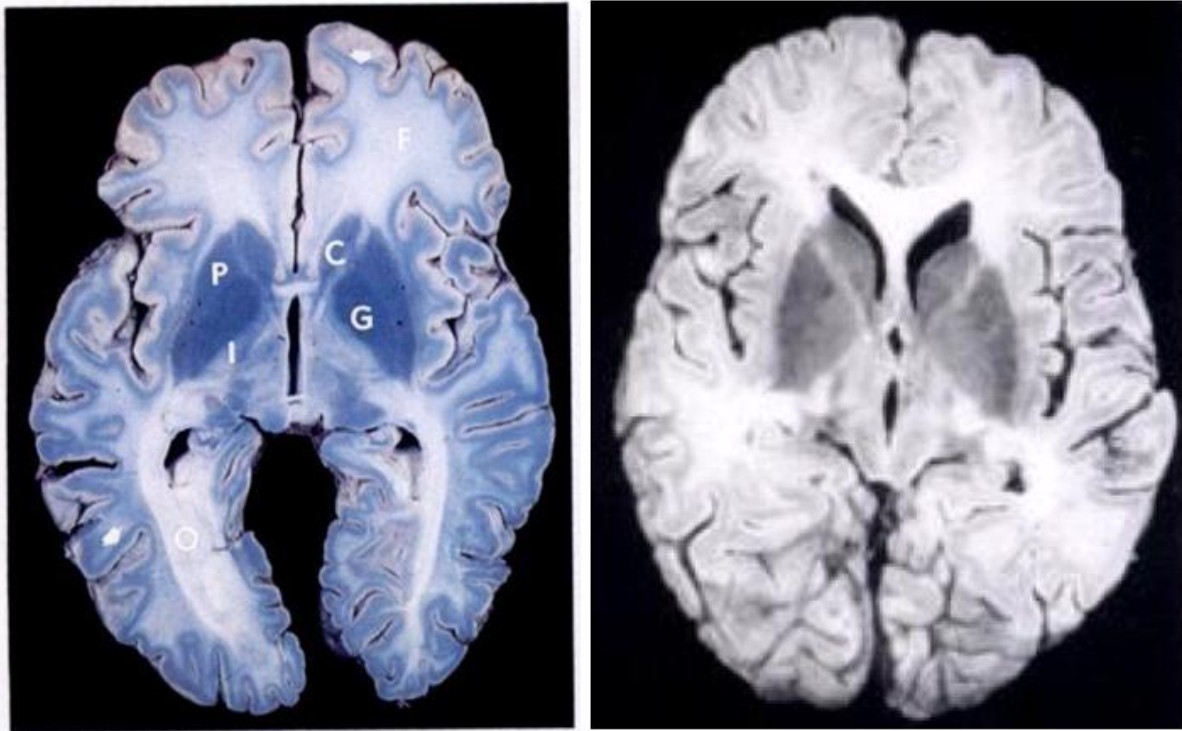


Iron concentration in the putamen as a function of age. While iron is accumulating in the first 4<sup>th</sup> decades of life, they remain fairly constant afterwards, a finding consistent in most deep gray matter structures. Figure taken from (Hallgren and Sourander, 1958).

After publishing these findings, the work of Hallgren and Sourander only received moderate attention because postmortem studies per se only allow insights at the final stage of diseases but cannot be applied in vivo or cannot serve to monitor disease progression. Owing to this limitation, only a limited number of studies have been conducted, mainly focusing on disease mediated alternations in Parkinson's disease and Alzheimer's disease (Dexter et al., 1991; Griffiths and Crossman, 1993; House et al., 2007).

However, with the advent of MRI into clinical research, a visual correspondence between T2 weighted MR images and histological staining for iron was recognized and ascribed as suggestive for the impact of iron to MR relaxation rates (Figure 3) (Drayer et al., 1986).

Figure 3



Perls' staining (left) and T2 weighted MR image (right) of a healthy human brain. The basal ganglia structures with know high iron concentrations (C,G,P) show pronounced hypointense signal areas which is suggesting an impact of iron to MR relaxation rates. Figure is taken from (Drayer et al., 1986).

This and subsequent findings nourished speculations that iron can be quantitatively assessed by MRI *in vivo*. Due to the high number of postmortem cases included, Hallgren and Sourander could also look for the effects of normal ageing. Since no bigger study followed, their work is still used as a look-up table to obtain putative iron values.

## MOTIVATION

Reliable and precise techniques for *in vivo* assessment of iron content are a prerequisite to study the role of iron in neurological diseases and normal ageing. MRI offers several techniques that are based on the susceptibility and relaxivity effects of ferritin-bound iron, but their sensitivity and specificity is lacking validation. Unfortunately, the magnetic susceptibility and relaxivity of iron are also confounded by other tissue components such as diamagnetic myelin or other trace elements. In addition, there is evidence that the orientation of the brain microstructure can affect the MR properties. This makes the *in vivo* assessment of iron even more challenging.

In this dissertation, several current and new approaches for iron mapping have been implemented and evaluated on a clinical whole body scanner to assess regional iron accumulation in brain tissue. The following sections describe the steps that have been undertaken to measure iron in the human brain, to validate those measurements using postmortem studies and to translate the finding into clinical research.

## **OUTLINE OF THE THESIS**

The chapter “**Methods for MRI of brain iron**” describes state-of-the-art MRI techniques for iron mapping. This chapter incorporates selected material from the review “*MRI assessment of iron deposition in multiple sclerosis*” (Journal of Magnetic Resonance Imaging. 2011 Jul;34(1):13-21) and the review “*Relaxation time mapping in multiple sclerosis*” (Expert Review of Neurotherapeutics. 2011 Mar;11(3):441-50) where the author substantially contributed to the Methods section and supplied figures representative for the techniques explained.

**Study 1** contains the study “*Quantitative MR imaging of brain iron: a postmortem validation study*” (Radiology. 2010 Nov;257(2):455-62). Various methods have been proposed in literature to assess iron concentrations, however, a systematic validation in the human brain is lacking because no other in vivo method is available to verify the findings from MRI. In this work, we circumvented this problem by acquiring MRI was shortly after death and the obtained relaxation rates were correlated with the transverse MR relaxation rates.

**Study 2** contains the work entitled “*Susceptibility induced gray-white matter MRI contrast in the human brain*” (Neuroimage. 2012 Jan 16;59(2):1413-9). This study investigated why phase contrast between cortical gray and white matter is about 10-fold more pronounced than the magnitude contrast, both obtained by the same gradient echo sequence. The work was carried out by taking tissue specimens from cortical gray and white matter and relating the iron concentrations and the myelin content to the MR relaxation rates and filtered phase values. The results of this work serve as a basis for the improved understanding of the biophysical mechanisms underlying MR signal generation based on the iron concentration and myelin content in human brain tissue.

**Study 3** contains the work entitled “*Quantitative susceptibility mapping as a means to measure brain iron: A postmortem validation study*” (submitted for publication). While it is commonly assumed that paramagnetic iron is the predominant source of susceptibility variations in the human brain, the extent to which QSM can serve to reliably assess brain iron levels is not yet fully clear. In this work we investigated the relationship between bulk tissue magnetic susceptibility and brain iron concentration in unfixed (in situ) postmortem brains. For this study, part of the image processing was carried out as joint work with the group of Prof. Reichenbach from Jena University Hospital.

**Study 4** contains the work entitled “*Mapping of iron deposition in conjunction with assessment of nerve fiber tract integrity in amyotrophic lateral sclerosis*” (Journal of Magnetic Resonance Imaging. 2010 Jun;31(6):1339-45). This study looked for differences in iron accumulation between 15 patients suffering from ALS and 15 healthy controls. Despite demonstrating the clinical application of MRI based iron mapping, this work also included diffusion tensor imaging (DTI) and extended findings from other groups in the corticospinal tract by additionally considering the aspect of co-localized increased iron deposition.

**Study 5** contains the work entitled “*Determinants of brain iron in multiple sclerosis: a quantitative 3T MRI study*” (Neurology. 2011 Nov 1;77(18):1691-7). A total of 113 patients with different clinical phenotype of multiple sclerosis and 35 healthy controls were enrolled in this study. Iron mapping was applied in the basal ganglia and the imaging results were subsequently related to disease duration, disease progression, demographic, and neuropsychological variables. In this study the author was in charge of data acquisition and image processing, however, the statistical analysis was conducted by Michael Khalil.

**Study 6** contains the work entitled “*Quantitative susceptibility mapping in multiple sclerosis*” (submitted for publication). Extending our own studies of iron deposition in MS, QSM was applied in a cohort of MS and CIS patients. We found QSM to be more sensitive for tissue changes in the basal ganglia at early stages of the disease than other susceptibility-driven MR measures. Despite iron as a dominant factor responsible for the bulk susceptibility, we interpret this finding as additive effect of demyelination in gray matter structures. Part of the image processing was carried out as joint work with the group of Prof. Wang from Cornell Medical College.

The last chapter summarizes the work and discusses the results obtained. Furthermore, an outlook how iron mapping could provide a means for investigating longitudinal disease related changes of cerebral tissue is given. Work in progress includes iron mapping in white matter, the dependence of MR magnitude, phase and susceptibility with respect to the orientation of white matter fibers in respect to the main magnetic field as well as postmortem validation study using fresh (non-formalin fixed) brains.

## METHODS FOR MRI OF BRAIN IRON

### RELAXATION TIME MAPPING

The Bloch Equations are a set of 3 equations that describe the macroscopic magnetization in space as a function of time and relaxation and were introduced by Felix Bloch (Bloch, 1946). For protons in simple solutions, solving the Bloch Equation provides a single exponential recovery function with the time constant T1, i.e. the time after approximately 63% of the longitudinal magnetization has recovered or T2 i.e. the time after approximately 63% of the transverse magnetization has decayed. Additionally to be basic Bloch equations, diffusion has to be accounted for which was considered by the introduction of diffusion terms (Torrey, 1956).

### T1 relaxation time mapping

#### Phenomenon

Dipolar relaxation is a further relaxation mechanism that occurs in the presence of paramagnetic compounds such as ferritin. Dipolar relaxation is caused by a fluctuation in the magnetic field sensed by water protons due to fluctuations in the direction of the magnetic moment of the iron as well as the diffusion of the protons in the vicinity of the iron compound (Koenig and Kellar, 1995). This relaxation mechanism affects the longitudinal relaxation time T1, also known as spin-lattice relaxation time, is an intrinsic property of hydrogen protons and describes how fast the macroscopic longitudinal component of magnetization recovers after excitation by radio frequency (RF) radiation at the Larmor frequency. From the perspective of quantum physics, longitudinal relaxation corresponds to a process where protons excited by RF release their energy to the lattice, i.e. the surrounding protons. The rate at which this process occurs strongly depends on the correlation times of the proton. This in turn depends on the size of the molecules to which the protons are bound and on their molecular environment. The longest T1 relaxation times can be observed in liquids such as cerebrospinal fluid (CSF) because unbound and freely diffusible protons cannot release their energy efficiently to the lattice.

## **T1 relaxation in brain tissue**

The T1 relaxation time of a specific tissue largely depends on the water content (Fatouros et al., 1991) as well as of macromolecules. The MR signal obtained from brain tissue comes from mainly hydrogen protons of intra- and extracellular tissue water. These protons largely relax single exponentially, but their relaxation process is also influenced by hydrogen protons bound to macromolecules such as myelin lipids and proteins. The bound protons do not directly contribute to the MR signal due to their ultra-short transverse relaxation times. However, through cross-relation they act as an additional relaxation sink and therefore can speed up the T1 relaxation process of tissue water and thus can cause a double relaxation behavior which may provide relevant information on myelin or the macromolecular content of investigated tissue. The amplitude and time constant of the second (macromolecular induced) exponent are usually too small to be detected by conventional T1 mapping but can be assessed in a quantitative MT analysis as discussed below. Recently, another T1 component around 300 ms has been observed which is believed to represent water trapped between the myelin sheets (Labadie C, 2008, 2009).

Myelin is assumed to be the major source for T1 differences between GM and white matter (Koenig et al., 1990), yet the strongest determinants of T1 are the strength of the magnetic field and temperature (Koenig et al., 1984). While the latter is relevant only in postmortem studies (Tofts et al., 2008), the effect of field strength is becoming more important due to the trend towards high field imaging.

Another intrinsic factor that can influence T1 relaxation in brain tissue is the accumulation of iron which causes a reduction of T1 due to its paramagnetic effect (Ogg and Steen, 1998).  $R_1$ , which is the inverse of the T1 relaxation time, shows a linear dependency on iron but the effect is weaker compared to transverse relaxation rates (Ogg and Steen, 1998; Vymazal et al., 1996). It has been suggested that brain iron contributes to regional variations and age effects of T1 (Gelman et al., 2001; Ogg and Steen, 1998). However, for practical reasons T1 mapping is rarely used to assess brain iron concentration because of the weak effect and the long acquisition time needed for precise T1 mapping. Additionally, the sensitivity of this approach varies between brain regions (Ogg and Steen, 1998) and does not significantly increase with higher field strengths (Vymazal et al., 1992).

## **Methods for T1 relaxation time mapping**

Several methods have been proposed for mapping T1 in brain tissue. They all provide various advantages with respect to acquisition time, precision and accuracy, whole brain coverage,



and also the ability to detect double-exponential relaxation behaviour of the underlying tissue. Although time consuming, calculating T1 from a series of inversion recovery (IR) sequences with varying inversion times (TI) is still considered as gold standard because it is largely insensitive to non-uniformities of the main magnetic field (B0) and the RF transmission field (B1) (Axel, 1984; Lacomis et al., 1986). Hereby, the equilibrium longitudinal magnetization (M0) is inverted by a 180° RF pulse and is measured after different delays (TIs) when it recovers towards the equilibrium value. At least two measurements with different TIs are needed, but to account for B1 (RF transmission field) inhomogeneities, incomplete inversion and recovery, usually more measurements are required which limits the clinical utility of this sequence. To speed up acquisition time, various fast readout techniques have been proposed including echo planar imaging (EPI), turbo fast low angle shot (FLASH), and fast spin echo (FSE) (Bluml et al., 1993; van Walderveen et al., 2003; Wright et al., 2008). FSE imaging provides a mean to efficiently readout the IR prepared magnetization with whole brain coverage (Fig1). However, it is often overlooked that the echo train in adjacent slices acts like an off-resonant saturation pulse which can saturate bound protons resulting in an underestimation of T1 (Dixon, et al. 1990; Wright, et al. 2008). Additional limitations by the specific absorption rate (SAR) can arise when moving towards higher field strengths. In such a situation an EPI readout seems to be more suitable but may provide only limited image resolution and a higher propensity for susceptibility-induced artefacts (van Walderveen et al., 2003; Wright et al., 2008). With regard to image resolution and acquisition time, spoiled gradient echo imaging such as fast low angle shot (FLASH) with variable flip angle is a further option. Although not yet in clinical practice, it is of particular interest because it is readily available on clinical scanners (Venkatesan et al., 1998). More recent developments are also based on this concept. Driven-equilibrium single-pulse observation of T1 (DESPOT1) calculates T1 from a pair of FLASH images with different flip angles (Deoni et al., 2003). High resolution (1 mm isotropic) T1 maps of the entire brain can thus be acquired in clinically acceptable time of approximately 10 min (Deoni et al., 2005). When optimized flip angles are used and B1 maps are incorporated, an accuracy of better than 5% can be achieved (Deoni, 2007).

### **Quantitative magnetization transfer (qMT)**

Although it is not an intrinsic relaxation rate, magnetization transfer is linked closely to T1. Most T1 mapping techniques cannot account for multi-exponential T1 relaxation which, however, occurs in compartmentalized spin systems such as the brain. In this context, brain

tissue is usually modeled by a two-pool model of protons, where one large pool represents the hydrogen protons of the tissue water and a much smaller pool represents protons that are bound to macromolecules such as the myelin lipids and proteins (Ropele and Fazekas, 2009). Quantitative magnetization transfer (qMT) intends to determine the relaxation times in each pool, the relative pool sizes, and the amount of magnetization transfer between the pools which is caused by dipolar coupling and chemical exchange (Fralix et al., 1991). The most interesting pool parameters are the magnetization transfer rate and the bound pool fraction (BPF), i.e. the relative size of the bound pool. The latter is commonly believed to reflect myelin content. To assess fundamental pool parameters such as the BPF, the bound pool has to be saturated with variable resonance offsets and saturation rates. Based on a continuous wave saturation of the bound pool, the first mathematical framework for a full description of the two-pool model was provided by Morrison and Henkelman (Morrison and Henkelman, 1995). As continuous saturation is not applicable in vivo due to restriction by the SAR, others have developed more complex methods with pulsed MT saturation (Ramani et al., 2002; Sled and Pike, 2001; Yarnykh, 2002). Thereby, a saturation pulse with variable resonance offset is applied prior to each excitation pulse of a spoiled 2D or 3D gradient echo sequence. These methods differ slightly in their post processing efforts and in the way how various assumptions are made regarding direct saturation effects and relaxation times of the bound pool. Common to all approaches is the need for T1 mapping (apparent T1 because T1 is double-exponential) which results in a total scan time of about 30 min or even more when aiming at a full coverage of the brain.

A different concept proposed for BPF mapping is based on a stimulated echo preparation instead of a steady state saturation scheme (Ropele et al., 2003). The stimulated echo signal decays due to T1 relaxation and dilution into the bound proton pool. By using indicator dilution theory, the BPF then can be calculated from the relative signal drop. The advantages of this approach are its robustness (because no fitting is required) and its low SAR which means that it can be used also at high field strengths.

Most recent developments are based on a balanced steady state free precession (SSFP) sequence. Balanced SSFP is a fully refocused gradient echo sequence with very short repetition times (Bieri and Scheffler, 2009). It provides high scan efficiency in terms of signal-to-noise ratio (SNR) per square root of measurement time. Fundamental pool parameters can be obtained from a series of SSFP sequences at a very high resolution (Gloor et al., 2008), however, the additional need for B1 and relaxation time mapping can significantly prolong the total acquisition time.

## **Transverse relaxation time T2**

### **Phenomenon**

The transverse relaxation time T2, also called the spin-spin relaxation time, of hydrogen protons is an intrinsic property of tissues and describes how fast the macroscopic transverse component of the magnetization decays after being excited by radio frequency (RF) radiation at the Larmor frequency. The magnetization decay results from a loss of coherence (dephasing) due to random and time-dependent field variations induced by neighboring spins, since not all spins have exactly the same precession frequency. When hydrogen protons diffuse through microscopic field gradients induced, they accumulate a random phase shift which is not fully reversible; this results in an additional loss of coherence and consequently in T2 shortening. Similar to T1, the phenomenon of T2 relaxation can also be modeled by the Bloch Equation, however, T2 relaxation is independent from T1. In contrast to T1, T2 values are much less dependent on the magnetic field strength and show a slight decrease with increasing field strength.

### **T2 in brain tissue**

T2 relaxation in brain tissue is multi-exponential and largely determined by the compartmentalization of water protons within cellular elements and their adhesion to macromolecules. In contrast to T1 relaxation, transverse relaxation usually occurs on a time scale where contributions from different compartments are not fully averaged out by proton exchange. A multi-component analysis therefore allows assigning specific T2 components to hydrogen protons in different compartments. At least three components have been detected in WM: extracellular water and cytoplasm with a T2 of about 100 ms, partial contributions of cerebrospinal fluid (CSF) with a T2 longer than 1s, and a so-called “short component” in the range of 20–50 ms (Beaulieu, et al. 1998; MacKay, et al. 1994). The short component has been associated with the hydration water trapped in between the myelin sheets and therefore is associated with myelin (Gareau et al., 2000; Moore et al., 2000).

T2 relaxation in brain tissue can also be influenced by iron accumulation. In brain tissue, T2 shortening due to iron accumulation can often be observed as hypointensity on T2 weighted images (Drayer et al., 1987). It has been shown for gray matter that R2, which is the inverse of T2, linearly scales with iron concentration over the entire range of physiological concentrations (Langkammer et al., 2010; Mitsumori et al., 2009; Vymazal et al., 1996; Vymazal et al., 1992) - whether this relationship also holds true for white matter is still

unclear (Langkammer et al., 2010; Vymazal et al., 1996). A simple assessment of iron deposition, e.g. in the basal ganglia, can be achieved by means of visual rating (Bakshi et al., 2000) or by taking the signal intensity of the ventricular cerebrospinal fluid as internal reference (Bakshi et al., 2002). However, such approaches are not sensitive enough for smaller regions or to detect more subtle changes.

### **Methods for T2 relaxation time mapping**

T2 mapping is usually based on a Carr-Purcell-Meiboom-Gill (CPMG) sequence, a spin echo sequences with multiple echoes (Rinck et al., 1985; Schneiders et al., 1983). This sequence is typically performed with 16 to 32 echoes and an echo spacing between 5 – 10 ms. Identification and quantification of the various T2 components can be done with chi-square minimization techniques like non-negative least-squares (NNLS) (Hwang and Du 2009; Jones, et al. 2004; MacKay, et al. 1994; Whittall and MacKay 1989). Due to the long acquisition time, the sensitivity for the active RF field (B1), and possible MT effects, the CPMG sequence is restricted to single slice measurements. Imperfect refocusing pulses can generate stimulated echoes which in turn can contribute to the sampled echoes and lead to altered T2 values (Pell, et al. 2006; Poon and Henkelman 1992; Stewart, et al. 1993). Recent attempts to improve whole brain coverage while not prolonging acquisition time include 3D and multi-slice approaches (Oh et al., 2006). When focusing on myelin water fraction (MWF) only, i.e. the relative amount of myelin water, other T2 components can be filtered or suppressed which allows a faster generation of MWF maps. Following this approach, double inversion-recovery and triple inversion-recovery preparations in combination with CPMG acquisitions have been used to selectively excite myelin-water (Travis and Does, 2005). Alternatively, a 3-echo linear combination myelin imaging method using an uniform T2 filter which maximizes the contributions from myelin-water and suppresses signals from other T2 components has been demonstrated to provide NNLS comparable results within 5 minutes (Vidarsson et al., 2005). Theoretically, the MWF can also be derived from a series of balanced SSFP experiments, by making some assumption of other pool parameters. However, numerical simulations have indicated that due to the strong dependency of the pool parameters and their variation in MS, MWF may be miscalculated (Lenz et al., 2010).

In case one is not interested in a multi-component analysis of brain tissue, one can also estimate a mean or apparent T2 value of the tissue water from a dual echo spin echo sequence. Although this would imply a single-exponential relaxation behavior, this approach is not infrequently chosen because such a sequence is often part of the clinical MRI protocol. The

DESPOT2 technique also does not account for multi-component relaxation but can provide T2 maps with very high resolution (Deoni et al., 2005). DESPOT2 calculates T2 from a series of fully balanced SSFP scans with constant TR and variable flip angles. It should be noted, that also DESPOT1 is needed to eliminate T1 terms in the SSFP signal intensity (Deoni et al., 2005).

## **Effective transverse relaxation time T2\***

### **Phenomenon**

In contrast to T1 and T2, T2\* is not an intrinsic relaxation parameter but rather reflects the effective decay of transverse magnetization due to all effects that can cause loss of spin coherence (dephasing), i.e. microscopic changes of the precession frequency within a single voxel. While non-random and static dephasing effects can be refocused in a spin-echo sequence with its 180° refocusing pulse(s), this is not possible with a gradient-echo sequence when sampling the free induction decay (FID). T2\* therefore is always shorter than T2.

### **T2\* in brain tissue**

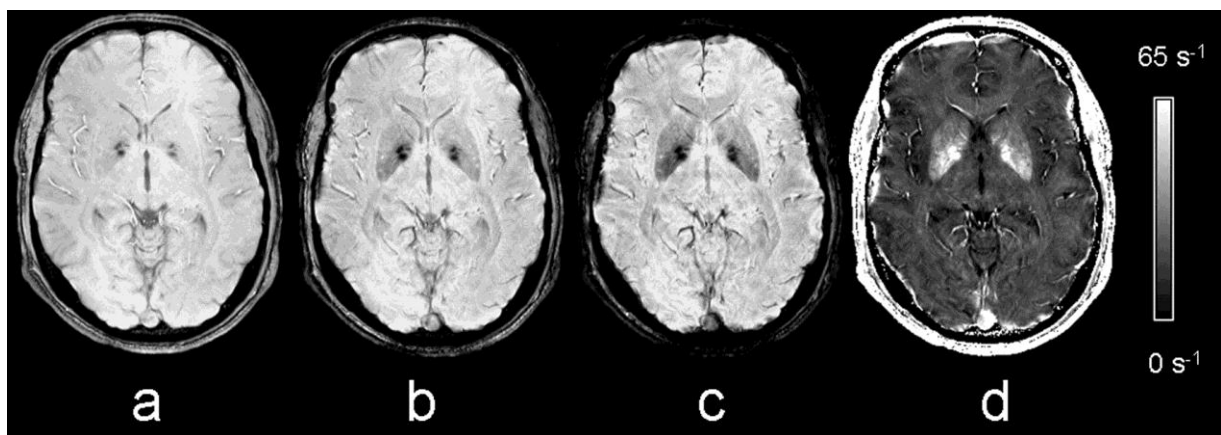
It has been suggested that R2\*, which is the inverse of T2\*, can be considered as the sum of all transverse relaxation rates according to  $1/T2^* = 1/T2 + 1/T2'$ , where 1/T2 is associated to intrinsic tissue properties as outlined above and the rate 1/T2' is attributed to microscopic field gradients such as induced by iron loaded ferritin (Gelman et al., 1999; Haacke et al., 2005; Ma and Wehrli, 1996). However, 1/T2' is not always clearly defined, in particular if the decay of the transversal magnetization is not monoexponential (Jensen and Chandra, 2000a; Yablonskiy and Haacke, 1994). T2\* mapping is expected to be more sensitive for iron than T2 mapping because the iron induced field gradients are not refocused. Similar to T2, the T2\* sensitivity also linearly scales with magnetic field strength and favors iron mapping at higher field strengths (Yao et al., 2009).

### **Methods for T2\* relaxation time mapping**

T2\* mapping is performed with a spoiled gradient-echo sequence with multiple echoes and by fitting these echoes to a single exponential decay function (Figure 1). Such a sequence can be run in multi-slice or 3D acquisition mode and can provide whole brain coverage in less than 10 minutes. Limitations typically come from macroscopic susceptibility effects which cause a signal loss due to dephasing along the gradient between tissues with different magnetic susceptibility which makes it often difficult to measure T2\* in the cerebral cortex. Proximity

to nasal sinuses also accounts for artifacts only in the frontobasal brain area. The susceptibility effect increases with longer echo times and higher field strengths (Fig. 3). Approaches to suppress these artefacts include high order shimming and a smaller voxel size, i.e. a higher image resolution. Image resolution is usually lowest in the slice selection direction. Another approach therefore is to estimate field variations along the slice selection direction from the phase of multiple echoes and to use this information to recover the gradient induced signal loss (Dahnke and Schaeffter, 2005).

Figure 1



T2\* mapping at 3T from an image series acquired with a multi-echo FLASH sequence from a healthy volunteer. Three out of 12 echoes are shown with an echo time of 9.2 ms (a), 20 ms (b), and 31 ms (c). A R2\* map can be derived by pixel-wise fitting a single exponential function, which is shown in (d). In the R2\* map, a high signal intensity represents a high R2\* or a short T2\*, respectively.

## PHASE IMAGING

Due to the nature of Fourier image encoding, MR images can represent the magnitude or the phase of the complex transversal magnetization, although the latter is virtually never used in clinical routine (apart from flow measurements). In contrast to MR magnitude images, phase images are not dependent on intrinsic relaxation parameters of the brain but represent local variations of the precession frequency. Iron induced changes of the magnetic susceptibility cause phase shifts that are proportional to the iron concentration (Hopp et al., 2010). Unfortunately, even larger shifts can be induced by magnetic field inhomogeneities which typically occur at air-tissue interfaces but also may result from imperfect shimming and therefore have to be filtered with a high-pass filter. In addition, phase images can only represent a phase range between  $-\pi$  and  $+\pi$  which means that phase wrapping can occur for

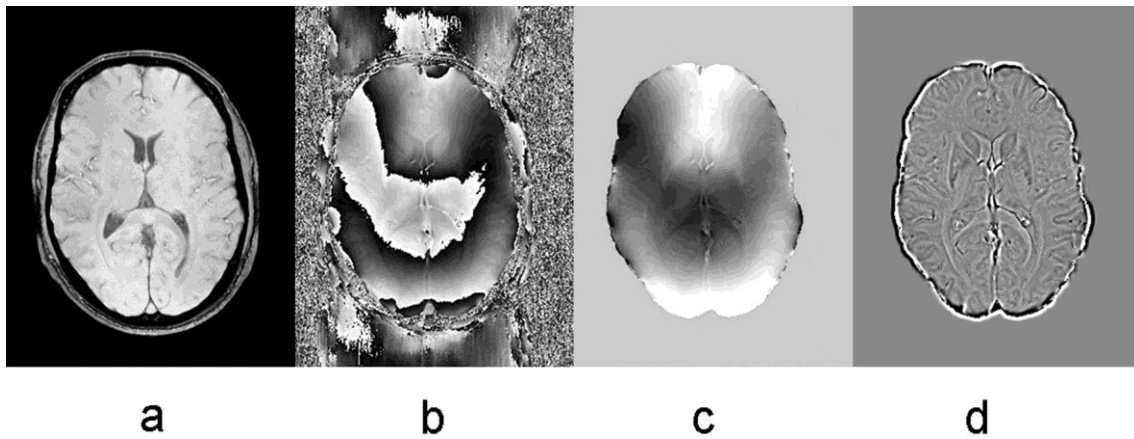
larger phase shifts. Phase unwrapping with an appropriate algorithm (Cusack and Papadakis, 2002; Rauscher et al., 2003) is the first and most important step when processing phase images (Figure 2). Recently, Hammond et al. have proposed a procedure to obtain iron induced local field shifts (LFS) from filtered phase images. The image processing steps comprise the subtraction of a reference phase from a region such as the posterior internal capsule and the division by a term that includes the echo time and the field strength to make the LFS independent from scanner and sequence (Hammond et al., 2008).

One drawback of phase imaging is the post processing step necessary to remove the background phase components using a high-pass filter. Although several methods using different filters have been proposed, this step is always altering the spatial distribution of phase dependent on the orientation to the main magnetic field and thus, alters the apparent underlying tissue properties in an unpredictable manner (Schweser, et al. 2011; Walsh and Wilman 2011).

### **SUSCEPTIBILITY WEIGHTED IMAGING (SWI)**

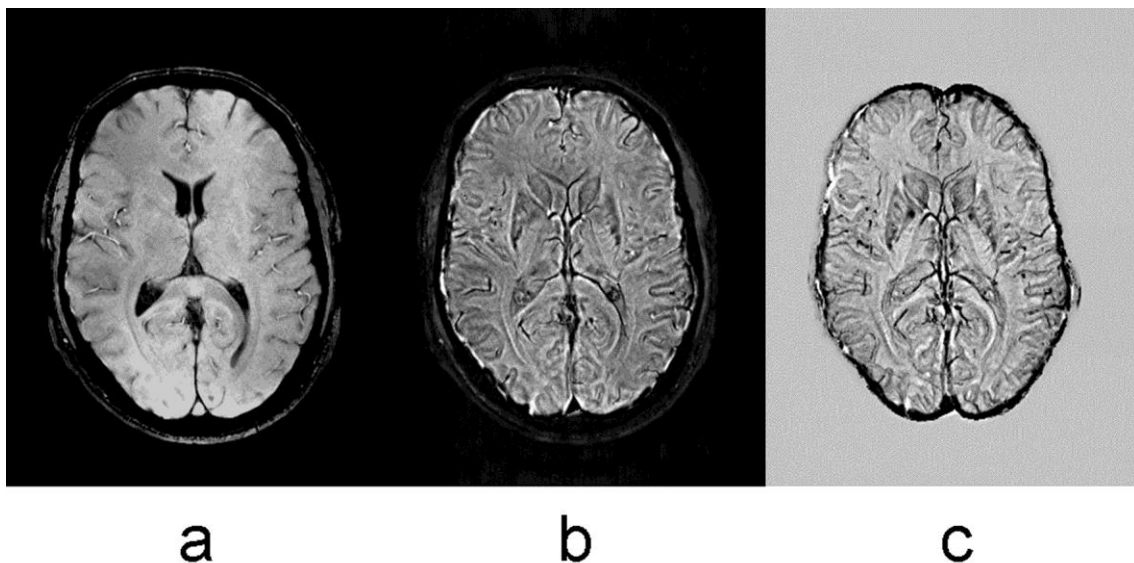
SWI combines a corresponding set of phase and magnitude images from a gradient-echo sequence to form an enhanced contrast magnitude image (Haacke et al., 2009; Mittal et al., 2009; Rauscher et al., 2005). SWI requires a high-resolution, three-dimensional spoiled gradient-echo with fully flow-compensating gradients. After phase unwrapping and filtering as described above, SWI images are calculated by multiplying the magnitude image with the phase image. To increase the susceptibility effect, phase values between  $-\pi$  and  $+\pi$  are usually mapped to a range between 0 and 1 using a 4th power function. In the resulting SWI images, veins and structures containing iron appear dark. To better visualize vein connectivity and small susceptibility variations, a minimum intensity projection through a limited number of slices is performed (Figure 3). However, due to the incorporation of an (arbitrary scaled) magnitude image, SWI is not a true quantitative method and therefore cannot be used as an indirect measure of iron.

Figure 2



Magnitude (a) and corresponding phase image (b) acquired from a healthy volunteer with a gradient-echo sequence at 3T. The raw phase image is characterized by phase wraps and inhomogeneities. Mandatory image processing steps comprise phase unwrapping (c) and removing of global inhomogeneities. After high-pass filtering, a phase image can be derived (d) that directly represents susceptibility induced variations of the Larmor frequency.

Figure 3



Magnitude image (a) and corresponding SWI image (b) from a healthy volunteer at 3T system, which was calculated by multiplying the magnitude image with the unwrapped and filtered phase image. A minimum intensity projection over a stack of 5 slices is shown in (c).

## QUANTITATIVE SUSCEPTIBILITY MAPPING

Quantitative susceptibility mapping (QSM) aims to calculate the local intrinsic bulk susceptibility based on the MR phase provided by gradient echo sequences. Magnetic susceptibility ( $\chi$ ), the physical property representing the response of magnetization in a



specific material when being exposed to an external magnetic field, describes the relation between the applied magnetic field (H) and the magnetization (M) of the material. When neglecting saturation effects, thus assuming a linear response between H and M and isotropic susceptibility of the material:

$$\chi = M / H$$

The relation to the magnetic field induction (B) is additionally including the vacuum permeability ( $\mu_0$ ).

$$B = \mu_0 (1 + \chi) H$$

When relating to the so-called susceptibility in the context of MRI, two remarks have to be considered. First, because of the limited spatial resolution the different susceptibility contributions within a certain volume are integrated and subsequently termed *bulk susceptibility*. Second, susceptibilities measured by MRI are not absolute values, but are given as differences in respect to the susceptibility of water. This is based on the fact, that the MRI system is mixing the Larmor frequency (of  $^1\text{H}$  protons) with the received RF signal (FID). Susceptibility as material constant per se is dimensionless and because of the relatively small variations in brain tissue it is often presented in ppm. Consequently in MRI literature and in this work, all susceptibilities represent bulk susceptibilities and are given with respect to water ( $\chi = -9.035$  ppm).

Theoretical considerations of the iron-loaded ferritin protein show, that the paramagnetic contributions ( $\chi > 0$ ) of iron to susceptibility are about 30 times greater than from other trace elements combined, making quantitative susceptibility mapping an interesting candidate for iron mapping (Schenck, 1992). Excluding the contribution of iron, brain tissue has been shown as diamagnetic ( $\chi < 0$ ), which was ascribed to the proteins of myelinated neuronal fibers (Liu et al., 2011a; Schweser et al., 2011). Furthermore, while both, excessive iron deposition and calcification have similar appearances in T2- and T2\*-weighted images, they have totally converse appearances in QSM maps (Schweser et al., 2010) which therefore allows disentangling different contributions to transverse relaxation.

The local magnetic field perturbation, which is a regional offset of the magnetic induction ( $\Delta B$ ), can be calculated by measuring the signal phase of the FID ( $\varphi$ ) and by considering the gyro-magnetic ratio  $\gamma$ . Furthermore, the MR phase evolves linearly with the echo time (TE).

$$\varphi = \gamma \Delta B * TE$$

However, although a relation with the magnetic bulk susceptibility exists, the magnetic field perturbation is locally dependent on the spatial distribution as well as the orientation with respect to the main magnetic field. This means that the same MR phase at different locations does not reflect identical underlying bulk susceptibility, but is a convolution of the bulk susceptibility and the unit dipole function (d).

$$\Delta B = \mu_0 M \otimes d$$

The unit dipole function (d) is defined as the magnetic field generated by a unit dipole and dependent on the angle ( $\theta$ ) between the main magnetic field axes and the vector ( $r$ ) in spherical coordinated (Liu et al., 2009):

$$d(\vec{r}) = \frac{1}{4\pi} \frac{3\cos^2(\theta) - 1}{|\vec{r}|^3}$$

In Fourier domain this convolution becomes a multiplication of the Fourier transform of  $\chi$  with the kernel  $(1/3 - k_z^2/k^2)$  with  $k$  being the spatial frequency vector defined as  $k^2 = k_x^2 + k_y^2 + k_z^2$ , where the subscripts denote the respective axis (Salomir et al., 2003).

$$\Delta B(x, y, z) = FT^{-1} \left\{ \left( \frac{1}{3} - \frac{k_z^2}{k^2} \right) * FT[\chi(x, y, z)] \right\}$$

While the forward problem, the calculation of the  $\Delta B$  based on a know susceptibility distribution, is straightforward, the inverse problem is challenging because of its ill-posed nature caused when the multiplication with the kernel response becomes zero at  $(1/3 - k_z^2/k^2) = 0$ , respectively for an angle to  $k_z$  of approximately  $54.7^\circ$  (magic angle).

Current QSM methods are solving this underdetermined ill-posed inverse problem by using regularization and/or by including additional information to stabilize the calculation of bulk susceptibility maps.

An elegant approach to stabilize the solution is to sample the object positioned at different angles with respect to the main field axis. This approach has been termed COSMOS, calculation of susceptibility through multiple orientation sampling and by including multiple angle acquisition (MAA) the inverse problem becomes over-determined and data missing at one k-space magic angle is included from other orientations (Liu et al., 2009). The COSMOS method is considered as reliable and relatively robust against reconstruction artifacts and Figure 4 is showing a reconstructed QSM map, which has been calculated from three gradient echo scans. However, due to the fact that several scans are needed, this method is costly in terms of scan time and studies involving patients are hampered because patient's comfort is significantly restricted. However, this approach still serves as golden standard, when single angle acquisition (SAA) methods are compared regarding their accuracy.

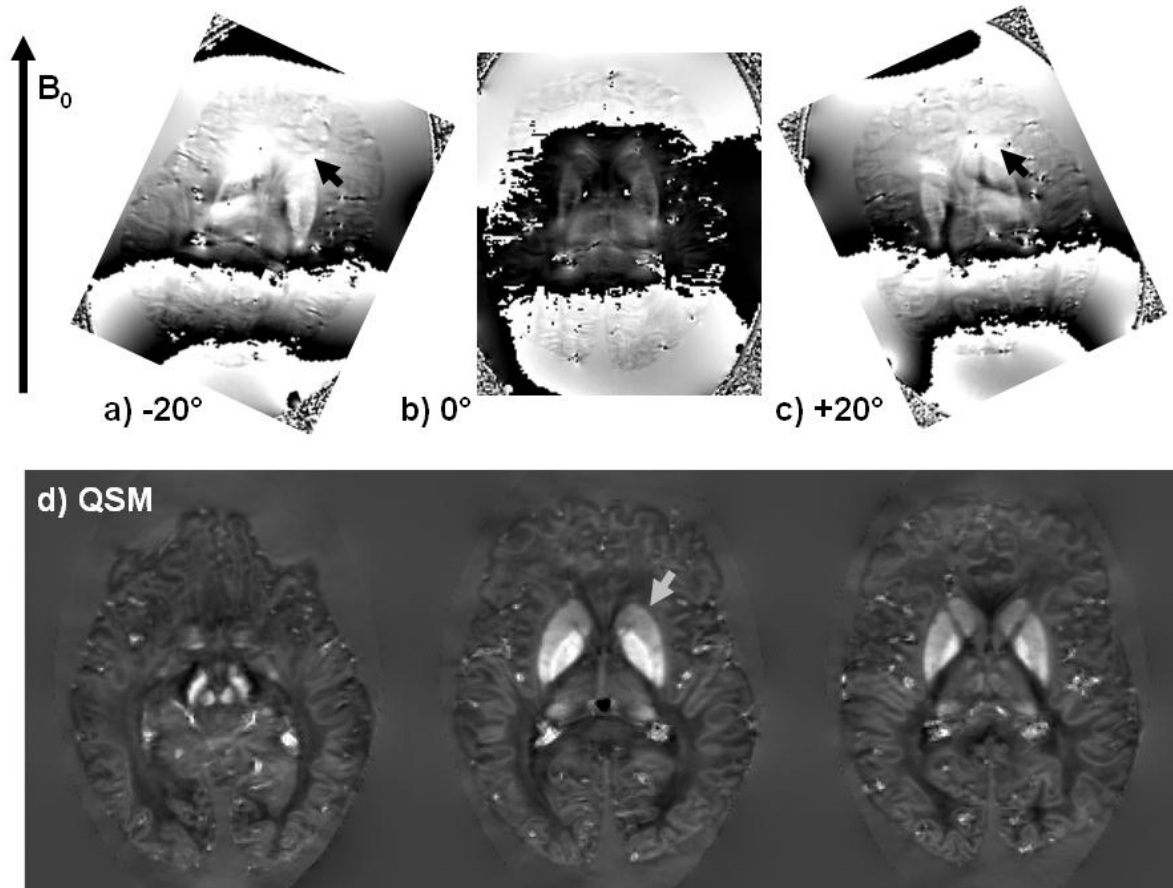
Nevertheless, multiple angle acquisition QSM methods such as COSMOS are restricted to phantom, ex-vivo and small animal studies and therefore efforts to calculate QSM maps from a single scan orientation have been made. An additional motivation for establishing appropriate single angle acquisition methods is that QSM maps can be retrospectively reconstructed from already collected gradient echo data.

An approach to reconstruct quantitative susceptibility maps from single orientation data is the so called truncated k-space division also known as threshold method. Here, the division by zero of the kernel is avoided by replacing the kernel with a tuning parameter when being close to the magic angle (Shmueli et al., 2009; Wharton et al., 2010). This tuning parameter has to be determined experimentally based on the input data available and represents a compromise between the quality of reconstruction and artifacts. Apart from streaking artifacts and effects of noise amplification in the reconstructed images, the calculated QSM values from this underdetermined k-space data tend to be underestimated in comparison with COSMOS measurements. Definite advantages of this method are its computational speed and that no prior information is needed thus possibly affecting the reconstruction process.

Morphology enabled dipole inversion (MEDI) includes the magnitude images as an additional constraint in the minimization problem (Liu et al., 2012). It is based on the observation that edges in the magnitude images are also likely to be edges of the bulk susceptibility. By adding a term to the minimization problem, which is penalizing voxels that are not part of an anatomical edge, the resulting QSM maps have been shown to be close to the results of the COSMOS method (Liu et al., 2011c). MEDI is applying a novel method called projection onto dipole fields for the elimination of background phase (Liu et al., 2011b). However, when

the contrast between anatomical structures is low, MEDI is underestimating also differences of the bulk susceptibility, a problem which is still challenging for future work.

Figure 4



Formalin-fixed brain positioned in three different orientations (approx.  $-20^\circ$ ,  $0^\circ$ ,  $20^\circ$ ) in the scanners with respect to the main magnetic field axis (a,b,c) While the phase wraps are orthogonal to the field axis ( $B_0$  is orientated up-down), the different spatial distribution of the gradient echo phase close to regions with high iron content is clearly aligned to the main magnetic field (black arrows). By solving the inverse problem (d) this becomes invariant from orientation in the reconstructed quantitative susceptibility map (gray arrow).

A novel approach for removing the background phase is sophisticated harmonic artifact reduction for phase data (SHARP) (Schweser et al., 2011). Sources of the background phase are assumed to be located outside of the region measurable by MRI and the resulting background fields are therefore harmonic functions with superimposed non-harmonic contributions from brain tissue. This is satisfying the Laplacian equation and therefore background fields can be separated from local contributions inside a region of interest using a spherical mean value filter (SMV). A SMV filter is assuming that the harmonic contributions have the property that the mean value of the entire sphere's phase values is equal to the value

in the sphere's middle. After these two components have been separated, the QSM values are obtained by subsequent deconvolution with the unit dipole response.

Beside those mentioned above, a variety of other methods has been presented and were evaluated for the calculation of the intrinsic bulk susceptibility. These included Bayesian regularization approach (de Rochefort et al., 2009), L1- and L2-norm regularized inversion techniques (Bilgic et al., 2011), using a piece-wise constant regularized inversion of the magnetic field (de Rochefort et al., 2008), or using additionally the first order derivatives of the kernel which is not zero at the same angle (Li et al., 2011).

In conclusion, the individual methods proposed for mapping of the bulk susceptibility have specific advantages and drawbacks regarding computational efforts, accuracy of the results, effort of implementation, robustness against artifacts and it is also not clear yet how anisotropic susceptibility sources such as myelinated fibers are affecting their outcome (Lee et al., 2010b). However, QSM is a very recent technique and subject to ongoing algorithmic improvements which may overcome the current pitfalls.

## **MAGNETIC FIELD CORRELATION IMAGING**

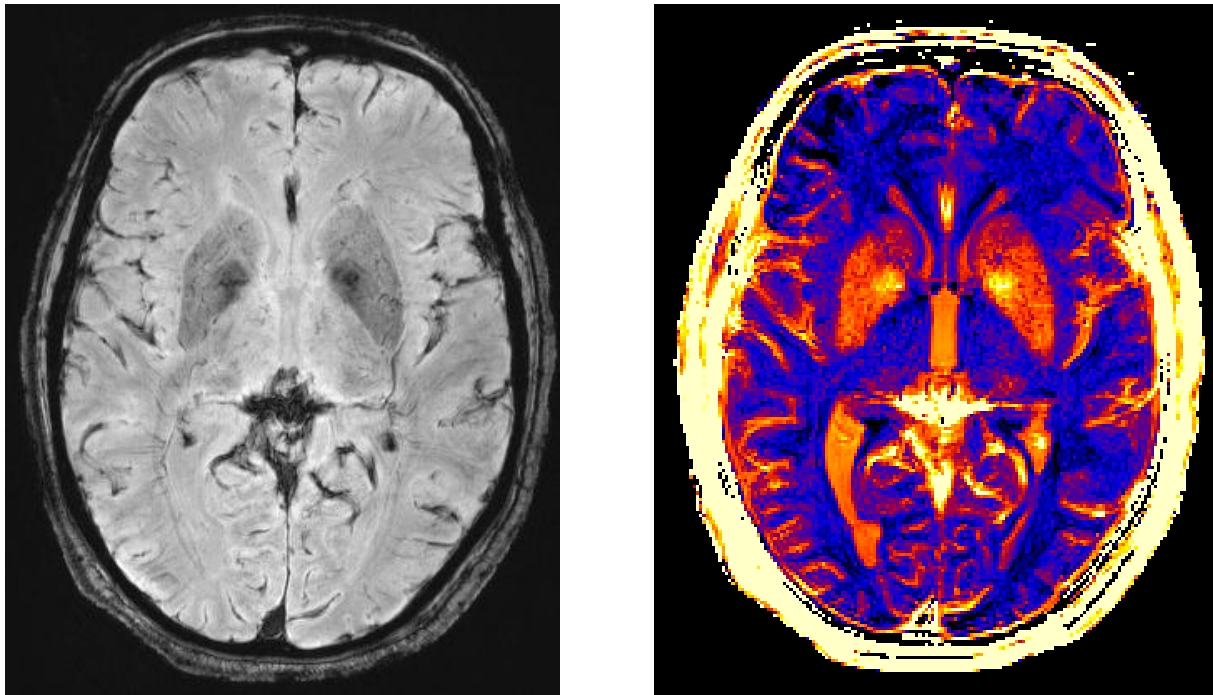
Magnetic field correlation (MFC) imaging is another technique that allows assessing iron accumulation because the MFC is directly related to iron induced microscopic (on a sub-voxel scale) field variations. The MFC can be estimated from a series of asymmetric spin echo sequences where the 180° echo pulse is slightly shifted (Jensen et al., 2006; Jensen et al., 2009). While T2 and T2\* are also affected by microscopic field variations, the MFC is expected to be independent from dipolar relaxation mechanisms and therefore less sensitive for the underlying tissue structure. When employing a single - shot EPI acquisition, MFC imaging can be done within a clinically reasonable acquisition time but at the cost of a limited image resolution. Similar to T2\* mapping with gradient echo sequences, MFC imaging is also susceptible to macroscopic field variations and motion.

## **DIRECT SATURATION IMAGING**

As outlined above, iron shortens the T2 relaxation time of water protons which in turn leads to a broadening of the saturation line shape (Wismer et al., 1988). This effect is utilized by a recent development termed direct saturation imaging (DSI). Similar to conventional magnetization transfer (MT) imaging, DSI employs off-resonant RF saturation pulses that

cause a reduction of the longitudinal tissue magnetization. However, in contrast to MT imaging, DSI aims to reflect the “direct” saturation of tissue water only. The reduction of the signal intensity relative to a reference measurement is expressed by a direct saturation ratio (DSR) which is expected to scale with iron concentration (Smith et al., 2009). Confounding effects due to MT between tissue water and bound protons can be minimized by applying long lasting (> 200 ms) RF saturation pulses with low power. If the DSI maps (Figure 5) are calculated from a series of examinations with different offset frequencies of the saturation pulse, it is also possible to correct the maps for magnetic field inhomogeneities. Although the DSI mechanism is mainly based on T2, DSI maps offer a sensitivity for iron detection that slightly differs from T2 or R2 maps (Smith et al., 2009).

Figure 5



T2\* weighted image (left) and a direct saturation image (right) of a postmortem brain. Note the correspondence of iron deposits in the globus pallidus, putamen and caudate nucleus in both imaging modalities reflecting high iron concentrations. (CSF is bright in the DSI map due to a short echo time and resulting residual saturation effects in compartments with long T1).

## **METHODOLOGICAL CONSIDERATIONS OF IRON MAPPING APPROACHES**

As outlined above, there are several approaches to assess iron concentration from MRI contrasts and relaxation parameters such as relaxation rates, phase imaging, SWI, direct saturation imaging, magnetic field correlation imaging, and bulk susceptibility.

Despite differences of their sensitivity to variations in brain iron concentration, as investigated in this work, they provide intrinsic characteristics regarding accuracy, specific absorption rate (SAR), SNR, measurement time and sensitivity to system imperfections including B0 and B1 inhomogeneities. However, a comparison between different MRI sequences applied is challenging due to the fact that the individual approaches have different prerequisites: While acquisition time, patient movement and SAR are considered crucial in every-day clinical usage, phantom experiments and postmortem MRI provide a completely different situation, but on the other hand can serve for the assessment of the accuracy. In this context, the MR sequences applied in this thesis will be discussed below concerning those factors mentioned.

### *R2 mapping*

Transverse relaxation rate mapping was solely done in postmortem and phantom scans by using a gold standard 32-echo spin-echo sequence. To prevent off resonant saturation and slice-profile effects which are both well-known effects in slice-selective spin-echo experiments, the R2 measurements were restricted to a single slice. While this approach is obviously very inefficient in terms of SNR because of the long measurement times of about 10 minutes per slice, the most important drawback is limited brain coverage, thus hampering consequent comparison with other measurements for several other brain regions. However, when R2 has to be assessed for the entire brain, either a multi-slice approach (e.g. turbo spin-echo) or an indirect approach such as 3D gradient echo imaging with varying flip angles and subsequent fitting procedure can be applied. For the reasons mentioned above, non gold standard measurements may introduce a bias, but the feasibility to image the entire brain renders those techniques relevant and valuable in a clinical setting. It should also be mentioned that the train of 180° RF pulses may limit the application at higher field strengths because of the SAR that scales with the square of the flip angle.

### *R2\* mapping*

In comparison with R2, R2\* can be rapidly acquired for the entire brain by using a standard multi-echo spoiled gradient echo sequence. Being one of the most efficient classical, non-balanced MRI sequence, gradient echo data can be either acquired in 2D or in 3D mode, with the three-dimensional acquisition clearly favored due to its higher SNR efficiency. However, while absolutely advantageous from a technical point of view, some clinical applications require 2D image acquisition. This is especially important when imaging patients suffering from Parkinson's disease or dementia, where patients' movement becomes a severe problem

and 2D acquisition leads to less motion induced artifacts. Because  $R2^*$  is not an intrinsic relaxation rate of tissue, but merely reflecting susceptibility induced effects, resolution and slice thickness are also affecting the relaxation rates obtained. Basically, increased in-plane resolution and thinner slices reduce the occurrence of macroscopic susceptibility artifacts, as commonly observed at air-tissue interfaces (pharynx, larynx) or closely to tissue-blood borders (sinus caroticus, sinus cavernosus). Those inhomogeneities induce background field gradients, resulting in faster signal decay and thus in an overestimation of  $R2^*$  rates. This effect can be corrected for each acquired echo according to:

$$S(T_E) = S_0 \exp(-T_E \cdot R2^*) \cdot \left| \text{sinc}\left(\frac{\gamma \cdot G \cdot \Delta z \cdot T_E}{2}\right) \right|$$

where  $S_0$  is the signal at  $T_E=0$ ,  $\Delta z$  the slice thickness and  $G$  the field gradient in the slice direction. Additionally, it has been shown that not only the slice thickness, but also the voxel-aspect-ratio, which is the ratio of in-plane resolution with slice thickness, plays a role for the observed  $R2^*$  relaxation rates. Gradient echo sequences optimized for clinical assessment of microbleeds typically have an echo time in the range of 20 to 40ms at 3 Tesla. Independent from the number of additional echoes inserted in the repetition interval, the acquisition time for  $1 \times 1 \times 2 \text{ mm}^3$  is typically below 5 minutes if parallel imaging strategies are incorporated, making it feasible as part of a clinical MRI protocol. Gradient echo sequences are frequently applied in high field imaging ( $>7$  Tesla) because SAR scales by the square of the emitted energy of the RF-pulses and, conversely to spin-echo sequences, gradient echo sequences apply fewer pulses with relatively small flip angles. These are the main reasons why gradient echo based sequences are best suited for high field imaging.

### *Phase imaging and QSM*

MR phase information, typically observed in non HF-refocused gradient echo sequences, is derived from an offset of the local magnetic field as induced by e.g. iron. Given this relation, the considerations about acquisition and echo times also hold true for phase imaging and derived imaging modalities such as QSM. One advantage using phase derived information for further computational analysis is that MR phase images are more robust to noise especially at lower signal amplitudes when compared with magnitude images obtained by the same sequence and assuming that noise variance of the real and imaginary signal is uncorrelated, equal and independent of the signal intensity (Conturo and Smith, 1990). This is founded by



the complex nature of the MR signal generation. Both, real and imaginary parts of the signal are individually subjected to Gaussian distributed noise which affects the magnitude image subsequently by incorporating a Rice distributed noise term. Therefore magnitudes of later echoes are relatively more affected and it is desirable to choose early echo times for the measurement. Conversely, SNR formulation of phase signal is less straightforward as it is additionally dependent of the time (t), the resonance frequency (f) as well as T2\*:

$$SNR(t) = \frac{2\pi f * t * M_0 e^{(-t/T2^*)}}{\sigma}$$

Here  $\sigma$  is denoting the noise variance, assuming that the real and imaginary channel have equally noise variance ( $\sigma = \sigma_{re} = \sigma_{im}$ ) and  $M_0$  is the transverse magnetization at  $t_0$ . The echo time with the optimal SNR can be derived there from:

$$\frac{dSNR(t)}{dt} = 0 \Rightarrow t_{opt} = T2^*$$

However, the dependence from T2\* is introducing a tissue dependent factor into the SNR considerations which requires an incorporation of a priori tissue information which becomes an issue for structures with T2\* values having a great deviation from normal the average values observed in gray and white matter (Wu et al., 2012a).

#### *Direct saturation and magnetic field correlation imaging*

Both methods, DSI and MFC, have been suggested recently for the assessment of brain iron are rather in an experimental stage and need more complex post processing. Current investigations about these two methods are limited and methodical considerations about sequence design, SAR, SNR therefore are rather crude. Based on a spin-echo sequence, both techniques were implemented. In this work by either preparation of magnetization (DSI) or by shifting the echo center (MFC), respectively. Actually, the acquisition time of about 15 minutes is clinically feasible with a reasonable SNR for the subsequent post processing. SAR problems were not expected at 3T, however, due to the (turbo) spin-echo nature this might certainly become an issue at higher field strengths.

## VALIDATION OF IRON MAPPING METHODS

Relaxation rates scale with iron concentration. However, absolute quantification of iron with MRI remains difficult because relaxation characteristics may be confounded by variations of the water content, lipid content, magnetization transfer and other minerals (e.g. calcium). Thus only in vitro methods allow to measure iron concentration in brain tissue in absolute terms using colorimetry, X-ray fluorescence, or mass spectrometry. So far the largest study to quantify iron accumulation in brain tissue was done by Hallgren and Sourander (Hallgren and Sourander, 1958). They measured iron concentration in postmortem tissue with colorimetry after adding ortho-phenanthroline to the iron solution that was washed out from the tissue samples with N-hydrochloric acid. A cohort of 81 subjects and samples from many brain regions allowed studying the strongly age-dependent iron accumulation in different brain regions. Although dated back to 1958, Hallgren's and Sourander's work is still frequently used as a look-up table to obtain age corrected iron concentrations when validating new or existing iron mapping techniques indirectly.

Figure 6



Postmortem studies including in situ MRI directly after death and chemical analysis of regional brain iron concentrations enable a direct validation. In our work, the formalin-fixed brains were cut into 10mm-thick brain slices and tissue specimens were subsequently processed in an inductively coupled plasma mass spectrometer.

Direct correlations between the results of MRI techniques and subsequent biochemical analyses of brain tissue specimen are scarce. Also, such correlative studies in postmortem

tissue may be affected by the fixation process and by changes in water content and temperature. To circumvent this problem, we assessed transverse relaxation rates in situ and have related them to chemically obtained iron concentrations after brain extraction and confirmed a strong linear relationship between iron concentration and both R2 and R2\*, where the latter exhibited a higher sensitivity for depicting differences in iron concentration (Langkammer et al., 2010). In another recent chemical correlation study, Hocq et al. measured R2 relaxation rates (Hocq et al., 2009) in brain tissue samples at different field strengths up to 14 Tesla. They found that R2 increases quadratically with field strengths and depends on the inter-echo time of the multi-echo sequence at high fields, however, their observations were based on fixed samples from deep gray matter structures only.

**STUDY 1:**

**QUANTITATIVE MR IMAGING OF BRAIN IRON:**

**A POSTMORTEM VALIDATION STUDY**

Christian Langkammer<sup>1,2</sup>, Nikolaus Krebs<sup>2</sup>, Walter Goessler<sup>3</sup>, Eva Scheurer<sup>2</sup>, Franz Ebner<sup>4</sup>,  
Kathrin Yen<sup>2</sup>, Franz Fazekas<sup>1</sup>, and Stefan Ropele<sup>1</sup>

(1) Department of Neurology, Medical University of Graz, Austria

(2) Ludwig Boltzmann Institute for Clinical Forensic Imaging, Graz, Austria

(3) Institute of Chemistry - Analytical Chemistry, University of Graz, Graz, Austria

(4) Division of Neuroradiology, Department of Radiology, Medical University of Graz,  
Austria

*Radiology. 2010 Nov;257(2):455-62*

## **ABSTRACT**

### **PURPOSE:**

To investigate the relationship between transverse relaxation rates R2 and R2\*, the most frequently used surrogate markers for iron in brain tissue, and chemically determined iron concentrations.

### **MATERIALS AND METHODS:**

This study was approved by the local ethics committee, and informed consent was obtained from each individual's next of kin. Quantitative magnetic resonance (MR) imaging was performed at 3.0 T in seven human postmortem brains in situ (age range at death, 38-81 years). Following brain extraction, iron concentrations were determined with inductively coupled plasma mass spectrometry in prespecified gray and white matter regions and correlated with R2 and R2\* by using linear regression analysis. Hemispheric differences were tested with paired t tests.

### **RESULTS:**

The highest iron concentrations were found in the globus pallidus (mean  $\pm$  standard deviation, 205 mg/kg wet mass  $\pm$  32), followed by the putamen (mean, 153 mg/kg wet mass  $\pm$  29), caudate nucleus (mean, 92 mg/kg wet mass  $\pm$  15), thalamus (mean, 49 mg/kg wet mass  $\pm$  11), and white matter regions. When all tissue samples were considered, transverse relaxation rates showed a strong linear correlation with iron concentration throughout the brain ( $r^2 = 0.67$  for R2,  $r^2 = 0.90$  for R2\*;  $P < .001$ ). In white matter structures, only R2\* showed a linear correlation with iron concentration. Chemical analysis revealed significantly higher iron concentrations in the left hemisphere than in the right hemisphere, a finding that was not reflected in the relaxation rates.

### **CONCLUSION:**

Because of their strong linear correlation with iron concentration, both R2 and R2\* can be used to measure iron deposition in the brain. Because R2\* is more sensitive than R2 to variations in brain iron concentration and can detect differences in white matter, it is the preferred parameter for the assessment of iron concentration in vivo.

## INTRODUCTION

Increased iron deposition in the basal ganglia, often observed as hypointensities on T2 and T2\* weighted images, has been suggested as a marker for tissue damage in several neurological disorders, including Parkinson's disease, Alzheimer's disease and multiple sclerosis (Bartzokis, et al. 2004; Berg and Youdim 2006; Drayer, et al. 1986a; Drayer, et al. 1986b; House, et al. 2007; Khalil, et al. 2009; Michaeli, et al. 2007; Schenck, et al. 2006). Moreover, increased iron levels have been linked to motor and cognitive dysfunction in the elderly (Pujol et al., 1992). These observations nourish speculations that iron-mediated oxidative stress and formation of cytotoxic protein aggregates may trigger or promote neurodegeneration and therefore represent neuroradiologic and diagnostic findings of increasing interest (Schenck and Zimmerman, 2004; Stankiewicz et al., 2007).

Iron is an essential trace element vital for normal brain metabolism, playing an important role in brain oxygen transport, myelin production, neurotransmitter synthesis, and in the Fenton reaction which is critical to oxidative stress (Altamura and Muckenthaler, 2009; Andrews, 1999; Orino et al., 2001). While hemoglobin bound iron represents approximately two thirds of all iron in the body, brain iron is mainly stored in the proteins ferritin and hemosiderin which serve as a buffer against harmful iron deficiency or iron overload (Bothwell, 1995). According to early work of Hallgren and Sourander ferritin bound iron accumulates in the brain until the 4th decade of life in the course of normal aging, and highest brain iron concentrations are typically observed in the basal ganglia (Hallgren and Sourander, 1958).

Currently, several MRI techniques for assessing iron have been proposed including relaxation time mapping (Haacke et al., 2005), field dependent transverse relaxation rate increase (Bartzokis et al., 1993), phase mapping (Ogg et al., 1999), susceptibility weighted imaging (Reichenbach and Haacke, 2001), magnetic field correlation imaging (Jensen et al., 2006), and direct saturation imaging (Smith et al., 2009). The variety of these methods reflects that iron does not only change the relaxation behavior of tissue water surrounding ferritin but also introduces susceptibility changes and microscopic field gradients. In addition, in the human body there is approximately 30 times more iron than the total of all other transition elements, yielding to a paramagnetic effect strong enough to significantly affect the MRI signal intensity (Schenck, 1992). However, so far none of the proposed techniques has been validated with chemically determined iron concentrations as a gold standard and it still remains unclear which method is the most sensitive and correlates best with iron concentrations in the human brain.

Therefore, the goal of this study was to investigate the relationship between the transverse relaxation rates  $R_2$  and  $R_2^*$ , the most frequently used surrogate markers for iron in brain tissue, and the chemically determined iron concentrations.

## **MATERIALS AND METHODS**

### **Subjects**

Seven deceased male subjects (age range at death, 38-81 years; mean age, 52.3 years) with an autopsy request by the local health authority were included in this study. Corpses were examined by forensic pathologists to ensure compliance with the inclusion criteria, i.e., postmortem interval shorter than 72 hours, no history of a neurological disorder or evidence of damage to the brain, and absence of ferromagnetic material. The study was approved by the local ethics committee and informed consent was obtained from each individual's next of kin.

### **Magnetic resonance imaging**

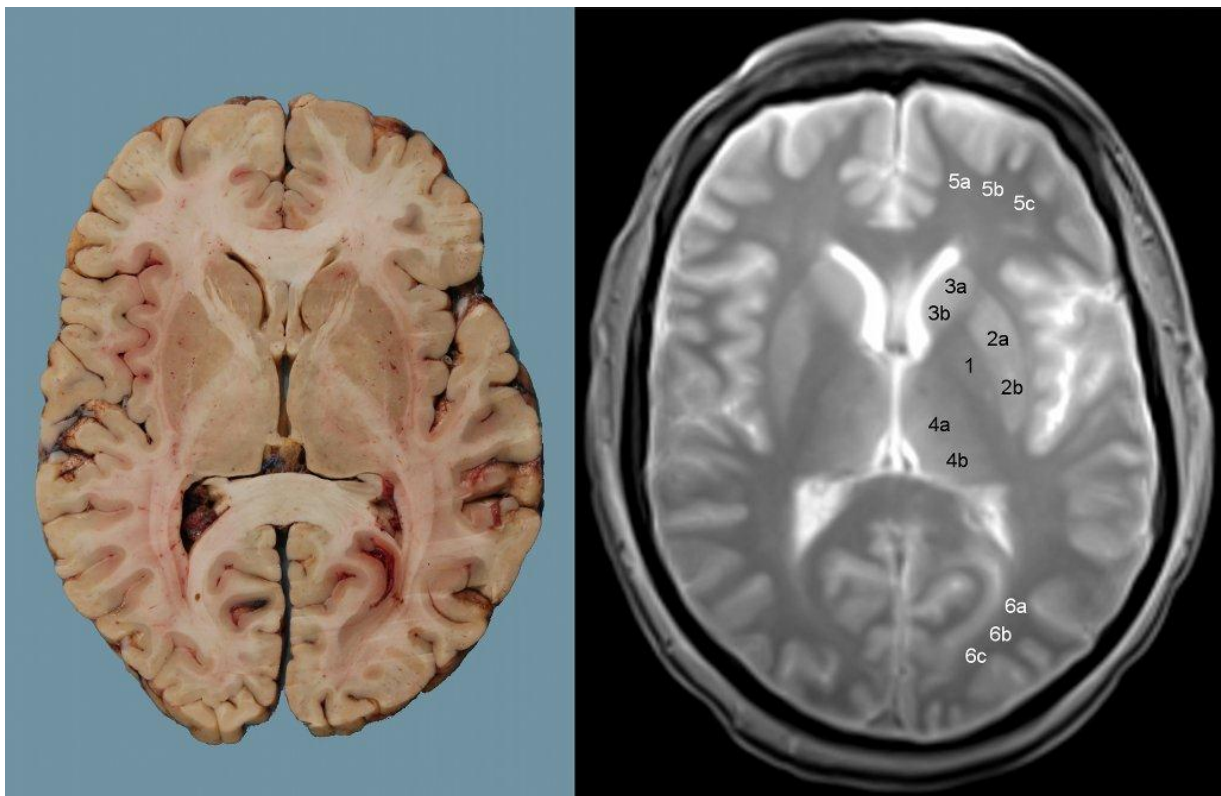
MR imaging of the brain in situ was performed within 72 hours after death at 3 Tesla (TimTrio, Siemens Healthcare, Erlangen, Germany) using a head coil array with 12 receive elements. The subjects were kept refrigerated at 4 °C and depending on the length of this period the body temperature at the beginning of the acquisition varied between 4 and 18 °C. Quantitative  $R_2$  relaxation data were acquired with a single slice 2D multi-echo spin-echo sequence with 32 equally spaced echoes (TR/TE1, 5000 ms/7 ms; inter-echo spacing, 7 ms; FOV, 256 x 256 mm<sup>2</sup>; in-plane resolution, 1 x 1 mm<sup>2</sup>; slices, 1; slice thickness, 4 mm; acquisition time, 6:27 min).  $R_2^*$  relaxation data were acquired with a spoiled 3D multi-echo gradient-echo sequence with 12 equally spaced echoes (TR/TE1, 68 ms/4.92 ms; inter-echo spacing, 4.92 ms; flip angle, 20°; FOV, 256 x 256 mm<sup>2</sup>; in-plane resolution, 1 x 1 mm<sup>2</sup>; slices, 44; slice thickness, 4 mm; acquisition time, 7:35 min). GRAPPA with an acceleration factor of 2 was used as parallel imaging technique. Additionally, a standard neuroimaging protocol including a fluid attenuation inversion recovery (FLAIR) and a high resolution magnetization prepared rapid gradient echo (MPRAGE) sequence were used to exclude subjects with acute cerebral damage. To reduce phase dispersion effects and to increase B<sub>0</sub> homogeneity second order shimming was applied. All scans were acquired in axial orientation and parallel to the most inferior parts of the occipital and frontal lobes. The single slice for  $R_2$  mapping was angulated parallel to the axial slices of the 3D gradient-echo sequence and was centered in the middle of the basal ganglia.

## **Brain fixation and autopsy**

Within 12 hours after MRI, brains were extracted and supplying arteries were ligated using surgical fibers to prevent the formation of air bubbles. The entire brains were fixed in 4% neutral buffered formalin for three to five weeks. Within four days after extraction the formalin was exchanged to ensure sufficient fixation of the entire brains (Dawe et al., 2009). To avoid contamination of the samples with iron dissection of the brains was done using ceramic knives. The brains were cut horizontally into 10 mm thick slices using an orientation identically to the MRI scans. Tissue specimens with 0.1 – 2.5 g wet mass were taken from globus pallidus (GP), putamen (PU), caudate nucleus (CN), thalamus (TH), the body of the corpus callosum (CC), and frontal (FWM), temporal (TWM), and occipital white matter (OWM). Grey matter (GM) structures were further cut in two subunits (anterior and posterior). Due to its small volume the globus pallidus was not divided into subunits. WM structures were cut in three subunits (anterior, central and posterior). All samples were taken from both hemispheres at identical positions. Figure 1 shows a brain slice and its corresponding MR image along with the positions of the dissected specimens. Autopsies and dissections were performed by forensic pathologists.



Figure 1:



A 10 mm thick slice of the formalin fixed brain covering the basal ganglia (left) and the corresponding axial slice of the multi-echo spin echo sequence (right) of a 48 years old male. Legend: globus pallidus (1), putamen (2), caudate nucleus (3), thalamus (4), frontal white matter (5) and occipital white matter (6).

## Chemical analysis

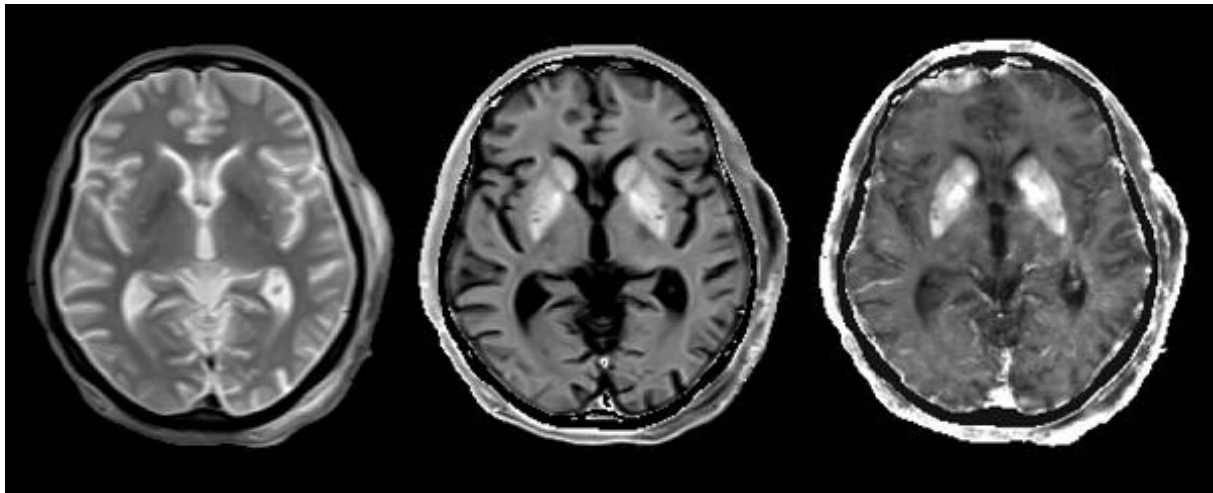
After freeze-drying, all specimens were mineralized with nitric acid in a microwave heated autoclave (UltraCLAVE III, EMLS, Leutkirch, Germany). The tissue iron concentrations were determined by inductively coupled plasma mass spectrometry (ICP-MS) (Agilent 7500ce, Agilent Technologies, Waldbronn, Germany) at  $m/z$  56. To reduce possible polyatomic interferences at  $m/z$  56 (e.g.  $^{40}\text{Ar}^{16}\text{O}^+$ ,  $^{40}\text{Ca}^{16}\text{O}^+$ ) He at a flow rate of 5.3 ml/min was added as a collision gas. The accuracy of the determined iron concentrations was validated with the NIST RM 8414 bovine muscle (NIST, Gaithersburg, USA) resulting in a good agreement with the certified results.

## Image analysis

Image analysis was performed blinded to the results of the chemical analysis. According to the position of the dissected tissue specimens, regions of interest (ROI) were outlined manually in each acquired sequence individually. To prevent partial volume effects the size of

the rectangular ROIs was always kept below  $5 \times 5 \text{ mm}^2$ . For these ROIs the transverse relaxation rates  $R_2$  and  $R_2^*$  ( $R_2=1/T_2$  and  $R_2^*=1/T_2^*$ ) were calculated by fitting a mono-exponential decay function to the averaged ROI signal intensities of the multi-echo data using a Levenberg-Marquardt algorithm and considering non-Gaussian distributed noise particularly impacting later echoes by a truncation model (He et al., 2008). Representative  $R_2$  and  $R_2^*$  maps are shown in Figure 2.

Figure 2:



Axial T2 weighted MRI (left) and corresponding maps showing the  $R_2$  (center) and  $R_2^*$  (right) relaxation rate of a 58 years old male subject. Brighter intensities represent higher  $R_2$  and  $R_2^*$  values.

### Statistical methods

Statistical analysis was performed using STATISTICA 7.1 (StatSoft, Tulsa, USA). Normal distribution of continuous data was tested with the Kolmogorov-Smirnov test. Paired t-tests were applied to test for hemispheric differences in chemical concentrations and relaxation rates for all investigated brain structures combined, as well as separately for the groups of GM and WM structures. Linear regression models were used to test for correlations between the iron concentrations assessed by chemical analysis and the corresponding transverse relaxation rates  $R_2$  and  $R_2^*$ . Subjects' age and temperature were not regarded as covariates in the statistical analysis. In all tests a p-value of  $p < 0.05$  was considered as statistically significant.

## RESULTS

### Chemical analysis

The chemical analysis of 235 tissue samples (GM, 88; WM, 147) revealed that the iron concentration in GM ranged from 35 to 250 mg/kg wet mass while iron concentrations in WM were all below 90 mg/kg wet mass. Highest iron concentrations were found in the globus pallidus followed by the putamen, the caudate nucleus and the thalamus. The detailed results for all analyzed brain structures are summarized in Table 1.

Table 1

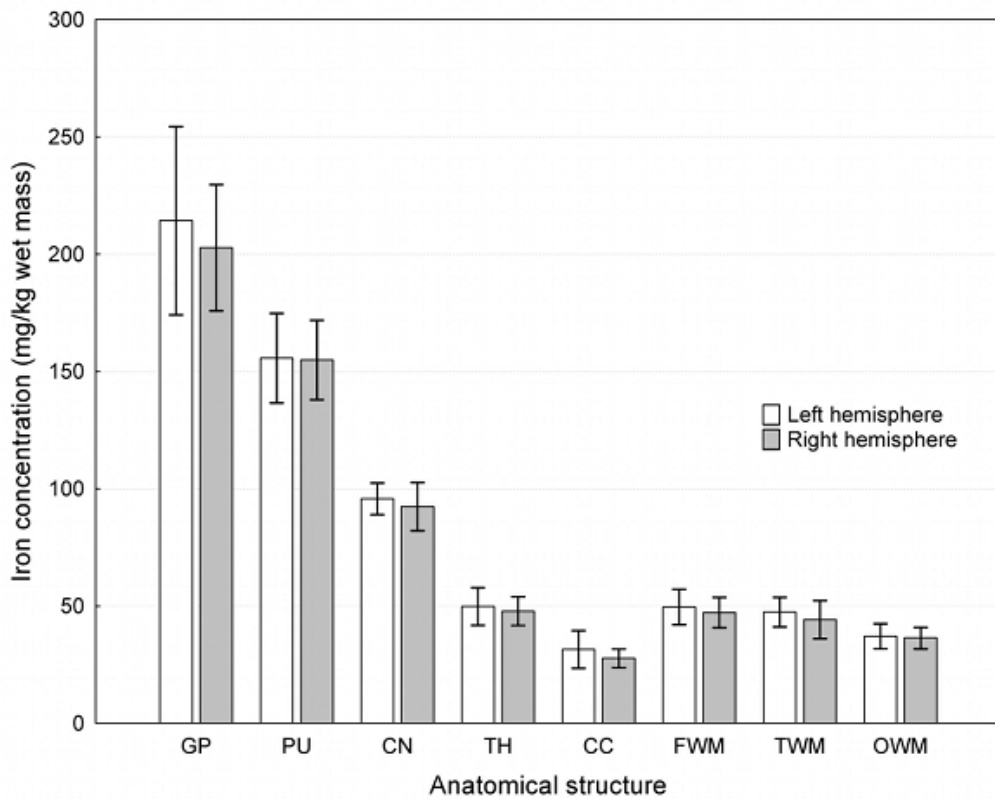
Iron concentrations from inductively coupled plasma mass spectrometry and corresponding transverse relaxation rates in white and grey matter structures

	N†	Iron concentration (mg/kg wet mass)			R2 (s-1)	R2* (s-1)
		Mean ± SD	Median	Range	Mean ± SD	Mean ± SD
Globus pallidus	13	205 ± 32	212	158 – 242	16 ± 2	72 ± 10
Putamen	25	153 ± 29	145	103 – 208	15 ± 1	56 ± 11
Caudate nucleus	25	92 ± 15	94	58 – 121	13 ± 1	40 ± 6
Thalamus	25	49 ± 11	48	35 – 81	11 ± 1	30 ± 6
Corpus callosum	37	30 ± 12	27	16 – 86	NA	22 ± 2
Frontal WM	37	48 ± 14	46	28 – 84	10 ± 1	25 ± 3
Temporal WM	36	46 ± 14	44	22 – 80	NA	26 ± 3
Occipital WM	37	37 ± 10	34	23 – 57	9 ± 1	25 ± 3

N, number of samples included († from one subject only one hemisphere was dissected); SD, 1 standard deviation; NA, structure was not covered by R2 mapping sequence;

As shown in Figure 3 chemically determined mean iron concentrations were significantly higher in the left than in the right hemisphere ( $p < 0.01$ ). This was true when considering all structures and WM structures only ( $p = 0.02$ ), but not for GM structures. The latter, however, also showed a trend for higher iron concentrations in the left hemisphere ( $p = 0.13$ ). Results for the hemispheric differences in iron concentration are given in Table 2.

Figure 3



Hemispheric differences revealed by inductively coupled plasma mass spectrometry. Significantly higher iron concentrations were observed in the left hemisphere when considering all regions. Bars indicate mean iron concentrations and whiskers denote the 95% confidence limits.

Legend: globus pallidus (GP), putamen (PU), caudate nucleus (CN), thalamus (TH), corpus callosum (CC), frontal WM (FWM), temporal WM (TWM) and occipital WM (OWM).

Table 2

Hemispheric differences in brain iron concentration

	N	Mean iron concentration		p	t
		Left hemisphere (mg/kg wet mass)	Right hemisphere (mg/kg wet mass)		
All structures	114	69.2	66.3	< 0.01	2.69
GM structures	42	116.7	113.3	0.13	1.51
WM structures	72	41.4	38.9	0.02	2.39

N, number of samples included; p, p – value; t, t – value;

## Magnetic resonance imaging

The transverse relaxation rates followed the same trend as the iron concentrations determined chemically. When including all brain regions both relaxation rates showed a strong and positive linear correlation with iron concentration (Figure 4 and Figure 5). The correlation

with R2 yielded a correlation coefficient of  $r^2 = 0.67$  while R2\* yielded an even higher coefficient of  $r^2 = 0.90$  ( $p < 0.001$ ). In addition, R2\* showed higher sensitivity to variations in iron concentration than R2 (regression slope = 0.27 for R2\* compared to 0.04 for R2). When considering GM structures only, the correlation coefficient was comparable for both transverse relaxation rates ( $r^2 = 0.58$  for R2 and  $r^2 = 0.87$  for R2\*,  $p < 0.001$ ). However, this relationship was less pronounced in WM. While R2\* showed a weak linear correlation with iron concentrations ( $r^2 = 0.20$ ,  $p < 0.001$ ), no correlation was found between iron concentrations and R2 in WM structures. Table 3 summarizes the results of the regional regression analyses. No significant hemispheric differences could be observed for both transverse relaxation rates, R2 and R2\*.

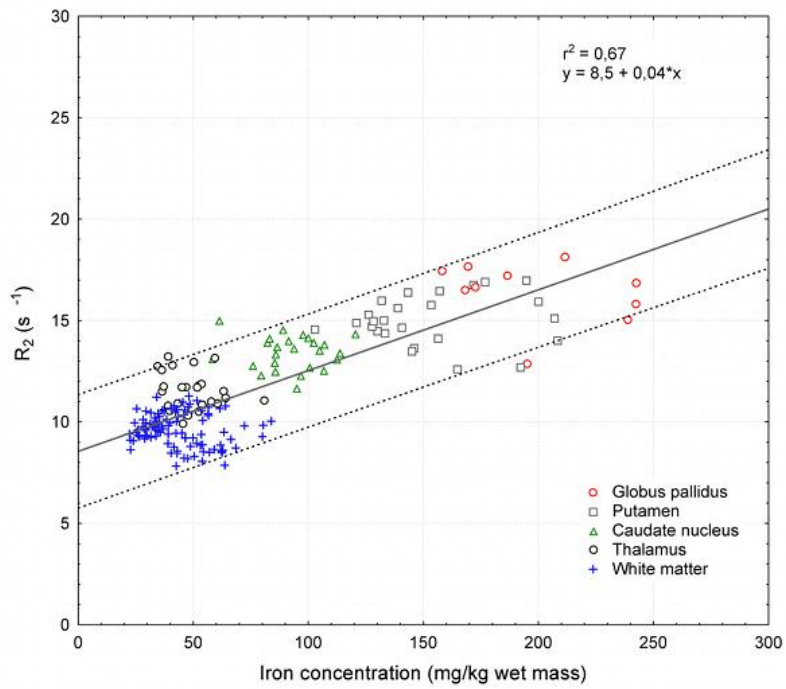
Table 3

Results of the linear regression analysis between iron concentrations and transverse MR relaxation rates

	R2				R2*			
	N	p	$r^2$	Regression (s-1)	N	p	$r^2$	Regression (s-1)
All structures	159	< 0.001	0.67	$8.5 + 0.04*[Fe]$	235	< 0.001	0.90	$14.3 + 0.27*[Fe]$
GM structures	85	< 0.001	0.58	$10.7 + 0.03*[Fe]$	88	< 0.001	0.87	$16.3 + 0.27*[Fe]$
WM structures	74	0.30	0.01	$9.9 - 0.006*[Fe]$	147	< 0.001	0.20	$20.5 + 0.10*[Fe]$

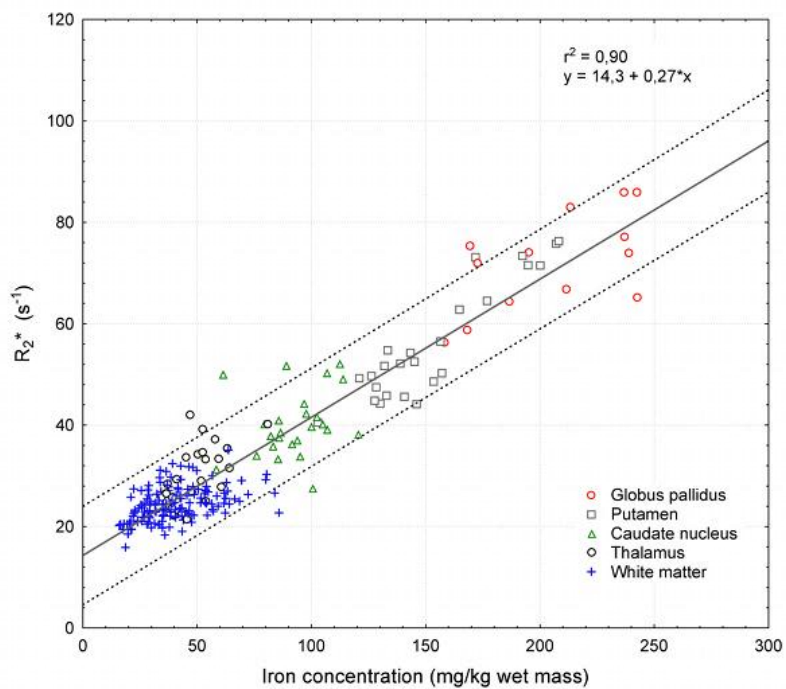
N, number of samples included; p, p – value; r, Pearson regression coefficient; Regression, denoted in intercept  $\pm$  slope \* iron concentration (in mg/kg wet mass);

Figure 4



Results of the linear regression analysis between iron concentrations and R<sub>2</sub> relaxation rates: The solid line indicates the regression line while the dotted lines represent the 95% confidence limits.

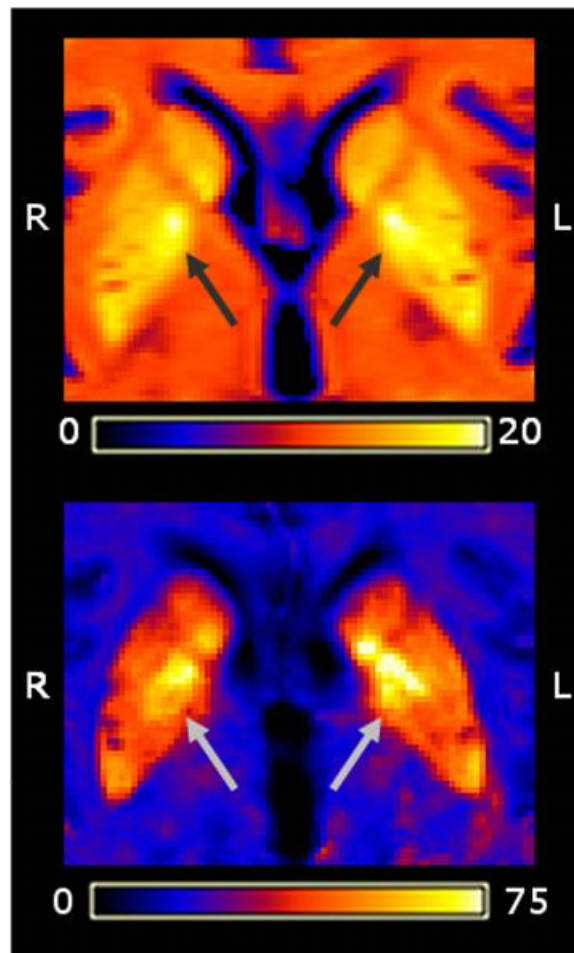
Figure 5



Results of the linear regression analysis between iron concentrations and R<sub>2</sub><sup>\*</sup> relaxation rates: The solid line indicates the regression line while the dotted lines represent the 95% confidence limits.

As a frequent finding local variations in image signal intensity even in single structures were observed that could be assigned to local changes in iron concentrations. This highlights the necessity of utilizing small specimens and ROIs to account for intra-structural variations in iron concentration as demonstrated in Figure 6.

Figure 6



Hemispheric differences in the basal ganglia of a 58 years old male as shown by the R2 (upper) and R2\* maps (lower). Note that the difference in the globus pallidus corresponds well with the chemical analysis which revealed a concentration of 211 mg/kg wet mass in the right hemisphere and a concentration of 242 mg/kg wet mass in the left hemisphere (indicated by arrows). Suggested differences of the lateral ventricles are caused by different windowing of the relaxation rate maps.

## DISCUSSION

This study attempted to validate the assessment of brain iron concentrations by MRI in unfixed brain tissue. For this purpose, quantitative MRI and chemical analysis were performed in deceased subjects where an autopsy had been requested by the local health

authorities, and without a history of neurologic disease or evidence of brain damage. Both relaxation rates, R2 and R2\* showed regional differences throughout the brain parallel to the results of the chemical analysis and exhibited a strong linear correlation with chemically determined iron concentrations. The observation that R2\* yielded a much higher sensitivity compared to R2 is not fully unexpected and in good agreement with theory and previous studies (Gelman, et al. 1999). According to MR relaxation theory R2\* is made up of the sum of two rates ( $R2^*=R2+R2'$ ), where the rate R2' is attributed to local magnetic field inhomogeneities and R2 is associated with intrinsic tissue properties (Haacke et al., 2005; Jensen and Chandra, 2000b; Yablonskiy and Haacke, 1994). Static magnetic field inhomogeneities such as caused by paramagnetic materials like iron are partially refocused in spin echo sequences and therefore should not impact R2 substantially. However, while 1H protons diffusely move through the microscopic field gradients induced by ferritin loaded cells, they acquire random phase shifts which can not be fully refocused due to the stochastic nature of the Brownian motion (Morris et al., 1992). Depending on the inter echo time of the applied spin echo pulse sequence, R2 is therefore also affected by diffusion mediated contributions of iron (Jensen, et al. 2001; Torrey 1956).

While observed correlations were strong within GM we did not find significant correlations of R2 with iron concentration when considering WM structures only. In contrast to GM, WM exhibits several different water pools with intrinsic R2 relaxation rates (MacKay et al., 1994). These pools exchange magnetization on the time scale of R2 relaxation and therefore individually contribute to the apparent R2 relaxation rate (Henkelman et al., 2001). As the water pools represent different tissue compartments, one possible explanation for the missing correlation could be that diffusion does not play a major role in all compartments such as the myelin water for instance (Stanisz and Henkelman, 1998). Moreover, the linear regression analysis revealed that R2\* is substantially more sensitive for probing changes in iron concentration than R2 (see Table 3). Considering these facts it cannot be excluded that there are also iron induced changes in R2 in WM structures below the limit of detection.

The observed correlation of R2\* with iron concentration in WM was significant but much lower than in GM. The overall lower amount and smaller range of iron concentrations in WM compared to GM are also likely to reduce the strengths of correlations. A recently published study did not find any correlation of R2\* with iron concentration in WM at all (Li et al., 2009). However, a direct comparison with our results is not appropriate as these authors investigated formalin fixated brain slices, while we examined entire brains in situ. Furthermore these authors based their conclusion on the investigation of a much smaller



number of tissue specimens obtained from few different WM structures (cingulum, superior corona radiata).

The relaxation rates found in GM in the present study are lower than the rates reported previously for fixed postmortem tissue (House et al., 2007; Shepherd et al., 2009; Xu et al., 2008) but it has been shown that formalin fixation substantially alters relaxation rates (Dawe et al., 2009; Shepherd et al., 2009). In contrast, the brains investigated in this work were scanned in situ – a condition that is not expected to significantly change transverse relaxation rates.

When considering the age range of our cohort, the iron concentrations found in our tissue samples are in good agreement with values reported by Hallgren and Sourander (Hallgren and Sourander, 1958). In contrast to their work, we included blood during preparation for the chemical measurements. This provided a situation closer to the conditions in vivo, where hem bound iron also contributes to the MR signal. However, given the good agreement with Hallgren and Sourander it seems that hem bound iron does only contribute little to overall iron content which can also be explained by the relatively low cerebral blood volume (Schenck, 1992). A significant effect of hem bound iron to transverse relaxation is therefore not expected.

The sensitivity and precision of the method used for the chemical analysis allowed us to look also for hemispheric differences. Such differences have been suggested by in vivo MRI measurements using phase shift imaging and T2 relaxometry (Supprian et al., 1997; Xu et al., 2008) but have not been validated histologically or chemically so far. The results of our chemical analysis support these MRI studies and revealed significantly higher iron concentrations in the left than in the right hemisphere. The leftward asymmetry of brain iron has been ascribed to motor lateralization and also to the co-localization of dopaminergic neurons and iron (Xu et al., 2008). Given the overall small difference in iron concentrations and the limited number of specimen investigated it is not surprising that on a group level these chemical findings were not paralleled by significant hemispheric differences in relaxation rates.

When interpreting our results some limitations also need to be considered. Our study was based on healthy brains and therefore the variability of iron concentration within a given region or structure was expectedly low. This precluded more in depths analysis of the regional correlations of relaxation rates which might be needed to clarify potentially confounding effects of tissue structure or composition. Also brain temperature was not considered in our analysis because its impact on transverse relaxation rates is controversial and unclear.

Published studies failed to find temperature mediated changes of transverse relaxation rates within experimental errors (Bottomley et al., 1984).

## **Conclusion**

This work indicates transverse MR relaxation rates as valid in vivo measures for brain iron concentration with  $R2^*$  as the preferred parameter because of its higher sensitivity and capability to detect differences in iron concentration also in white matter. Moreover, whole brain  $R2^*$  mapping can be accomplished quickly, which is of importance in a clinical setting.

**STUDY 2:**

**SUSCEPTIBILITY INDUCED GRAY-WHITE MATTER**

**MRI CONTRAST IN THE HUMAN BRAIN**

Christian Langkammer<sup>1,2</sup>, Nikolaus Krebs<sup>2</sup>, Walter Goessler<sup>3</sup>, Eva Scheurer<sup>2</sup>, Kathrin Yen<sup>4</sup>, Franz Fazekas<sup>1</sup>, and Stefan Ropele<sup>1</sup>

(1) Department of Neurology, Medical University of Graz, Austria

(2) Ludwig Boltzmann Institute for Clinical Forensic Imaging, Graz, Austria

(3) Institute of Chemistry - Analytical Chemistry, University of Graz, Graz, Austria

(4) Institute of Forensic Medicine, University of Heidelberg, Germany

*Neuroimage. 2012 Jan 16;59(2):1413-9*

## Abstract

MR phase images have shown significantly improved contrast between cortical gray and white matter regions compared to magnitude images obtained with gradient echo sequences. A variety of underlying biophysical mechanisms (including iron, blood, myelin content, macromolecular chemical exchange, and fiber orientation) have been suggested to account for this observation but assessing the individual contribution of these factors is limited in vivo.

For a closer investigation of iron and myelin induced susceptibility changes, postmortem MRI of six human corpses (age range at death: 56-80 years) was acquired in situ. Following autopsy, the iron concentrations in the frontal and occipital cortex as well as in white matter regions were chemically determined. The magnetization transfer ratio (MTR) was used as an indirect measure for myelin content. Susceptibility effects were assessed separately by determining  $R2^*$  relaxation rates and quantitative phase shifts. Contributions of myelin and iron to local variations of the susceptibility were assessed by univariate and multivariate linear regression analysis.

Mean iron concentration was lower in the frontal cortex than in frontal white matter ( $26 \pm 6$  vs.  $45 \pm 6$  mg/kg wet tissue) while an inverse relation was found in the occipital lobe (cortical gray matter:  $41 \pm 10$  vs. white matter:  $34 \pm 10$  mg/kg wet tissue). Multiple regression analysis revealed iron and MTR as independent predictors of the effective transverse relaxation rate  $R2^*$  but solely MTR was identified as source of MR phase contrast.  $R2^*$  was correlated with iron concentrations in cortical gray matter only ( $r=0.42$ ,  $p<0.05$ ).

In conclusion, MR phase contrast between cortical gray and white matter can be mainly attributed to variations in myelin content, but not to iron concentration. Both, myelin and iron impact the effective transverse relaxation rate  $R2^*$  significantly. Magnitude contrast is limited because it only reflects the extent but not the direction of the susceptibility shift.

## INTRODUCTION

Phase images from gradient echo sequences allow the depicting of brain structures with much more details than the corresponding conventional magnitude images (Rauscher et al., 2005). At higher field strength this phenomenon is even more pronounced and provides significantly improved contrast between gray and white matter structures (about an order of magnitude greater) (Duyn et al., 2007). These observations nourish expectations that phase imaging could serve to further improve the detection of cortical lesions in multiple sclerosis patients (Schmierer et al., 2010) and the detection of beta-amyloid plaques in the cortex of transgenic mouse brains (Wengenack et al., 2011).

However, the origin of susceptibility contrast between gray and white matter is not fully understood so far. Phase and magnitude images from gradient echo sequences with longer echo times are both sensitive to the magnetic susceptibility of the underlying tissue. It has been speculated that different levels of myelin (Fukunaga et al., 2010), the relative volume and oxygenation state of blood (Lee et al., 2010a; Marques et al., 2009; Sedlacik et al., 2008), iron deposition (Fukunaga, et al. 2010; Ogg, et al. 1999; Yao, et al. 2009), chemical exchange between water and macromolecular protons (Luo et al., 2010; Shmueli et al., 2011; Zhong et al., 2008), variations in the macromolecular mass fraction (Mitsumori et al., 2009), and the orientation of underlying white matter fibers with respect to the main magnetic field (Denk, et al. 2011b; He and Yablonskiy 2009) may play a significant role for contrast mechanism. But also contributions from other trace elements such as calcium have been considered as sources of cortical susceptibility contrast (Marques et al., 2009; Yamada et al., 1996). More recent work clarified that chemical exchange between water and macromolecular protons (Shmueli et al., 2011) and also the contribution from heme-bound iron in blood (Marques et al., 2009; Petridou et al., 2010; Sedlacik et al., 2008) are not sufficient to explain the extent of the MR phase shifts typically observed.

Because of its well known paramagnetic effect and its abundance, iron was suggested as a major determinant of susceptibility induced contrast (Schenck and Zimmerman, 2004). However, although the effective transverse relaxation rate  $R2^*$  shows a strong linear correlation with iron concentration in gray matter, this relationship is much weaker in white matter indicating that also other factors may play a dominant role (Langkammer et al., 2010; Schweser et al., 2011). In this context it was suggested that the diamagnetic effect of myelin proteins may counteract the paramagnetic effect of iron and therefore might contribute to the susceptibility induced contrast between gray and white matter (Fukunaga, et al. 2010; He and

Yablonskiy 2009). Despite all these considerations, the sources of these contrasts are still a matter of debate and a validation of the underlying biophysical mechanisms is lacking.

The aim of the present study therefore was to investigate possible contributions of myelin and iron to the susceptibility induced contrast between cortical gray and white matter. As there is no in vivo method available for reliably assessing iron concentration in white matter, this study was conducted in deceased subjects shortly after death. High resolution gradient echo magnitude and phase images were acquired in the brain and then related to myelin content and chemically obtained iron concentration. The myelin content was assessed by magnetization transfer imaging (Schmierer et al., 2004). Additionally, R2 relaxation rate mapping was done to disentangle the effect of intrinsic tissue properties.

## **MATERIALS AND METHODS**

### **Subjects**

The local ethics committee approved this study and informed consent was obtained from each individual's next of kin.

Six deceased subjects (median age: 66.5 years; age range at death: 56-80 years; 2 female) with an autopsy requested by the local health authority were included in this study. Forensic pathologists examined the corpses to ensure compliance with the inclusion criteria, i.e., postmortem interval shorter than 72 hours, no history of a neurological disorder or evidence of damage to the brain, and absence of ferromagnetic material.

### **Postmortem MRI**

Corpses underwent MRI of the brain within 40 hours after death at 3 Tesla (TimTrio, Siemens Healthcare, Erlangen, Germany) using a head coil array with 12 receive channels. The subjects were kept refrigerated at 4 °C and, depending on the length of this period, the body temperature at the beginning of the acquisition varied between 11 and 24 °C.

High resolution susceptibility weighted MR images (Deistung et al., 2008) were acquired with a spoiled 3D dual echo gradient echo sequence (TR/TE1/TE2 = 39/9.2/20 ms; flip angle = 20°; FOV = 256 x 256 mm<sup>2</sup>; in-plane resolution: 500 x 500 μm<sup>2</sup>; 88 slices with 2 mm thickness; 2 averages; acquisition time = 17 minutes 27 seconds).

Myelin content was assessed by the magnetization transfer ratio (MTR) because it has been demonstrated that the extent of magnetization transfer between tissue water and myelin bound protons is directly coupled to the density of myelin in white matter (Schmierer et al., 2004).

Magnetization transfer data was acquired with a spoiled 3D gradient-echo sequence (TR/TE = 40/7.38 ms; flip angle = 15°; FOV = 256 x 256 mm<sup>2</sup>; in plane resolution = 1 x 1 mm<sup>2</sup>; 44 slices with 4 mm thickness; acquisition time = 6 minutes 27 seconds) which was performed with and without a Gaussian shaped saturation pre-pulse (offset frequency = 1.2 kHz; duration = 10ms; flip angle = 500°).

R2 relaxation data was acquired with a double-echo fast spin echo sequence (TR/TE1/TE2 = 5260/10/73 ms, FOV = 256 x 256 mm<sup>2</sup>; in plane resolution = 1 x 1 mm<sup>2</sup>; 30 slices with 3 mm thickness; acquisition time = 9 minutes 19 seconds).

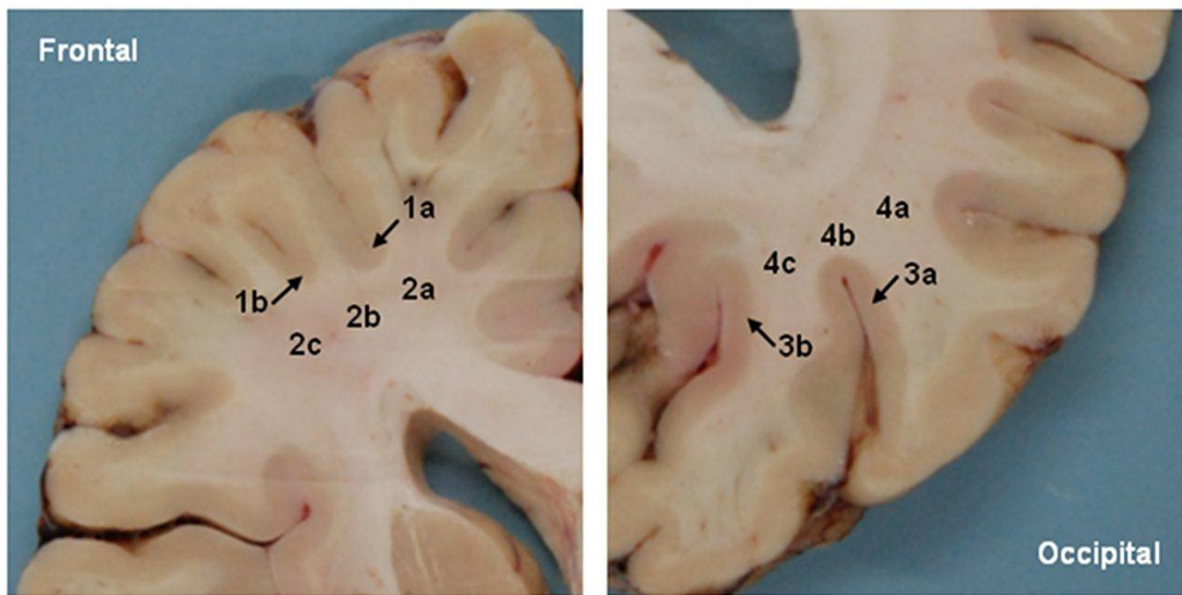
MRI examination additionally included a standard neuroimaging protocol (FLAIR, high resolution MPRAGE sequence) to exclude subjects with acute cerebral damage. All scans were acquired in axial orientation using GRAPPA with an acceleration factor of 2 and were angulated parallel to the most inferior parts of the occipital and frontal lobes.

### **Autopsy and preparation of specimens**

Brains were extracted at autopsy within 12 hours after MRI and main supplying arteries (A. basilaris, Aa. carotides internae) were ligated using surgical fibers to prevent any formation of air bubbles and wash out of blood. Brains were examined exteriorly in detail by a forensic pathologist to exclude any findings of traumatic brain injury, cerebral bleedings, and cicatrices. Brains were fixed in a 4% phosphate buffered (pH 7.0 ± 0.5) formaldehyde solution, (Carl Roth GmbH, Karlsruhe, Germany) for three to five weeks (Yong-Hing et al., 2005). Within four days after extraction the formalin was exchanged to ensure sufficient fixation throughout the brains (Dawe et al., 2009). The brains were cut horizontally into 10 mm thick slices using an orientation identical to the MRI scans and to avoid contamination of the samples with iron, dissection of the tissue was done using ceramic knives.

Tissue specimens were taken from cortical gray matter regions and from adjacent white matter regions. Figure 1 shows a brain slice along with the positions of the dissected specimens. Given the limited number of available samples, these two regions (frontal and occipital) were selected because of their substantial variation in iron concentration (Hallgren and Sourander, 1958). Gray and white matter structures were cut in two and three subunits, respectively, whereas the results of the chemical analysis were averaged for the statistical analysis. Tissue specimens were always taken from both hemispheres at identical positions.

Figure 1



Formalin fixed brain slice from a 64-years-old subject representatively showing the regions where tissue specimens were obtained for mass spectrometry. Legend: frontal cortex (1), frontal white matter (2), occipital cortex (3) and occipital white matter (4). Subunits are denoted by (a,b,c).

### **Chemical assessment of iron concentration**

Dissected tissue specimens were dried in a Gamma 1-16 LSC freeze-dryer (Martin Christ GmbH, Osterode am Harz, Germany) and aliquots of the dried tissue samples were weighed to 0.1 mg into 12 cm<sup>3</sup> quartz vessels. After addition of 5 cm<sup>3</sup> nitric acid the vessels were closed with Teflon caps and placed in the rack of a microwave-heated autoclave UltraCLAVE III (EMLS, Leutkirch, Germany). The samples were heated at 250°C for 30 minutes. Iron concentrations were determined with an Agilent 7500ce inductively coupled plasma mass spectrometer (Agilent Technologies, Waldbronn, Germany) at a mass-to-charge ratio (m/z) of 56. Helium at a flow rate of 5.3 ml/min was added for reduction of the polyatomic interferences <sup>40</sup>Ar<sup>16</sup>O<sup>+</sup> and <sup>40</sup>Ca<sup>16</sup>O<sup>+</sup>. The accuracy of the method was checked with the NIST RM 8414 bovine muscle (NIST, Gaithersburg, USA) and obtained results agreed well with the certified concentrations.

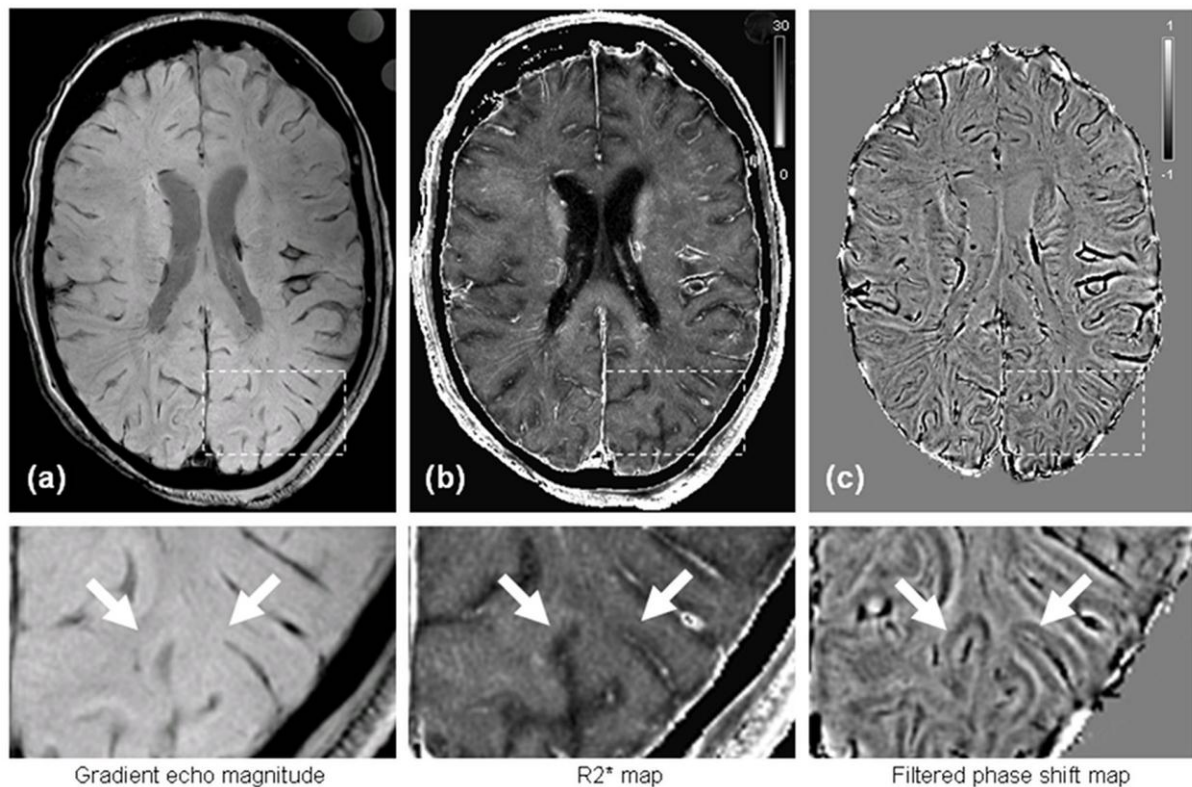
### **Image processing and analysis**

Assuming monoexponential relaxation, maps of the relaxation rates R2 and R2\* were calculated from the dual echo gradient echo and spin echo data, respectively. MTR maps were produced by normalizing the signal intensities obtained with MT saturation to the reference



scan without MT saturation (Henkelman et al., 2001). Phase maps were obtained by unwrapping the raw phase images of the gradient echo sequence with a region growing algorithm implemented in FSL (Smith et al., 2004) followed by high pass filtering with a 8 mm Hamming kernel to remove low frequency background fields (Haacke et al., 2004). Finally, phase shift maps were calculated from the phase difference between the first and the second echo and those maps were used in all further analyses. Exemplarily, gradient echo images (magnitude, R2\* and phase shift) are shown in Figure 2.

Figure 2



MR images from an 80-years-old subject including magnified cortical region. Magnitude (a), calculated R2\* (b) and filtered phase shift (c) images were acquired by a gradient echo sequence at an echo time of 20 ms. The contrast observed between cortex and white matter is substantial greater in phase (c) than in magnitude or R2\* (a,b) images.

According to the position of the dissected tissue specimens, regions of interest (ROI) were outlined manually in the first echo of the fast spin echo sequence, because this image series showed the best contrast between gray and white matter. Then, the outlined ROIs were transformed automatically to the registered R2\*, phase shift and MTR images using an affine registration and transformation algorithm from FSL (Smith et al., 2004). Blood vessels in corpses usually contain deoxygenated blood that can lead to rapid MR signal decay in highly

vascularized regions. For this reason, ROI analysis was done distantly from larger vessels. Therefore and to prevent transformation induced partial volume effects, all ROIs were manually checked after automatic affine transformation. Image analysis was performed blinded to the results of the chemical analysis.

### **Statistical methods**

All analyses were performed using STATISTICA 7.1 (StatSoft, Tulsa, USA) and a p-value of  $p < 0.05$  was considered as statistically significant. Linear regression models were used to evaluate the effect of iron and myelin content on susceptibility related MRI parameters. Multivariate linear regression analysis was used to identify independent determinants of  $R2^*$  and phase shifts. All statistical analyses were first carried out for all brain regions included, and then separately for gray or white matter regions only. Subjects' age was not regarded as covariates in the statistical analyses.

## **RESULTS**

### **Quantitative MRI**

The results of the regional analysis of relaxation rates, MTR and phase shifts are presented in detail in Table 1. The transverse relaxation rates  $R2$  and  $R2^*$  yielded only moderate differences between cortical gray matter and white matter. In contrast, the MTR and the phase shifts were substantially different in the cortical gray compared to the adjacent white matter regions. Most remarkably, the mean phase shift in all cortical gray matter regions was positive indicating that overall paramagnetic contributions to the bulk susceptibility are larger than their diamagnetic counterparts. Conversely, the mean phase shifts in white matter regions were all negative.

It should be noted that the sign of the phase is vendor specific and therefore arbitrary. Herein, positive values denote paramagnetic while negative values denote diamagnetic shifts with respect to the resonance frequency of water.

### **Regional variations of iron**

A total of 120 specimens from six brains were analyzed with inductively coupled plasma mass spectrometry, 48 from cortical gray matter and 72 from white matter. The wet tissue weight ranged between 0.1 and 1.5 g. Mean iron concentration was lower in the frontal cortex ( $26 \pm 6$  mg/kg wet mass) than in frontal white matter ( $45 \pm 6$  mg/kg wet mass) while occipital an inverse relation was found (cortical gray matter,  $41 \pm 10$  vs. white matter,  $34 \pm 6$  mg/kg

wet mass). For comparison, the regional iron concentrations reported by Hallgren and Sourander (Hallgren and Sourander, 1958) are also included in Table 1, where available.

Table 1

Regional analysis of iron concentration, myelin content and corresponding measures of susceptibility.

	Iron concentration (mg/kg wet mass)		MTR (%)	R2 (s-1)	R2* (s-1)	Phase shift (Hz)
Frontal cortex	25.5 ± 6	†29 ± 4	27.0 ± 2.4	6.0 ± 1.1	23.9 ± 3.0	0.17 ± 0.47
Frontal white matter	44.8 ± 6	†42 ± 8	32.6 ± 2.4	6.8 ± 1.3	27.9 ± 2.6	-0.34 ± 0.37
Difference frontal	18.3	13	5.6	0.8	4.0	0.51
Occipital cortex	40.7 ± 10	†45 ± 7	28.1 ± 1.7	7.9 ± 0.5	26.3 ± 3.1	0.51 ± 0.34
Occipital white matter	34.3 ± 6	-	33.4 ± 2.3	7.7 ± 1.1	29.0 ± 2.2	-0.36 ± 0.35
Difference occipital	-6.4		5.3	*-0.2	2.7	0.87

Values are given in means ± 1 standard deviation unless otherwise noted.

† Iron concentrations reported by Hallgren and Sourander (Hallgren and Sourander, 1958).

\* “Inverse transverse relaxation contrast”

### Univariate regression analysis

When considering all gray and white matter samples, R2\* showed a significant linear correlation with iron concentration ( $r=0.38$ ) and an even stronger linear correlation with the MTR ( $r=0.57$ ). In contrast, the MR phase shift was correlated with myelin content only ( $r=-0.43$ ). Scatter plots of these analyses are shown in Figure 3 and the results of all univariate regression analyses are summarized in Table 2.

When including only cortical gray matter regions, R2\* showed an even stronger correlation with iron ( $r=0.42$ ,  $p<0.05$ ) which, however, was absent for the MR phase shift.

When considering only white matter regions a significant negative correlation of iron and the MTR was found ( $r=-0.47$ ,  $p=0.02$ ) which is depicted in Figure 4.

Table 2

Results of the univariate linear correlations (given for cortical gray and white matter combined and separately)

Included specimens	Dependent variable	Independent variable	r	p	Regression equation
All regions	R2*	Iron concentration	0.38	<0.01	$y = 22.38 + 0.12 x$
	R2*	MTR	0.57	<0.001	$y = 10.88 + 52.68 x$
	Phase shift	Iron concentration	-0.14	0.33	-
	Phase shift	MTR	-0.43	<0.005	$y = 1.78 - 5.89 x$
	MTR	Iron concentration	0.13	0.35	-
Cortical gray matter	R2*	Iron concentration	0.42	<0.05	$y = 21.18 + 0.12 x$
	R2*	MTR	0.38	0.07	-
	Phase shift	Iron concentration	0.25	0.24	-
	Phase shift	MTR	0.28	0.18	-
	MTR	Iron concentration	0.01	0.99	-
White matter	R2*	Iron concentration	-0.06	0.77	-
	R2*	MTR	0.21	0.32	-
	Phase shift	Iron concentration	-0.17	0.40	-
	Phase shift	MTR	0.12	0.59	-
	MTR	Iron concentration	-0.47	<0.02	$y = 38.59 - 0.142 x$

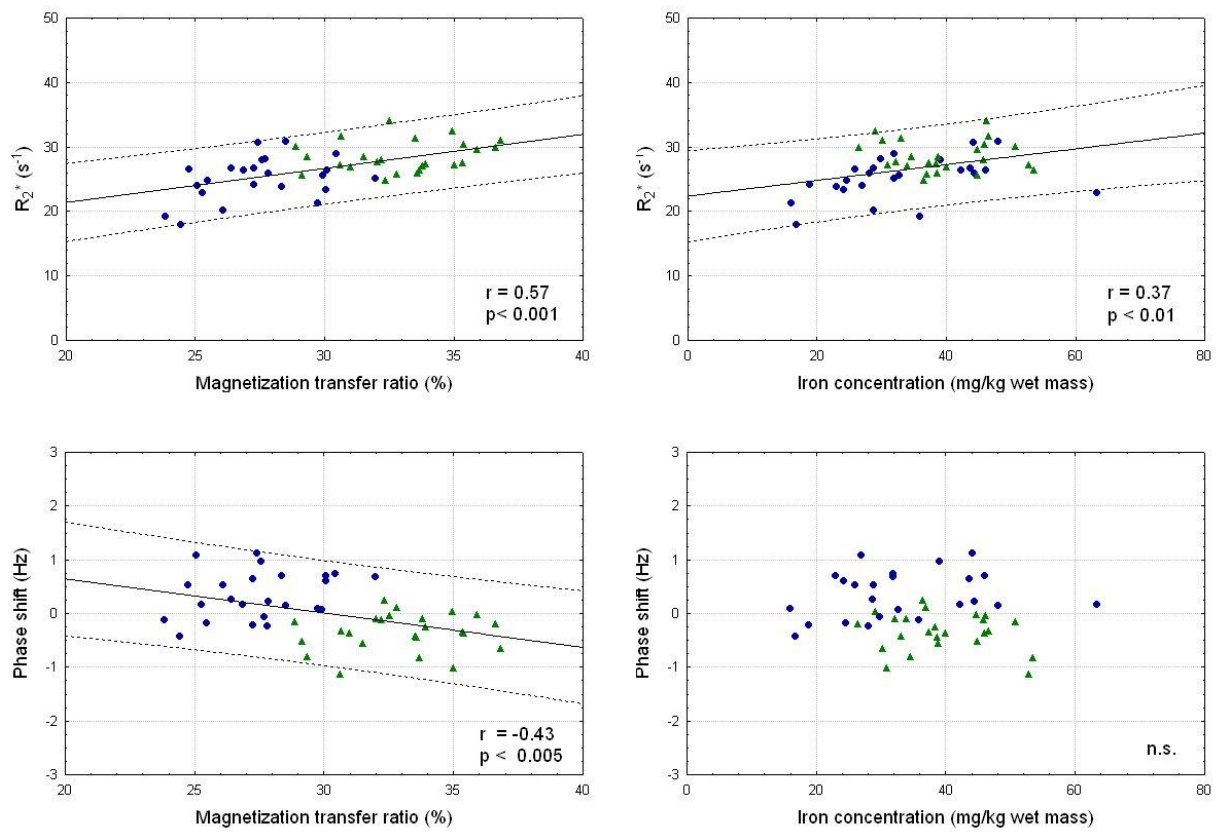
p = p – value, r = Pearson regression coefficient

### Determinants of susceptibility induced gray-white matter contrast

Multiple regression analysis revealed iron concentration and the MTR as independent predictors of the effective transverse relaxation rate R2\*. In line with the univariate results, the MTR was identified as the only independent predictor of the phase shift.

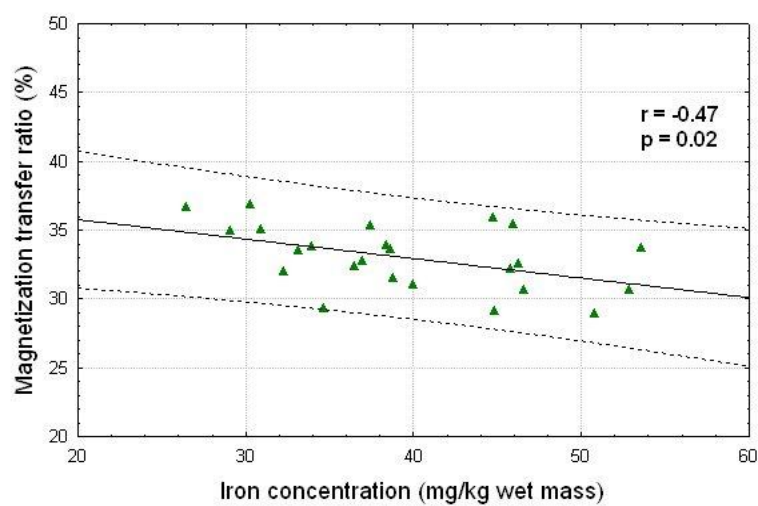
Results of the multiple regression analyses as well as the regression equations are summarized in Table 3 and these results suggest that phase contrast between gray and white matter can be mainly attributed to differences in myelin content.

Figure 3



Linear correlations of the MTR and iron concentration with  $R_2^*$  and phase shift. White matter is represented by triangles and gray matter by circles. The solid lines indicate the regression lines while the dotted lines represent the 95% confidence limits.

Figure 4



The MTR showed a negative correlation with iron in white matter. The solid line indicates the regression line while the dotted lines represent the 95% confidence limits.

Table 3

Results of the multiple regression analyses for R2\* and phase shift for all specimens.

Dependent variable	Independent variable	Beta	p	Regression equation
R2*	Iron concentration	0.30	<0.05	R2*=0.098*[Fe] + 48.78*MTR +8.46
	MTR	0.52	<0.001	
Phase shift	Iron concentration	-0.08	0.52	Phase shift = -5.73 * MTR + 1.87
	MTR	-0.42	<0.005	

p = p – value, [Fe] ... iron concentration is given in mg/kg wet mass

## DISCUSSION

In this postmortem study the susceptibility induced contributions of iron and myelin content to cortical gray and white matter MRI signal generation in unfixed brain tissue were investigated. Recent studies demonstrated that blood volume and its oxygenation state as well as chemical exchange between water and macromolecular protons are not sufficient of explain the phase contrast observed between cortical gray and white matter. However, regional iron concentrations were not included in those studies because there is no complementary in vivo technique for the assessment of iron. To overcome this limitation, in situ MRI was performed in deceased subjects shortly after death and the regional iron concentrations were determined chemically.

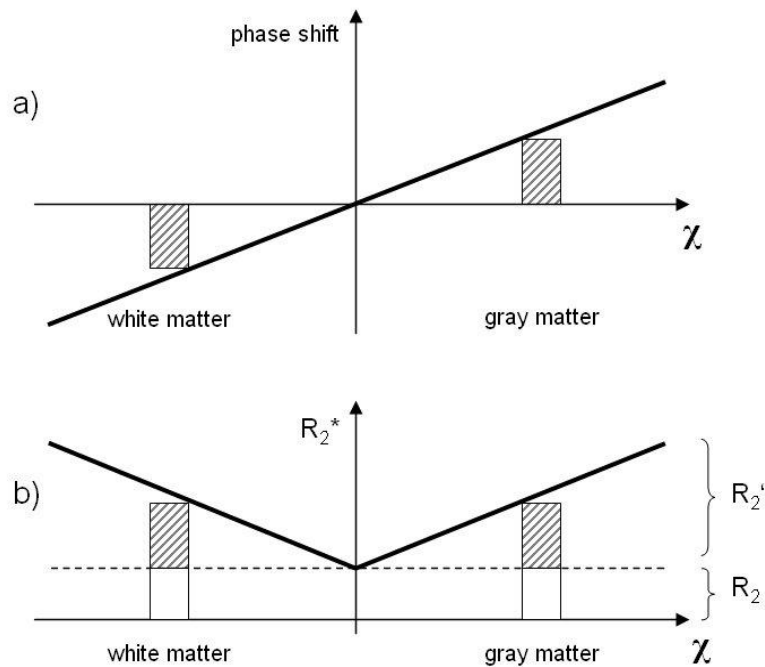
### Determinants of susceptibility induced contrast between cortex and white matter

Linear regression analysis revealed, that the R2\* relaxation rate is affected by both, significant contributions of paramagnetic iron and diamagnetic myelin where the latter was more dominant. In contrast, solely myelin content was identified as independent predictor for the phase shift. Given the fact, that both measures of susceptibility, R2\* and phase shifts, are derived from the same gradient echo sequence, these observations seem unexpected at a first glance.

The phase of a gradient echo is linearly related to differences of the bulk susceptibility with respect to water and therefore can yield positive and negative values. R2\* is the sum of the tissue intrinsic R2 relaxation rate and the rate R2' which is attributed to rf-reversible field inhomogeneities as induced by iron or myelin (Yablonskiy and Haacke, 1994). As R2\* reflects the net loss of spin coherence, it is not relevant whether the susceptibility difference (to water) arises from paramagnetic or diamagnetic origin. This implies that the mean bulk susceptibilities of cortical gray and white matter are of similar extent, but in opposite

directions as indicated by a different sign of the acquired phase signal. An illustration of this relationship is provided in Figure 5.

Figure 5



susceptibilities  $\chi$  are given in differences with respect to water.

MR phase shift and  $R_2^*$  relaxation rate as functions of the tissue susceptibility (all susceptibilities  $\chi$  are given relative with respect to water). While the different susceptibilities of cortical gray and white matter cause a reversed sign of the phase shifts (a), they provide similar  $R_2^*$  rates (b). This may explain well the limited cortical magnitude contrast when compared to the phase contrast.

(Note that the bars are not in scale with results of Table 1).

The rather small differences in mean  $R_2$  and  $R_2^*$  rates found between cortex and adjacent white matter regions ( $R_2$  range: 6.0 to 7.7 s<sup>-1</sup>,  $R_2^*$  range: 23.9 to 29.0 s<sup>-1</sup>) are in line with these considerations as well as the large mean phase shift difference (range: -0.36 to 0.51 Hz). These observations are supported by the results of recent quantitative susceptibility mapping studies and provide experimental evidence and an explanation, why the observed cortical phase contrast is superior in comparison with the magnitude contrast (Liu et al., 2011c; Schweser et al., 2011). Further evidence that myelin is responsible for the observed susceptibility related phase shift between gray and white matter comes from studies of the myelination process in neonates (Zhong et al., 2011) and also from transgenic shiverer mice

(Liu et al., 2012) which both offer the possibility to investigate a much broader range of myelination than in matured brains.

In this study, we used the MTR as an indirect measure for the myelin content. While this concept is commonly applied for white matter, it has not been validated for cortical gray matter so far. Basically, the two-pool model for magnetization transfer between myelin and tissue water can also be applied to cortical gray matter with the difference that myelin content is lower and T1 is higher than in white matter (Stanisz et al., 2005). The latter is responsible why the MTR in the cortex is much higher than one would expect this from the myelin content. In the context of our study this suggests that the effect of the myelin content on the susceptibility may have been underestimated in the multiple regression analysis.

### **R2\* is correlated with iron concentration in cortical gray matter**

Given the overwhelming effects from diamagnetic myelin in comparison to paramagnetic iron in white matter, R2\* and phase shift mapping can not serve for reliably assessing iron concentrations in white matter unless the contribution of myelin is corrected for.

However, when including cortical gray matter structures only, a positive correlation between iron concentration and R2\* rate was revealed. This finding is in line with other postmortem work where this relationship was found in deep gray matter structures (Langkammer et al., 2010) and is not unexpected considering the similar tissue microstructure of cortical and deep gray matter.

### **Relationship between myelin content and iron concentration**

Another interesting finding was the significant negative correlation of iron and myelin content within white matter regions (Figure 4). In white matter, iron is linked with the process of myelination and was found in the proximity of myelin producing oligodendrocytes suggesting a co-localization of iron deposits with neuronal fibers (Fukunaga et al., 2010). Conversely, our results indicate an inverse relationship. However, related studies including iron chemical assessment in white matter regions (corpus callosum, frontal, temporal and occipital) also revealed that the iron concentration in the body of the corpus callosum, which is commonly considered as a region with very a high density of myelinated fibers in the human brain (Oh et al., 2006; Salat et al., 2005), is substantially smaller than in frontal or temporal white matter (Langkammer et al., 2010). However, the cause of this inverse relationship is unclear and needs further investigations.



## **The role of hem bound iron**

The mass spectroscopic analysis revealed a heterogenic distribution of iron in cortical gray and white matter structures. Where available, iron concentrations were in very good agreement with values reported by Hallgren and Sourander (Hallgren and Sourander, 1958). Noteworthy, these authors excluded blood in their colorimetric measurements while in this study blood was maintained in the tissue samples during preparation. The good agreement with the values reported by of Hallgren and Sourander suggests that the total amount of heme-bound iron is marginal compared with ferritin-bound iron in the tissue specimens. To rule out that some of the hem bound iron was washed out during fixation, we additionally performed mass spectrometric iron measurements of the formalin at the beginning and the end of the brain fixation period. However, mass spectroscopy could not proof significant iron levels in the formalin solutions.

## **Iron is responsible for inverse transverse relaxation contrast in the cortex**

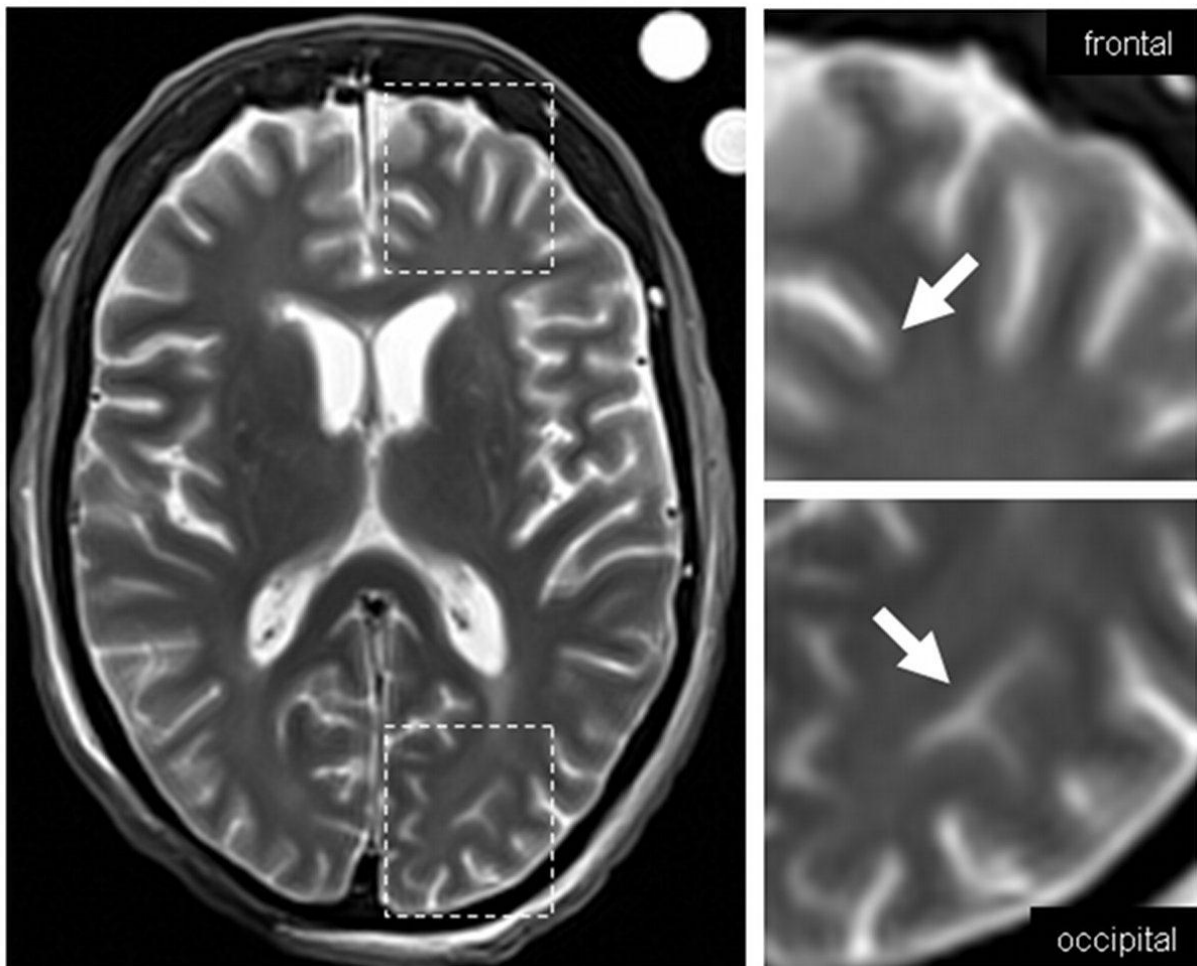
Several MRI studies using T2-weighted scans have observed an unexpected behavior of contrast in the occipital lobe when compared with other cortical regions. Because it is commonly assumed that the transverse relaxation rate  $R_2$  in cortical gray matter is lower than in white matter this was entitled as “inverse transverse relaxation contrast” and the effect has been attributed to variations in iron (Zhou et al., 2001) and dipolar interactions (Grohn et al., 2005).

In the present study we also decided to assess  $R_2$  rates because they are intrinsically included in  $R_2^*$  relaxation rates (see discussion above). The  $R_2$  rates obtained were lower compared to aforementioned studies, which can be ascribed to the fact that spin diffusion occurring during the application of imaging gradients in a CPMG sequence accelerates the transverse MR signal decay. This effect is less pronounced in a dual-echo approach and in addition, intra-voxel incoherent motion is smaller in postmortem tissue.

$R_2$  rates in frontal gray matter were lower than in white matter, while occipital  $R_2$  rates were virtually identical in cortical gray and white matter (Table 1). This can also be seen directly in the T2 weighted spin echo images, where the cortical gray-white matter contrast was less prominent in the occipital lobe (Figure 6). Significantly lower mean iron concentrations were found in frontal cortical gray matter than in frontal white matter while this relationship was reversed occipital. When considering that  $R_2$  in white matter is not affected by iron (Langkammer et al., 2010) and changes of  $R_2$  in gray matter can be mainly assigned to variations in iron content, these results argue that iron deposition is the responsible

mechanism underlying the observed loss of contrast in T2 weighted images. However, an inversion of the contrast can not be observed in the magnitude and phase images of a gradient echo sequence (as can be seen in Figure 2) because cortical susceptibility induced gray-white matter contrast is mostly driven by differences in myelin content.

Figure 6



The inverse transverse relaxation contrast can be observed in T2 weighted spin echo images. Cortical gray-white matter contrast is prominent in the frontal lobe, while it can disappear between occipital gray and white matter as a consequence of different iron levels (Arrows).

### **Orientalional dependency of myelinated fibers**

In addition to theoretical considerations it was recently shown in vivo that  $R2^*$  rates and phase shifts depend on the orientation of the underlying white matter fibers with respect to the main magnetic field (Denk et al., 2011; He and Yablonskiy, 2009). Also an experimental ex vivo study confirmed the dependency of gradient echo phase shift to the orientation in highly

myelinated corpus callosum tissue specimens (Lee et al., 2010b). However, in our study, we did not include the orientation as a further covariate, because the selected white matter regions did not vary substantially in their fiber directions with respect to the main magnetic field. Nevertheless, the corpses included in this work were all positioned axial in the MR system – identical to clinical routine examinations – which allows a direct comparison with the transverse relaxation rates and phase shifts obtained in related in vivo studies.

## **CONCLUSION**

Variations in myelin content, but not in iron concentration are responsible for the MR phase contrast observed between cortical gray and white matter. Both, myelin content and iron affect the effective transverse relaxation rate  $R2^*$  independently whether the bulk susceptibility is paramagnetic or diamagnetic. Therefore, magnitude contrast is limited because it only reflects the extent but not the direction of the susceptibility shift.

Because of the lower myelin content in cortical gray matter,  $R2^*$  rates can be used for the assessment of cortical iron concentrations. However, neither  $R2^*$  nor phase shift mapping can serve for reliably assessing iron concentrations in white matter unless the contribution of myelin is corrected for.

**STUDY 3:**

**QUANTITATIVE SUSCEPTIBILITY MAPPING**

**AS A MEANS TO MEASURE BRAIN IRON?**

**A POSTMORTEM VALIDATION STUDY**

Christian Langkammer<sup>1,2\*</sup>, Ferdinand Schweser<sup>3\*</sup>, Nikolaus Krebs<sup>2</sup>, Andreas Deistung<sup>3</sup>,  
Walter Goessler<sup>4</sup>, Eva Scheurer<sup>2</sup>, Karsten Sommer<sup>3</sup>, Gernot Reishofer<sup>5</sup>, Kathrin Yen<sup>6</sup>, Franz  
Fazekas<sup>1</sup>, Stefan Ropele<sup>1</sup>, Jürgen R. Reichenbach<sup>3</sup>

(1) Department of Neurology, Medical University of Graz, Austria

(2) Ludwig Boltzmann Institute for Clinical-Forensic Imaging, Graz, Austria

(3) Medical Physics Group, Institute of Diagnostic and Interventional Radiology I, Jena  
University Hospital – Friedrich Schiller University Jena, Jena, Germany

(4) Institute of Chemistry - Analytical Chemistry, University of Graz, Graz, Austria

(5) Department of Radiology, Medical University of Graz, Austria

(6) Institute of Forensic Medicine, University of Heidelberg, Germany

\* Authors contributed equally to this work

*Submitted*

## **ABSTRACT**

Quantitative susceptibility mapping (QSM) is a novel technique which allows determining the bulk magnetic susceptibility distribution of tissue *in vivo* from gradient echo magnetic resonance phase images. It is commonly assumed that paramagnetic iron is the predominant source of susceptibility variations in the human brain as many studies have reported a reasonable correlation of magnetic susceptibility with brain iron concentrations *in vivo*. Instead of performing direct comparisons, however, all these studies used the putative iron concentrations reported in the hallmark study by Hallgren and Sourander for their analysis. Consequently, the extent to which QSM can serve to reliably assess brain iron levels is not yet fully clear. To provide such information we investigated the relation between bulk tissue magnetic susceptibility and brain iron concentration in unfixed (*in situ*) postmortem brains of 13 subjects using MRI and inductively coupled plasma mass spectrometry. A strong linear correlation between chemically determined iron concentration and the bulk magnetic susceptibility was found in gray matter structures ( $r=0.84$ ,  $p<0.001$ ), whereas the correlation coefficient was lower in white matter ( $r=0.27$ ,  $p<0.001$ ). The slope of the overall linear correlation was consistent with theoretical considerations of the magnetism of ferritin supporting that most of the iron in the brain is bound to ferritin proteins. In conclusion, iron is the dominant source of magnetic susceptibility in deep gray matter and can be assessed with QSM. In white matter regions the estimation of iron concentrations by QSM is less accurate and more complex because the counteracting contribution from diamagnetic myelinated neuronal fibers confounds the interpretation.

## INTRODUCTION

Quantitative susceptibility mapping (QSM) is a novel post-processing technique which allows to calculate the bulk magnetic susceptibility distribution of tissue *in vivo* from gradient echo (GRE) magnetic resonance phase images (Li and Leigh 2004; Reichenbach 2012). QSM based on single-scan clinical data recently became feasible due to increased computational power and novel algorithms that enable both improved pre-processing of the input GRE data (Liu, et al. 2011c; Schweser, et al. 2011) and reconstruction of susceptibility maps with reduced artifact level (Wharton and Bowtell, 2010). Susceptibility maps acquired from volunteers have been shown to demonstrate unprecedented anatomical contrast in both white and gray matter regions (Liu et al., 2011c; Petridou et al., 2009; Schafer et al., 2011; Schweser et al., 2011; Shmueli et al., 2009; Wharton and Bowtell, 2010). The clinical potential of QSM is still under investigation but it is anticipated that susceptibility maps of patients will provide novel insights into disease induced tissue changes (Reichenbach, 2012). In particular, at magnetic field strengths greater than 1.5 Tesla, the contrast-to-noise characteristics of GRE phase images are superior to magnitude images (Duyn et al., 2007) substantiating that QSM has the potential to be more sensitive with respect to magnetic tissue properties than conventional magnitude-based techniques such as mapping transverse relaxation rates (Aquino, et al. 2009; Haacke, et al. 2005; Langkammer, et al. 2010). Moreover, susceptibility maps can be calculated from any single-echo GRE dataset that is routinely acquired with the well-established susceptibility weighted imaging (SWI) technique (Deistung, et al. 2008; Reichenbach and Haacke 2001) and, thus, comes at no additional cost with routine clinical protocols.

Variations of the magnetic susceptibility of brain tissue can have several different biophysical origins. It is currently assumed that the susceptibility of the human brain is dominated by tissue iron which is predominantly stored in ferritin macromolecules (Hallgren and Sourander, 1958). The ferritin complex is a globular storage protein for iron and known to be paramagnetic so that iron increases the bulk magnetic susceptibility of the tissue (Schenck et al., 1992). Iron stores in the human brain have received increasing interest as abnormally increased brain iron concentrations have been found in a variety of neurological disorders including Alzheimer's disease, Parkinson's disease and multiple sclerosis (Berg and Youdim, 2006; Khalil et al., 2011b). Therefore, much interest has focused on techniques for reliable assessment of brain iron concentrations *in vivo*. Recent experiments in normal controls suggested relatively high correlations between tissue susceptibility assessed by QSM and the

presumed regional iron concentrations (Bilgic, et al. 2011; Wharton and Bowtell 2010; Wu, et al. 2012b) taken from the histochemical postmortem study by (Hallgren and Sourander, 1958). However, other studies indicate that bulk tissue susceptibility is also affected by myelin because of its overall diamagnetic property which counteracts the effect of iron (Langkammer et al., 2010; Lee et al., 2011; Liu et al., 2011a; Schweser et al., 2011). In addition, substances such as blood and contributions from calcium and trace elements have also been found to also affect the magnetic susceptibility of tissue (Mitsumori et al., 2009; Schweser et al., 2011; Sedlacik et al., 2007; Shmueli et al., 2011; Yamada et al., 1996). Valid information on the true correlation of QSM measurements with tissue iron concentrations in different regions of the brain can, however, can only be derived by direct comparison. Therefore, the goal of this study was to investigate the relationship between chemical determined brain iron concentration using inductively coupled plasma mass spectrometry and magnetic susceptibility in unfixed (in situ) postmortem brains.

## **MATERIALS AND METHODS**

### **Deceased subjects**

Thirteen deceased subjects (mean age: 63.5 years; age range at death: 38-81 years; 3 females) with an autopsy requested by the local health authority were included in this study. Forensic pathologists examined the corpses to ensure compliance with the inclusion criteria, i.e., postmortem interval shorter than 72 hours, no history of a neurological disorder or external evidence of brain trauma, and absence of ferromagnetic material. The local ethics committee approved the study and informed consent was obtained from each individual's next of kin.

### **MRI**

Corpses underwent MRI of the brain within 40 hours after death at 3 Tesla (Magnetom TimTrio, Siemens Healthcare, Erlangen, Germany) using a head coil array with 12 receive channels. The subjects were kept refrigerated at 4 °C and, depending on the length of this period, the body temperature  $T_{body}$  at the beginning of the MR data acquisition varied between 4 °C and 24 °C (mean body temperature of all subjects: 13.8°C). High resolution GRE MR images (Deistung et al., 2008) were acquired with an rf-spoiled, flow compensated 3D gradient echo sequence (TR/TE = 39/20 ms; flip angle = 20°; FOV = 256 × 256 mm<sup>2</sup>; voxel resolution: 0.5 × 0.5 × 2 mm<sup>3</sup>; 88 slices; 2 averages; receiver bandwidth = 200 Hz/px; acquisition time approximately 18 minutes). A double-echo, fast spin echo sequence

(TR/TE1/TE2 = 5260/10/73 ms, FOV = 256 × 256 mm<sup>2</sup>; voxel resolution = 1 × 1 × 3 mm<sup>3</sup>; 30 slices; acquisition time approximately 9 minutes) was used for assessing brain anatomy. Additionally, a FLAIR and a high resolution MP-RAGE sequence were included in the MRI examination protocol. All scans were acquired in axial orientation using GRAPPA with an acceleration factor of 2. To provide a reference for quantitative susceptibility contrast in vivo, one healthy (living) 58 years old male volunteer was recruited and the same protocol was applied. This experiment was approved by the local ethics committee and informed written consent was obtained from the volunteer.

### **Autopsy and preparation of specimens**

Brains were extracted at autopsy within twelve hours after MRI and main supplying blood vessels were ligated using surgical sutures to prevent the formation of air bubbles and wash out of blood. The extracted brains were subsequently fixed in a 4% phosphate buffered (pH 7.0 ± 0.5) formaldehyde solution, (Carl Roth GmbH, Karlsruhe, Germany) for three to five weeks. Within four days after extraction the formalin was exchanged to ensure sufficient fixation throughout the brains (Dawe et al., 2009).

The fixed brains were cut axially into 10 mm thick slices using an orientation identical to the MRI scans. Tissue specimens with a wet weight of 0.1 g to 2 g were taken from several pre-specified gray (globus pallidus, putamen, caudate nucleus, and thalamus) and white (frontal-, occipital- and temporal white matter, body of corpus callosum) matter structures. Tissue specimens were taken from both hemispheres at identical positions and ceramic knives were used to avoid contamination with iron. To increase the statistical power of the analysis the samples were cut in two or three subunits, respectively. Due to its relatively small size the globus pallidus was not divided into subunits. Finally, to prepare samples for the mass spectrometry all specimens were freeze dried and weighed before and after freeze drying to enable calculation of wet tissue iron concentrations.

### **Mass spectrometry**

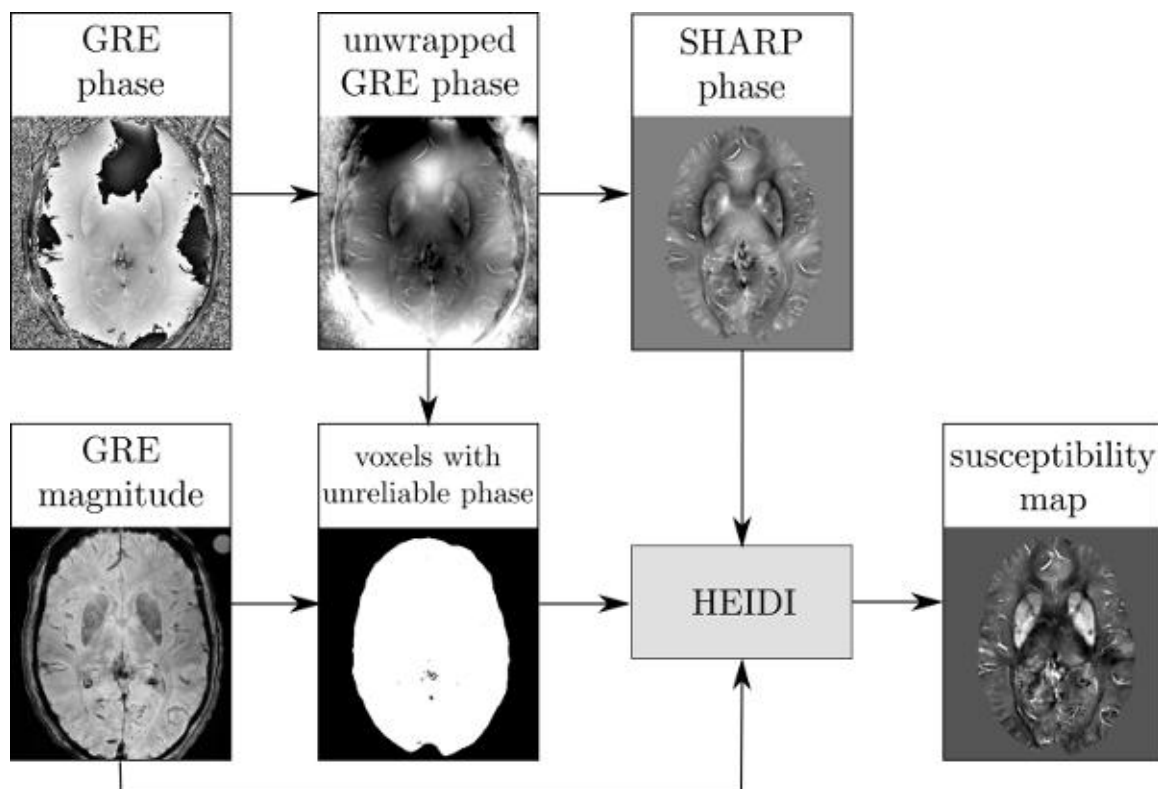
Iron concentrations were determined with an inductively coupled plasma mass spectrometer (Agilent 7500ce, Agilent Technologies, Santa Clara, CA, USA) at a mass-to-charge ratio of 56 in Helium-mode. Helium was added at a flow rate of 5.3 ml/min to reduce polyatomic interferences of <sup>40</sup>Ar<sup>16</sup>O<sup>+</sup> and <sup>40</sup>Ca<sup>16</sup>O<sup>+</sup>. The accuracy of the method was checked with the NIST RM 8414 bovine muscle (NIST, Gaithersburg, MD, USA) and obtained results (69.7 ± 5.1; n=38) agreed well with the certified concentrations (71.2 ± 9.2; n=38).



## Image processing and analysis

Image analysis was performed blinded to the results of the chemical analysis. Aliasing of the GRE phase was resolved with a Fourier-domain unwrapping technique (Li, et al. 2011a; Schofield and Zhu 2003) and background phase contributions were eliminated with the SHARP technique (radius 5 mm, regularization parameter 0.05). Additionally, voxels with unreliable phase values were identified based on the local phase gradient and by thresholding the GRE magnitude image (Schweser et al., 2011). Finally, quantitative susceptibility maps with well suppressed streaking artifacts were reconstructed from the background corrected phase images using the Homogeneity Enabled Incremental Dipole Inversion (HEIDI) algorithm (Schweser et al., ISMRM 2012, #2359). This algorithm solves the inverse field-to-source problem from GRE phase to susceptibility as a weighted total-variation problem incorporating a priori information on the susceptibility distribution that has been derived from the complex GRE signal. The process of QSM is schematically depicted in Figure 1.

Figure 1



Schematic illustration of the QSM framework with data from a deceased 89-years-old subject: the gradient echo phase was unwrapped and preprocessed with the SHARP algorithm while the magnitude additionally served for the identification of unreliable voxels. Using a total variation regularization strategy incorporating a priori information from the complex gradient echo signal, the resulting QSM maps were reconstructed.

According to the Curie law the magnetic susceptibility of paramagnetic materials, such as ferritin-bound brain iron, is approximately inverse proportional to temperature. The susceptibility maps in this study were, therefore, corrected for each subject with respect to the measured body temperature,  $T_{body}$ , and converted to the in vivo condition ( $T=36.5^{\circ}\text{C}$ )(Schenck et al., 1992):

$$\chi_{36.5} = \chi_{measured} * \left( \frac{273 + T_{body}}{273 + 36.5} \right)$$

Subsequently, the zero-points of all resulting susceptibility maps were shifted for each subject individually to the average susceptibility value of occipital white matter because this region had the lowest inter-subject variance in iron concentration (standard deviation of 9 mg/kg wet tissue in this study (Table 1) or 10 mg/kg wet tissue in (Langkammer et al., 2010), respectively). This procedure was required because QSM is intrinsically limited to providing susceptibility differences rather than absolute susceptibility values(Cheng et al., 2009).

According to the position of the dissected tissue specimens, regions of interest (ROI) were outlined manually on the first echo images of the fast spin echo sequence. The ROIs were then transformed automatically to the susceptibility maps using an affine registration and transformation algorithm from FSL (Smith et al., 2004).

## **Statistical methods**

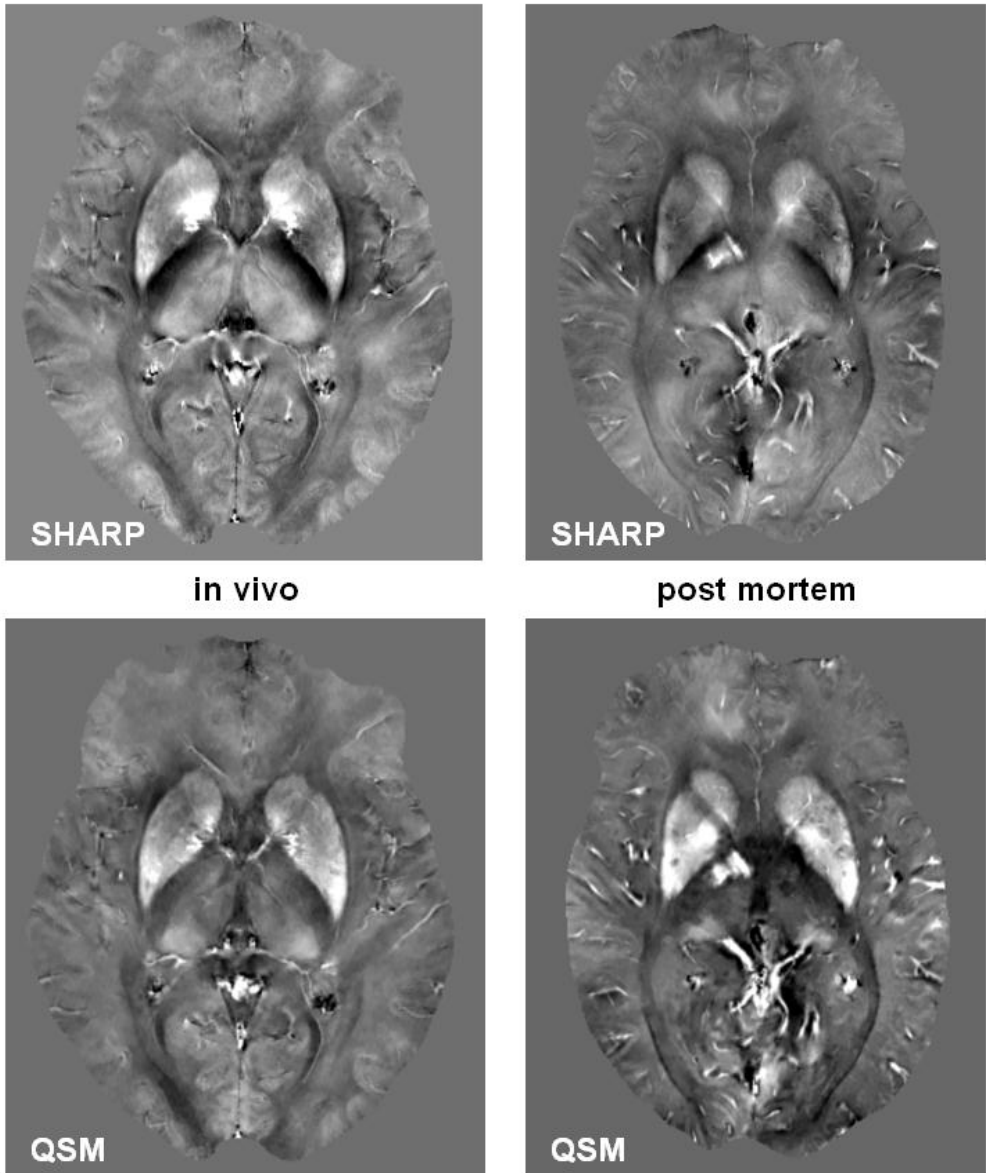
Statistical analyses were performed using STATISTICA 7.1 (StatSoft, Tulsa, USA) and a p-value below 0.05 was considered as statistically significant. Linear regression models were employed to investigate the relation between chemically determined iron concentrations and the bulk tissue susceptibility. All statistical analyses were first carried out for all brain regions, and then for gray and white matter regions separately.

## **RESULTS**

Iron concentrations were obtained from 457 specimens (172 from deep gray matter and 285 from white matter structures). From one subject only one hemisphere was dissected and accidentally contaminated samples were excluded. Inductively coupled plasma mass spectrometry revealed the highest mean iron concentration in the globus pallidus, followed by the putamen, the caudate nucleus, and the thalamus. Mean iron concentrations were lower in white matter than in deep gray matter structures (Table 1). The analysis of the formaldehyde solution before and after the fixation process did not reveal any iron content, indicating that no leakage of tissue iron into the buffer solution had occurred.

The visual appearance of susceptibility maps (Figure 2) was in line with previous QSM work, although visibility of small vessels was substantially increased, which may be attributed to the increased deoxygenation level of the blood. The results of the regional QSM analysis are summarized in detail in Table 1 where positive and negative values represent paramagnetic and diamagnetic magnetic susceptibilities, respectively, relative to occipital white matter. All deep gray matter structures were paramagnetic relative to white matter structures.

Figure 2



SHARP processed phase (top row) and resulting quantitative susceptibility maps (bottom row) of an in vivo 58-year-old subject (left) with a deceased 57-year-old subject (right). Substantially more vessels are visible in the postmortem map because of the fully deoxygenated blood. The contrast in the images is equal (SHARP phase from -1 to 1 rad; QSM from -0.1 to 0.2 ppm).

Table 1

Chemically determined iron concentrations and bulk tissue magnetic susceptibilities grouped by brain regions.

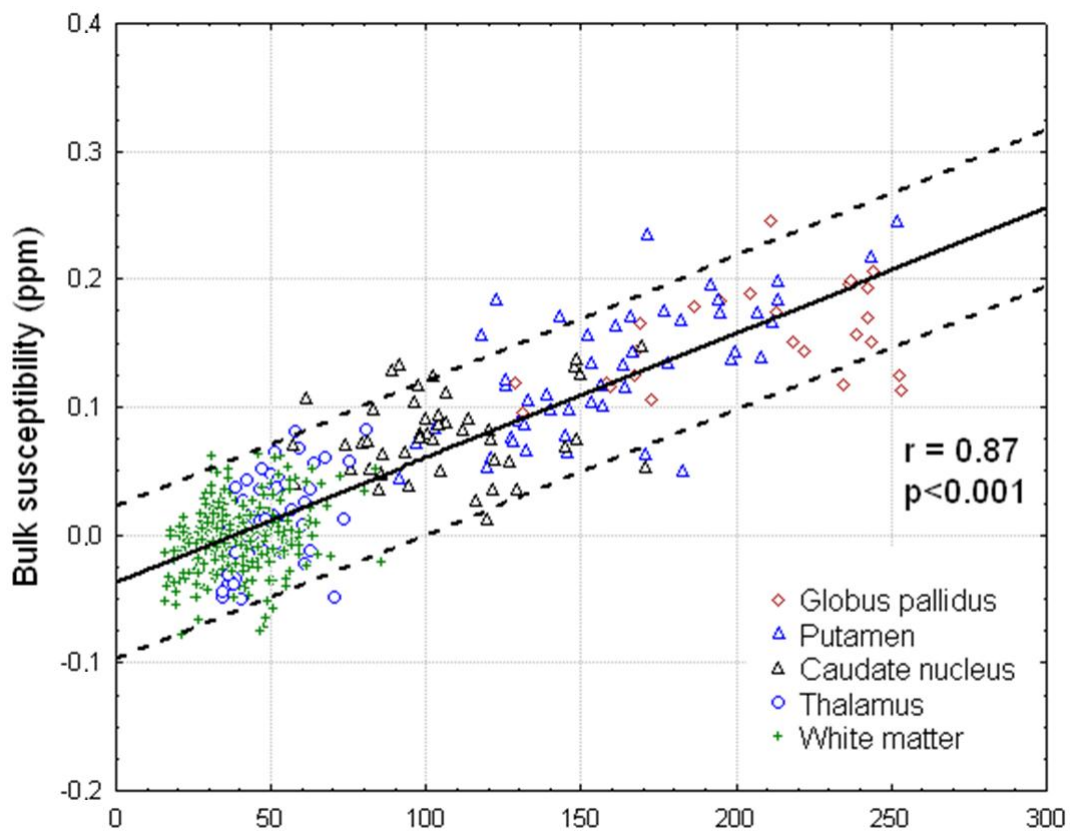
	N	Iron concentration (mg/kg wet tissue)		Bulk susceptibility (ppm)	
Globus pallidus	25	205 ± 39	(169 – 239)	0.155 ± 0.038	(0.119 – 0.182)
Putamen	49	160 ± 37	(132 – 183)	0.129 ± 0.051	(0.085 – 0.170)
Caudate nucleus	49	105 ± 27	(86 – 121)	0.078 ± 0.032	(0.053 – 0.097)
Thalamus	49	50 ± 12	(41 – 58)	0.012 ± 0.035	(-0.014 – 0.039)
Corpus callosum	67	29 ± 10	(21 – 32)	-0.012 ± 0.028	(-0.031 – 0.005)
Frontal white matter	73	47 ± 11	(36 – 54)	-0.009 ± 0.026	(-0.008 – 0.026)
Temporal white matter	72	46 ± 11	(39 – 52)	-0.003 ± 0.028	(-0.021 – 0.015)
Occipital white matter	73	36 ± 9	(29 – 42)	-0.000 ± 0.016	(-0.007 – 0.010)

Values are given in mean ± standard deviation (inter-quartile range).

Susceptibilities values are given relative to the reference region (occipital white matter) so that positive and negative values represent more and less diamagnetic bulk magnetic susceptibility relative to the reference region, respectively. N represents the number of samples included the analysis.

Regional magnetic susceptibilities were highly correlated with the results from mass spectrometry, in particular with higher iron concentrations. Figure 3 illustrates the strong positive linear correlation found between chemical iron concentration and bulk magnetic susceptibility when all regions were included in the analysis ( $r=0.87$ ,  $p<0.001$ ). The correlation remained high when only gray matter structures were included ( $r=0.84$ ,  $p<0.001$ ) and substantially decreased when only white matter structures were considered in the analysis ( $r=0.27$ ,  $p<0.001$ ). Including all regions, linear regression yielded  $\chi = 0.0097 \text{ ppm} * [\text{Fe}] - 0.040 \text{ ppm}$ , where  $[\text{Fe}]$  is the iron concentration in mg/kg wet tissue mass and the susceptibility value  $\chi$  is again referenced to the mean susceptibility of occipital white matter. When only including gray matter or white matter regions in the regression, slopes of 0.00089 ppm/(mg/kg) and 0.00055 ppm/(mg/kg), respectively, were obtained. Detailed results of the regression analysis are listed in Table 2.

Figure 3



Correlation of bulk magnetic susceptibility with measured iron concentration. The line represents the regression of all data points and the dotted lines indicate the 95% confidence intervals.

Table 2

Results of the linear regression analysis of bulk magnetic susceptibility and measured iron concentration.

	bulk susceptibility		
	r	regression slope (ppm per mg/kg wet weight)	regression offset (ppm)
all structures	0.87	0.00097 ± 0.00003	-0.037 ± 0.002
gray matter	0.84	0.00089 ± 0.00005	-0.022 ± 0.006
white matter	0.27	0.00055 ± 0.00012	-0.023 ± 0.005
theory for ferritin (36.5°C)	-	0.00127	-

Slope and offset values are given in mean ± standard deviation. The p-values were below 0.001 in all analyses. r = Pearson regression coefficient; Regression equation:  $\chi = \text{slope} * \text{iron concentration (in mg/kg wet tissue)} \pm \text{offset}$ .

## DISCUSSION

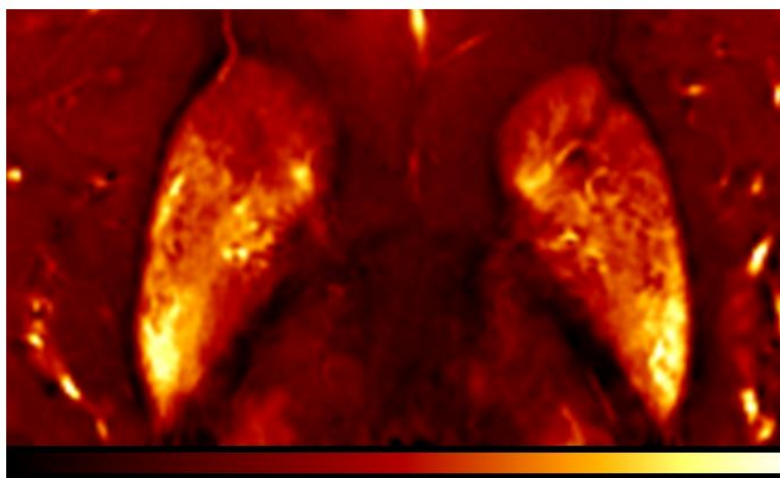
In this study, the relation between iron concentration and magnetic susceptibility in the human brain was investigated by QSM and inductively coupled plasma mass spectroscopy of postmortem tissue specimens. The results confirmed that the magnetic susceptibility is very sensitive for variations in iron concentration in the human brain.

The experimentally determined slopes of the linear correlation functions using all and using only deep gray matter regions are in line with the susceptibility of ferritin as predicted by theoretical considerations (Schenck et al., 1992): Considering the effective number of Bohr magnetons (3.78) and an estimated density of brain tissue of  $1 \text{ g/cm}^3$ , the paramagnetic contribution of ferritin to the tissue susceptibility may be estimated to be  $0.00127 \text{ ppm} * [\text{Fe}]$  at  $36.5 \text{ }^\circ\text{C}$  which corresponds to a susceptibility of  $0.00137 \text{ ppm} * [\text{Fe}]$  at the mean tissue temperature of the present study of  $13.8 \text{ }^\circ\text{C}$  ( $[\text{Fe}]$  in  $\text{mg/kg}$  wet tissue mass) because the susceptibility of paramagnetic substances is inverse proportional to the temperature (Schenck et al., 1992). This agreement between theoretical and experimental findings supports the notion that most of the iron in the brain is bound to ferritin proteins (Hallgren and Sourander, 1958). The slightly smaller susceptibility values (see Table 2) compared to the theoretical values may be explained by either abundance of iron in chemical forms that are less paramagnetic (such as oxygenated heme or other low spin iron species) (Schenck et al., 1992) or by a systematic underestimation of the calculated susceptibility (Wharton and Bowtell, 2010). In particular in white matter, the lower slope might additionally be explained by the high abundance of diamagnetic myelin (Li et al., 2012; Schweser et al., 2011): The increased myelin content of white matter compared to gray matter systematically decreases the susceptibility of the white matter regions and, due to the low mean susceptibility value of white matter regions, slightly biases the linear fitting. This is also reflected by the regression offset which was significantly lower when all structures were considered compared to only white or gray matter structures (Table 2).

The observed higher correlation coefficient for the deep gray matter structures compared to the white matter structures was also recently found when transverse relaxation rate mapping was used for the assessment of brain iron (Langkammer et al., 2010) and may be attributed to the much broader range of iron concentrations in deep gray matter (about 4-times higher concentrations). The small variation in iron concentration in white matter enhances the relative contribution of confounding effects of several other factors. The scattering of the values is, for example, likely to originate from spatial mismatch of dissected tissue specimens

and analyzed regions in the MR images. The tissue samples were collected from identifiable anatomic structures and not based on the magnetic susceptibility maps so that the relatively strong regional variations of susceptibility values within single nuclei (see Figure 4) may have impacted the results. Substances such as deoxygenated blood, transferrin, hemosiderin, myelin, calcium (Schweser et al., 2010), and orientation dependency of susceptibility (Denk, et al. 2011a; Liu 2010) naturally change the bulk voxel susceptibility, thus, compromising the correlation with ferritin-bound iron. Iron in transferrin or deoxygenated heme, for example, is also assessed quantitatively by mass spectroscopy but is in different electronic states with spin quantum numbers of  $S=5/2$  and  $4/2$ , respectively, and thus is more paramagnetic than iron bound to ferritin which has an effective spin quantum number of approximately  $3/2$  (Schenck, 1992). On the other hand, iron in white matter is collocated to oligodendrocytes which play a major role in myelination (Connor and Menzies, 1996). Myelin and calcium, on the other hand, are diamagnetic and thus counteract the effect of iron on susceptibility (Li, et al. 2011a; Schweser, et al. 2011). These factors and the abundance of other trace elements could modify the measured susceptibility. The current understanding of the magnetic susceptibility of brain tissue is still rather limited and thus needs input from histochemical correlation studies. Further work also has to include surrogate markers for myelin and should consider white matter fiber orientations with respect to the main magnetic field to determine this contribution to the total voxel susceptibility. These will be prerequisites for a more accurate assessment of iron in highly myelinated regions (Lee et al., 2010b; Li et al., 2012).

Figure 4



Regional variations of bulk magnetic susceptibility within the basal ganglia in a 54-years-old deceased subject. Image contrast is from -0.1 ppm (red) to 0.25 ppm (yellow).

The present study was not compromised by changes due to formalin fixation of the brain, which is known to degrade the tissue microstructure and consequently changes the MR signal behavior (Dawe et al., 2009; Schmierer et al., 2008). However, we cannot rule out that a lower tissue temperature than in vivo as well as some degree of autolysis might have impacted our measurements. Little is known about the temperature dependence of tissue susceptibility and whether the magnetic susceptibilities of white and gray matter exhibit different temperature dependences. For example, the structure of the myelin lipid bilayer might change with decreasing temperature and proceeding autolysis may affect its diamagnetism. However, the strong correlation with iron concentration as observed in the present study suggests that iron induced susceptibility changes dominate other potential contributions. This is also supported by the visual comparison of postmortem QSM maps with in vivo QSM maps as exemplarily shown in Figure 2. Despite the stronger visibility of vessels, which may be explained by the increased abundance of deoxyhemoglobin, no significant changes in the bulk susceptibility of tissue were observed.

Recent work employing QSM has revealed a substantially increased cortical gray-white matter contrast in susceptibility maps when compared to magnitude images (Li et al., 2011; Liu et al., 2011c; Schweser et al., 2011). The absence of this pronounced cortical contrast in our subjects is most likely due to normal aging. To demonstrate methodical developments recent studies mainly relied on young volunteers around 30 years. In contrast the mean age of our cohort was 63.5 years, which is an age where cortical gray-white matter contrast is reduced also in conventional MRI (Salat et al., 2009). The similar appearance of in vivo and postmortem susceptibility maps and the lack of cortical contrast even in the SHARP phase images (Figure 2) demonstrates that this is neither a limitation of the utilized QSM technique nor an effect of postmortem changes, but may be ascribed to aging.

When comparing the results of the present QSM study to recently published work employing the effective transverse relaxation rate  $R2^*$ , both techniques revealed similar correlations with iron and, thus, represent reasonable measures for the assessment of regional iron concentrations (Aquino, et al. 2009; Langkammer, et al. 2010). There are, however, several substantial differences of magnetic susceptibility mapping and relaxation rate mapping. First, susceptibility is more specific to the underlying biophysical tissue composition because diamagnetic substances counteract the effect of paramagnetic substances while the abundance of both substances has an additive effect on the  $R2^*$  rate, which confounds the interpretation of  $R2^*$  particularly in regions with low iron concentrations such as white matter (Langkammer, et al. 2010; Schweser, et al. 2011). Moreover, susceptibility maps can be



calculated from single echo GRE measurements that are routinely acquired in the course of SWI, while  $R2^*$  measurements require a multi-echo GRE sequence. However, this comes along with the drawback that QSM only allows determining susceptibility differences rather than absolute susceptibility values. Due to this relative nature, normalization of the maps with respect to a certain reference region (occipital white matter in the present study) is required which may induce minimal susceptibility shifts. While relaxation rate mapping is a robust and established approach that has been applied in a number of clinical studies, QSM, on the other hand, is a very recent technique and subject to ongoing algorithmic improvements which may overcome the current pitfalls.

Nevertheless, quantitative magnetic susceptibility mapping provides novel information on the intrinsic biophysical tissue properties which is, to a certain extent, complementary to relaxation rate mapping. It may, therefore, be expected that the combination of relaxation rate mapping and QSM will provide further insight and will be instrumental for disentangling the main contributors yielding an increased accuracy of measurements of iron concentration and non-iron contributions in white matter. Future studies are certainly required to elaborate and compare relaxation rate mapping and QSM with respect to their sensitivity and accuracy as well as specificity to the underlying tissue composition and, in particular, for investigations of pathological conditions.

## **CONCLUSION**

Variations of the magnetic susceptibility of brain tissue are strongly driven by ferritin-bound iron. While iron is the dominant source of magnetic susceptibility in deep gray matter, the counteracting diamagnetism of myelin reduces the sensitivity of QSM based iron measurements in white matter.

**STUDY 4:**

**MAPPING OF IRON DEPOSITION IN CONJUNCTION WITH  
ASSESSMENT OF NERVE FIBER TRACT INTEGRITY IN  
AMYOTROPHIC LATERAL SCLEROSIS**

Christian Langkammer<sup>1</sup>, Christian Enzinger<sup>1,2</sup>, Stefan Quasthoff<sup>1</sup>, Paula Grafenauer,<sup>1</sup>  
Michaela Soellinger<sup>1</sup>, Franz Fazekas<sup>1</sup>, and Stefan Ropele<sup>1</sup>

(1) Department of Neurology, Medical University of Graz, Austria

(2) Section of Neuroradiology, Department of Radiology, Medical University of Graz, Austria

*Journal of Magnetic Resonance Imaging. 2010 Jun;31(6):1339-45*

## **ABSTRACT**

### **PURPOSE:**

To test if and where increased iron accumulation occurs in amyotrophic lateral sclerosis (ALS) by quantitative mapping of iron deposition and to relate these findings to white matter tract degeneration assessed by diffusion tensor imaging (DTI).

### **MATERIALS AND METHODS:**

Fifteen patients with ALS and 15 age- and gender-matched controls underwent MRI of the brain to obtain R2\* relaxation rate and DTI measurements, focusing on the corticospinal tract (CST) and on deep gray matter structures, using tract-based spatial statistics (TBSS).

### **RESULTS:**

Compared with controls, ALS patients showed reduced fractional anisotropy values along the mesencephalic CST, suggesting disintegration of fiber tracts. A trend for R2\* values to be elevated was found in the CST of ALS patients. Regarding other brain areas examined, increased R2\* values in ALS patients were observed solely in the caudate nucleus.

### **CONCLUSION:**

This study extends previous findings on fiber disorganization by additional quantitative evidence for increased iron deposition in closely localized regions along the CST in ALS patients. Longitudinal studies are needed to further explore the pathophysiologic and diagnostic implications of these findings.

## INTRODUCTION

Amyotrophic lateral sclerosis (ALS) is a chronic and relentlessly progressive CNS disease preferentially affecting the motor neuron system. Various diffusion tensor imaging (DTI) based techniques have revealed microstructural tissue changes in the corticospinal tract (CST) in ALS (Ellis, et al. 1999; Grosskreutz, et al. 2008; Toosy, et al. 2003). The approaches applied included streamline fiber tracking (Sage, et al. 2007; Wang, et al. 2006), probabilistic diffusion tractography (Behrens et al., 2003; Ciccarelli et al., 2006) and tract based spatial statistics (TBSS) (Ciccarelli et al., 2009; Smith et al., 2006). Advances in DTI validation nourished hopes that DTI could serve to differentiate whether axonal loss is primary or secondary (Beaulieu 2002; Song, et al. 2002; Song, et al. 2005; Sun, et al. 2006). Recent studies also suggested that tissue changes in ALS might not be restricted to the motor system (Abrahams et al., 2005; Phukan et al., 2007; Rippon et al., 2006). Apart from a more detailed description of ongoing morphologic changes, however, the aetiopathological understanding of ALS still remains limited (Turner, et al. 2009; Wang and Melhem 2005).

Increased accumulation of iron in the brain has been implicated in the pathophysiology of many neurodegenerative CNS disorders like Alzheimer's, Parkinson's, and Huntington's disease (Berg and Youdim 2006; Stankiewicz, et al. 2007). This comes from speculations that iron-mediated oxidative stress and formation of cytotoxic protein aggregates may trigger or promote neurodegeneration (Berg and Youdim, 2006; Gotz et al., 2004). Such mechanisms have been considered as a major culprit in the pathophysiology of ALS (Carri et al., 2003). Indeed, in ALS patients whose motor cortex appeared hypointense on T2-weighted scans, this was ascribed to elevated iron concentrations in association with neurodegeneration (Imon et al., 1995; Oba et al., 1993). Moreover, increased serum levels of ferritin have been reported in ALS (Goodall et al., 2008). However, whether and to what extent iron accumulation might also be directly associated with damage to specific fiber tracts in ALS and how this differs from normal ageing processes has not been investigated so far.

Ferric ions cause local changes of the magnetic susceptibility, an effect that is measurable by MRI using relaxometry, phase imaging, or magnetic field correlation (MFC) (Haacke et al., 2005; Jensen et al., 2006; Schenck and Zimmerman, 2004; St Pierre, 2003). Here, we therefore used R2\* relaxometry to quantitatively measure iron deposition in the brains of ALS patients with a focus on the CST. We also wanted to investigate how such measurements relate to microstructural tissue changes assessed by clinical findings and DTI.

## **MATERIALS AND METHODS**

### **Study Participants**

Fifteen patients with definite or probable ALS according to the El Escorial criteria (Brooks, 1994) defined by the World Federation of Neurology (mean age  $60.1 \pm 8.8$  years, range 42-82 years, 5 female) participated in this study. An experienced clinician diagnosed occurrence of ALS and rated their functional impairment using the revised Amyotrophic Lateral Sclerosis Functional Rating Scale - ALSFRS-R (Brooks et al., 2000). The mean ALSFRS-R was  $39.1 \pm 5.6$  and the mean estimated disease duration was  $25.5 \pm 16.2$  months. A mean disease progression rate (Ciccarelli et al., 2006) RDP of  $0.58 \pm 0.57$  was calculated according to:

$$\text{RDP} = (48 - \text{ALSFRS-R}) / \text{disease duration (in months)}$$

Nine patients presented with a limb-type onset and 6 patients presented with a bulbar-onset. Limb-type onset subjects primarily showed a degeneration of the upper and lower motor neuron, restricting their ability of voluntary muscle movement, whereas bulbar-onset subjects showed an additional impairment of brain stem motor neurons, resulting in dysarthria and dysphagia. In total eleven patients had mild to moderate limb paresis (3 to 4 out of 5 according to the Medical Research Council Scale).

Fifteen healthy subjects (mean age  $60.8 \pm 8.1$  years, range 41 - 80 years, 5 female), free of neuropsychiatric disease, were matched for age and gender to serve as a control group.

All study participants gave written informed consent in accordance with the requirements of the local ethics committee.

### **Magnetic resonance imaging**

Study participants underwent MRI at a 3 Tesla whole body system (Tim Trio, Siemens Healthcare, Erlangen, Germany) using a head coil array with 12 elements. Structural imaging included a fast FLAIR sequence (TR/TE/TI = 10 s/70 ms/2500 ms, in plane resolution =  $0.9 \times 0.9$  mm<sup>2</sup>, slice thickness = 4 mm and FOV = 220 mm) and a T1 weighted 3D MPRAGE sequence with 1mm isotropic resolution (TR/TE/TI/FA = 1900 ms/2.19 ms/900 ms/9°) and a matrix size of 256 x 256. Structural MRI data were jointly reviewed in a blinded manner by experienced observers to exclude the presence of morphological abnormalities.

To map R2\* a spoiled FLASH sequence (TR/FA = 68 ms/20°) with 12 equally spaced echoes (bipolar readout gradient with echo spacing of 4.92 ms, in plane resolution = 0.9 x 0.9 mm<sup>2</sup>, slice thickness = 4 mm, FOV = 230 mm) was used.

DTI data were acquired with a diffusion weighted single shot SE-EPI sequence (TR/TE/FA = 6700 ms/95 ms/90°, in plane resolution = 1.95 x 1.95 mm<sup>2</sup>, slice thickness = 2.5 mm, NEX = 4), where the diffusion sensitizing gradients were applied in 12 independent directions (b = 1000 s/mm<sup>2</sup>) and a reference scan was performed without diffusion weighting (b ≈ 0 s/mm<sup>2</sup>).

## **Image Analysis**

### **Regional R2\* and DTI Mapping**

To eliminate image shifts caused by the bipolar data acquisition, all subsequent echoes provided by the multiecho FLASH sequence were registered with the first echo using FLIRT (Jenkinson et al., 2002) from the FMRIB software library (FSL Version 4.1.0) (Smith et al., 2004). R2\* maps were then calculated by fitting a mono-exponential decay curve and by considering the contribution of non Gaussian image noise with a Least square approach (St Pierre, 2003; St Pierre et al., 2004):

$$S(TE) = S_0 * e^{(-TE * R2^*)} + c_{noise}$$

Based on the high resolution T1-weighted scan, seven deep grey matter structures in both hemispheres (amygdala, caudate nucleus, hippocampus, nucleus accumbens, globus pallidus, putamen and thalamus) were segmented fully automatically using FIRST, a segmentation and registration tool based on deformable models (Smith et al., 2004). The resulting masks for these structures were eroded by one pixel to avoid anatomical overlapping with adjacent regions as well as to minimize possible impacts of mis-registration and were then overlaid on the R2\* maps. Mean R2\* values and standard deviations were calculated for each structure by averaging the values from both hemispheres.

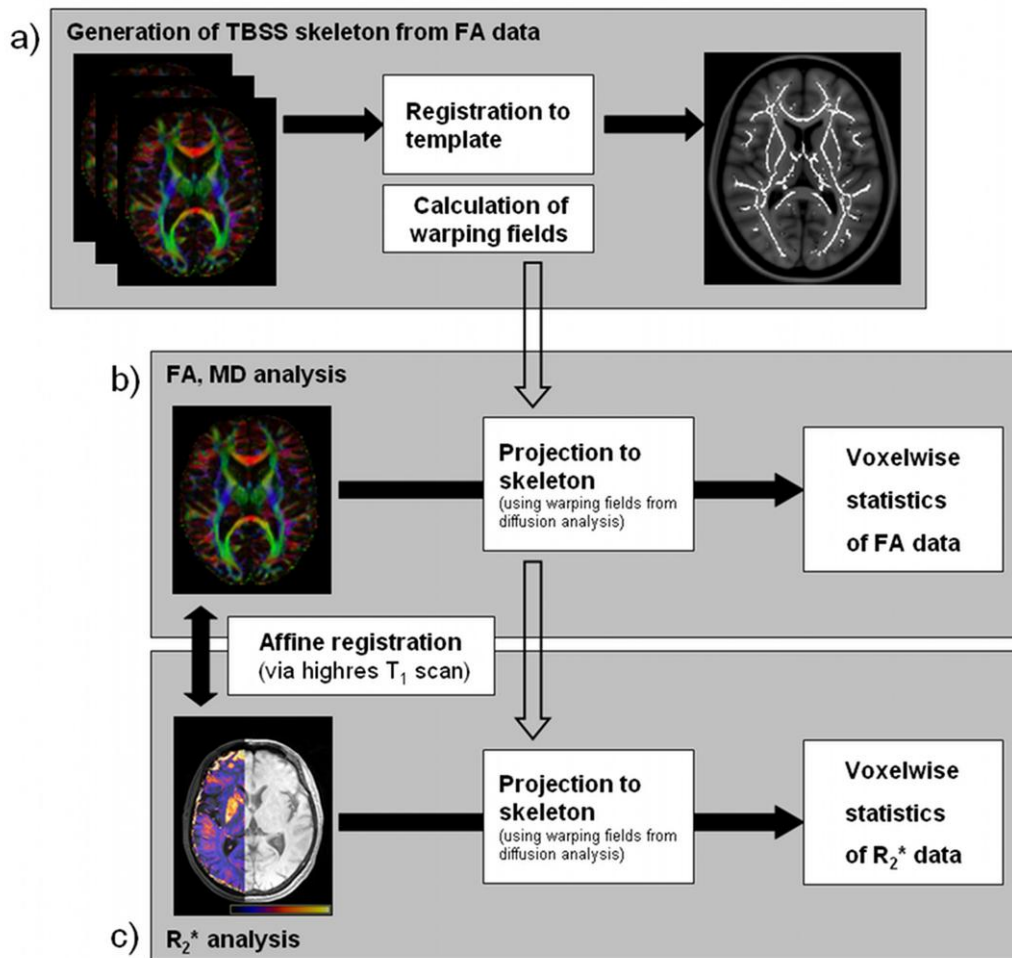
All DTI scans were pre-processed with FSL (Smith et al., 2004). The image processing steps included eddy current correction by affine registration to a reference scan without diffusion weighting, brain skull extraction and diffusion tensor calculation. Maps showing the fractional anisotropy (FA) and the mean diffusivity (MD) then were calculated from the tensor data. DTI data were registered affinely to the T1 weighted volume and the same regional masks that have been used in the R2\* analysis were used to mask and calculate FA and MD values for the deep grey matter structures.

### **Tract-based Analysis**

Tract-based spatial statistics (TBSS) (Smith, et al. 2006; Smith, et al. 2007) was employed to study diffusion characteristics along the major white matter tracts including the CST. The parameters utilized for TBSS analyses were: FA skeleton threshold 0.20, voxelwise permutation inference analysis with 5000 permutations and a cluster forming threshold of  $t = 3$  with a corrected cluster significance level of  $p < 0.05$  (2-tailed), including age, ALSFRS-R, disease subtype, estimated disease duration and disease progression rate as covariates.

To permit direct spatial comparison of DTI and  $R2^*$  data, the skeleton generated for the DTI analysis was also used for the voxelwise analysis of the  $R2^*$  maps. Therefore,  $R2^*$  maps were registered with the corresponding DTI data sets and transformed into DTI space by applying the same warping fields.  $R2^*$  maps were projected onto the skeleton using the same spatial coordinates as in the DTI TBSS analysis and then the same statistical analyses as with the DTI data were performed. Image processing is summarized schematically in Figure 1.

Figure 1



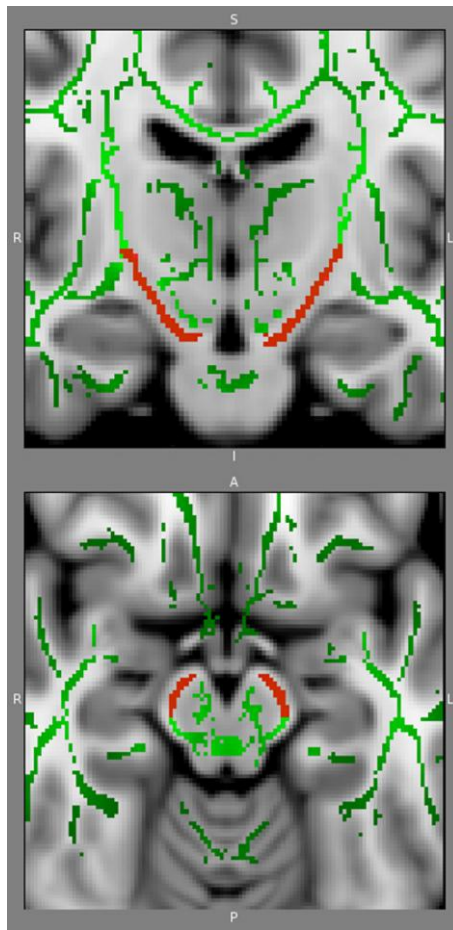
TBSS processing: FA images are registered non-rigid to a FA template and a white matter skeleton is generated. Using the calculated warping fields, FA and MD data is projected to the skeleton and voxelwise statistics are carried out. Using the same warping fields as for the diffusion analysis, R<sub>2</sub><sup>\*</sup> images are projected to the skeleton, which is allowing an investigation of R<sub>2</sub><sup>\*</sup> changes based on white matter information.

### Analysis of the Corticospinal Tract

A mask of the corticospinal tract (CST) was defined by two experienced observers (CE, FF) on the basis of the white matter skeleton generated by TBSS (Figure 2). Based on this, R<sub>2</sub><sup>\*</sup>, FA and mean diffusivity (MD) differences between ALS patients and controls were assessed along the CST.



Figure 2



Red areas show the white matter mask derived by TBSS that represents the mesencephalic part of the corticospinal tract used for subsequent analyses.

## Statistical Analysis

Statistical analyses were performed with STATISTICA 7.1 (StatSoft, Tulsa, Oklahoma, USA). Distribution of data was tested by the Kolmogorov-Smirnov test. Linear regression models and ANOVA were used to explore the impact of age, ALSFRS-R, disease subtype, estimated disease duration and disease progression rate on regional variations in iron deposition and diffusion characteristics. The significance level was set at  $P < 0.05$ .

## RESULTS

### Regional Changes in Deep Grey Matter

Assessing regional  $R2^*$  values across several structures of the brain (see Table 1) we found no evidence for possibly increased deposition of iron in ALS patients compared to controls

except for the caudate nucleus ( $R2^* = 29.29 \text{ s}^{-1}$  vs.  $26.61 \text{ s}^{-1}$ ,  $p = 0.029$ ). Overall, there was no significant correlation between age and  $R2^*$  values in the deep grey matter regions.

Analysis of regional FA showed a significant FA reduction in ALS patients compared to controls in the globus pallidus (FA = 0.478 vs. 0.406,  $p = 0.034$ ) and the putamen (FA = 0.275 vs. 0.241,  $p = 0.007$ ). In ALS patients, MD was also significantly increased in the putamen (MD =  $0.739 * 10^{-3} \text{ mm}^2 \text{ s}^{-1}$  vs.  $0.822 * 10^{-3} \text{ mm}^2 \text{ s}^{-1}$ ,  $p = 0.045$ ). There was no evidence for changes of FA or MD in the caudate nucleus.

Table 1

$R2^*$ , FA, and MD values for ALS patients and controls in deep grey matter regions (mean  $\pm$  standard deviation)

Structure		$R2^*$ (s-1)	FA	MD (* $10^{-3} \text{ mm}^2 \text{ s}^{-1}$ )
Nucleus accumbens	Controls	46.12 $\pm$ 7.83	0.27 $\pm$ 0.05	0.87 $\pm$ 0.18
	ALS	44.51 $\pm$ 7.82	0.25 $\pm$ 0.05	0.76 $\pm$ 0.17
Amygdala	Controls	35.87 $\pm$ 8.34	0.21 $\pm$ 0.03	0.95 $\pm$ 0.09
	ALS	32.71 $\pm$ 7.42	0.22 $\pm$ 0.03	0.92 $\pm$ 0.09
Caudate nucleus	Controls	*26.62 $\pm$ 2.29	0.15 $\pm$ 0.03	1.37 $\pm$ 0.29
	ALS	*29.29 $\pm$ 2.30	0.17 $\pm$ 0.03	1.23 $\pm$ 0.29
Hippocampus	Controls	24.89 $\pm$ 2.71	0.18 $\pm$ 0.04	1.12 $\pm$ 0.09
	ALS	24.73 $\pm$ 2.71	0.17 $\pm$ 0.04	1.19 $\pm$ 0.11
Globus pallidus	Controls	34.08 $\pm$ 1.83	*0.48 $\pm$ 0.07	0.72 $\pm$ 0.08
	ALS	34.31 $\pm$ 1.84	*0.41 $\pm$ 0.07	0.76 $\pm$ 0.08
Putamen	Controls	28.77 $\pm$ 2.99	*0.28 $\pm$ 0.03	*0.74 $\pm$ 0.05
	ALS	30.20 $\pm$ 2.99	*0.24 $\pm$ 0.03	*0.82 $\pm$ 0.08
Thalamus	Controls	21.01 $\pm$ 1.76	0.32 $\pm$ 0.02	0.93 $\pm$ 0.11
	ALS	21.13 $\pm$ 1.86	0.30 $\pm$ 0.02	0.94 $\pm$ 0.11

\* p-level < 0.05

Table 2

Analysis of  $R2^*$ , FA, and MD in the segmented corticospinal tract (CST) (mean  $\pm$  standard deviation)

	Controls	ALS Patients	p - level	Relative Difference, %
$R2^*$ (s-1)	26.28 $\pm$ 2.27	27.86 $\pm$ 2.33	0.080	6.01 %
FA	0.703 $\pm$ 0.032	0.687 $\pm$ 0.031	0.206	2.33 %
MD (* $10^{-3} \text{ mm}^2 \text{ s}^{-1}$ )	0.713 $\pm$ 0.061	0.685 $\pm$ 0.055	0.211	4.53 %

## **Changes in White Matter Tracts**

When performing a regional analysis along the entire CST no significant differences between ALS patients and controls regarding mean FA and MD were observed (Table 2). However, iron deposition ( $R2^*$ ) along the CST was elevated in patients and almost approached significance ( $p = 0.08$ ).

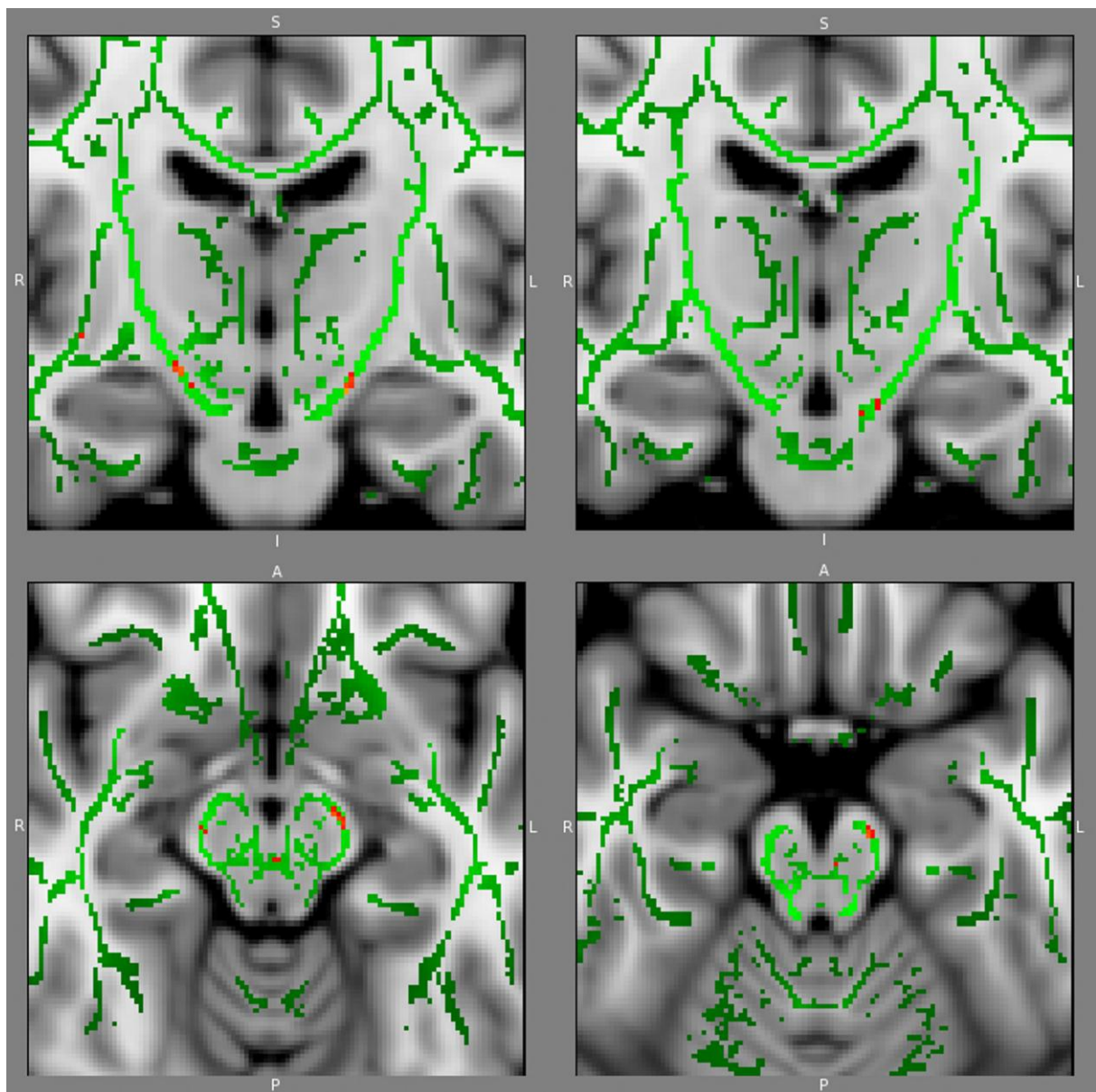
The TBSS analysis of the DTI data demonstrated significantly reduced FA values in the mesencephalic part of the CST in ALS patients compared to controls (Figure 3, left panel).

A similar TBSS analysis of the  $R2^*$  maps indicated that iron levels were significantly increased in adjacent regions of the CST in the ALS patients compared to the controls (Figure 3, right panel).

The TBSS analysis of  $R2^*$  data using the same permutation inference analysis with identical threshold parameters showed that these changes were more pronounced in the left than in the right hemisphere, suggesting some laterality of these effects.

Concerning other factors like disease duration, disease progression rate and disease severity (ALSFRS-R), no significant cluster differences for  $R2^*$  or water mobility in the major white matter tracts were found.

Figure 3



Tract based spatial statistics demonstrated significant FA reduction (left panel) and significantly increased R2\* (right panel) in ALS patients when compared to age and sex-matched controls (significant voxels at  $p < 0.05$  are shown in red). The regions with decreased FA and those with increased R2\* in the patients in the mesencephalic part of the CST are closely localized.

## DISCUSSION

This study simultaneously applied DTI and iron mapping in ALS patients, with the goal to assess disease related microstructural brain tissue changes in several deep grey matter structures and in the CST in comparison with a carefully age- and sex-matched control group. Whereas we were able to confirm previous studies demonstrating fiber tract degeneration via

FA decreases in the CST (Ciccarelli et al., 2009; Ellis et al., 1999; Toosy et al., 2003), we also extend these reports by providing evidence for increased iron accumulation parallel to the changes in diffusion characteristics. Altered homeostasis of metals and subsequent oxidative stress has been proposed as a potential element in the pathophysiology of ALS (Berg and Youdim, 2006), so our findings might bear some biological relevance.

We here decided to use R2\* relaxometry as a surrogate marker for iron deposition. Compared to other approaches, R2\* mapping is robust, provided appropriate shimming is done and scanning of the entire brain can be done in clinically feasible time. It also has a low specific absorption rate (SAR) profile which is an advantage at higher field strengths. There has been skepticism regarding the use of R2\* as a surrogate marker for brain iron deposition, but so far, a more sensitive method for the assessment of iron deposition has not been validated in a clinical setting.

Also, our results fit well into the ranges found by R2\* relaxometry in other studies (Haacke et al., 2005; Khalil et al., 2009; Peran et al., 2007). However, it should be noted that R2\* changes do not necessarily imply changes in iron content, but also could reflect microstructural tissue changes. This can be explained by the fact that R2\* is made up of the sum of two rates, where the rate R2' is attributed to local magnetic inhomogeneities caused by paramagnetic materials like iron and R2 is associated to intrinsic tissue properties (Haacke et al., 2005).

As within the CST of ALS patients the regions of significantly increased iron accumulation did not completely match the location of areas with significant diffusion changes this might suggest the presence of independent processes in the context of neurodegeneration. Alternatively, some regional variation may well have been introduced by imperfect co-registration and different voxel sizes of the DTI and R2\* scans consistent with the concept of two different expressions of the same pathophysiologic process. By interpreting the TBSS results it has to be considered that TBSS is doing a maximum FA search and projects nearby and higher FA values onto the skeleton. As the identical analysis was also applied to R2\* data, co-localization of the significant decreased FA pixels with the increased R2\* pixels might be implied by the different resolutions of R2\* and DTI data. In this context it could be speculated from our data that iron mapping might be more sensitive than DTI for detecting ALS related tissue changes. This comes from the observation that iron mapping suggested more diffuse and pronounced affection of the CST than revealed by TBSS and DTI in analyses based on the CST mask. It could be speculated from this that changes in iron

accumulation precede DTI changes at least to some extent. A higher sensitivity of R2\* than DTI measurements for depicting CST damage in ALS would be an alternative explanation.

When extending the analysis of R2\* values to other white matter tracts and deep grey matter structures we found no convincing evidence that iron deposition is a more diffuse and widespread process in ALS. Except for the caudate nucleus there were no significant differences in R2\* values between ALS patients and controls and this finding has to be viewed with caution given the multiplicity of comparisons. Otherwise, several deep grey matter structures appear to accumulate iron with increasing age independently of any degenerative process such as ALS. Different from R2\* measurements DTI characteristics were significantly changed in the globus pallidus and putamen, but not in the caudate nucleus. Whether these abnormalities occur secondary to CST damage or are indicative of a more diffuse component of the disease cannot be clarified from this or previous studies.

Several research groups reported correlations of DTI characteristics in the CST with clinical parameters such as disease duration and disease progression rate (Ellis et al., 1999; Wang et al., 2006). The fact that we like others could not confirm these findings (Hong, et al. 2004; Toosy, et al. 2003) is clearly disappointing from a clinical perspective. Interestingly, recent longitudinal studies also showed no impact of disease duration on DTI measurements, suggesting that information from diffusion derived analyses might be limited to early stages of the disease (Agosta, et al. 2009; Blain, et al. 2007). Otherwise the patient number and range of clinical abnormality of cohorts investigated may have been insufficient for establishing such associations in some studies including this one. Unfortunately, R2\* mapping did not improve upon clinicoradiologic correlations but this should be further investigated in a larger and more heterogenous group of patients.

In conclusion, this study extended previous findings on fiber disorganization by additional quantitative evidence for increased iron deposition in closely localized regions along the CST in ALS patients.

**STUDY 5:**  
**DETERMINANTS OF BRAIN IRON IN MULTIPLE SCLEROSIS:**  
**A QUANTITATIVE 3T MRI STUDY**

Michael Khalil<sup>1,5</sup>, Christian Langkammer<sup>1</sup>, Stefan Ropele<sup>1</sup>, Katja Petrovic<sup>1</sup>, Mirja Wallner-Blazek<sup>1</sup>, Marisa Loitfelder<sup>1,2</sup>, Margit Jehna<sup>1,2</sup>, Gerhard Bachmaier<sup>3</sup>, Reinhold Schmidt<sup>1</sup>, Christian Enzinger<sup>1,4</sup>, Siegrid Fuchs<sup>1</sup>, and Franz Fazekas<sup>1</sup>

(1) Department of Neurology, Medical University Graz, Austria

(2) Institute of Psychology, University of Graz, Austria

(3) Institute for Medical Informatics, Statistics and Documentation, Medical University Graz, Austria

(4) Division of Neuroradiology, Department of Radiology, Medical University Graz, Austria

(5) NUBIN, Department of Clinical Chemistry, VU University Medical Center Amsterdam, The Netherlands

*Neurology. 2011 Nov 1;77(18):1691-7*

## **ABSTRACT**

### **OBJECTIVES:**

Abnormal high cerebral iron deposition may be implicated in chronic neurological disorders, including multiple sclerosis (MS). R2\* relaxometry has been recently validated in a post-mortem study to indicate brain iron accumulation in a quantitative manner. We used this technique to assess brain iron levels in different stages of MS and healthy controls (HC) and determined their relation with demographic, clinical, neuropsychological and other imaging variables.

### **METHODS:**

We studied 113 consecutive patients [35 clinically isolated syndrome (CIS), 78 MS] and 35 HC with 3T MRI, clinical and neuropsychological examination. Iron deposition in subcortical gray matter structures was assessed by automated, regional calculation of R2\* rates.

### **RESULTS:**

Basal ganglia (BG) R2\* levels were significantly increased in MS compared to CIS ( $p < 0.001$ ) and HC ( $p < 0.005$ ). They were correlated with age ( $r = 0.5$ ,  $p < 0.001$ ), disease duration ( $r = 0.5$ ,  $p < 0.001$ ), the EDSS ( $r = 0.3$ ,  $p < 0.005$ ) and with the z-values of mental processing speed ( $r = -0.3$ ;  $p < 0.01$ ). Step-wise linear regression analysis revealed gray matter atrophy as the strongest independent predictor of BG R2\* levels ( $p < 0.001$ ), followed by age ( $p < 0.001$ ), and T2-lesion load ( $p < 0.005$ ).

### **CONCLUSION:**

BG iron accumulation in MS occurs with advancing disease and is related to the extent of morphologic brain damage, which argues for iron deposition as an epiphenomenon. The absence of increased iron levels in CIS patients indicates that iron accumulation does not precede the development of MS.



## **INTRODUCTION**

Brain iron is an essential cofactor for various physiological processes in neuronal metabolism, including myelination and mitochondrial energy generation (Kell, 2010). Excessive levels of iron, however, can also exert toxic effects by increased production of free radicals leading to oxidative stress (Campbell et al., 2001; Gutteridge, 1992). This may be important as several brain structures, in particular the basal ganglia, tend to accumulate non-haemin iron with normal ageing (Hallgren and Sourander, 1958). Furthermore increased brain iron levels have been noted in various chronic neurodegenerative disorders and it has been speculated that they play a role in their development (Stankiewicz, et al. 2007; Zecca, et al. 2004).

More than two decades ago, increased levels of cerebral iron have been reported in multiple sclerosis (MS) based on visual and therefore rather crude ratings of the intensity of signal reduction on T2-weighted images (Drayer et al., 1987; Grimaud et al., 1995). Subsequent technical developments based either on relaxation time mapping (Bakshi, et al. 2002; Burgetova, et al. 2010; Khalil, et al. 2009), phase imaging (Hammond et al., 2008) or on magnetic field correlation (Ge, et al. 2007), opened the possibility to assess brain iron in MS in a quantitative manner. Recently, R2\* relaxometry has been validated for the quantitation of brain iron (Langkammer et al., 2010).

Therefore, in extension to our previous work (Khalil et al., 2009), we quantitatively assessed regional brain iron levels using R2\* relaxometry in a larger series of MS patients and compared R2\* rates in defined cerebral structures between patients with different stages of the disease and age matched healthy controls. Besides a detailed neurologic examination investigated patients also underwent cognitive testing to allow for a more comprehensive assessment of the clinical impact of brain iron levels in MS.

## **MATERIALS AND METHODS**

### **Patients and Controls**

We enrolled 113 consecutive patients from our MS outpatient clinic to participate in this study. Patients were included if they had a diagnosis of a clinically isolated syndrome (CIS) suggestive of MS (n=35) (Miller et al., 2008) or of MS consisting of patients with relapsing remitting MS (RRMS) (N=70) or secondary progressive MS (SPMS) (N=8) (Polman et al., 2005). All patients underwent a detailed neurologic examination, neuropsychological testing and a comprehensive 3T MRI examination. Disability was measured using the Expanded

Disability Status Scale (EDSS) (Kurtzke, 1983). In MS patients we calculated the annualized relapse rate from the documented relapses as a measure of clinical disease activity. A relapse was defined as the appearance or reappearance of at least one neurological symptom or as the worsening of an old symptom attributed to MS that lasted for at least 24 h and was preceded by a relatively stable or improving neurological state of at least 30 days. Among the 113 patients, 51 received long-term disease modifying treatment (36 interferon-beta, 8 glatiramer-acetate, 4 intravenous immunoglobulins, 2 natalizumab and 1 mitoxantrone) (Table 1).

Thirty-five healthy volunteers (HC) served as controls for the regional brain iron distribution (Table 1). They were recruited amongst partners from MS patients or served as volunteers for ongoing fMRI projects and had to have normal clinical and MRI examinations.

Table 1

Clinical and demographic data

	CIS	MS	HC	p-value
N	35	78	35	NA
N female (%)	24 (68.6)	49 (62.8)	18 (51.4)	n.s. <sup>a</sup>
Age (y) *	33.7 (10.3)	37.3 (9.2)	36.7 (13.7)	n.s. <sup>b</sup>
Age at disease onset (y) *	32.9 (9.5)	27.2 (8.4)	NA	<0.005 <sup>b</sup>
Disease duration (y) **	0.2 (0.1-0.8)	8.0 (4.3-13.9)	NA	<0.001 <sup>c</sup>
Annualized relapse rate **	NA	0.5 (0.3-1.1)	NA	NA
EDSS (expanded disability status scale)	1.0 (0.0-2.0)	2.0 (1.0-3.5)	NA	<0.05 <sup>c</sup>
N (%) treated	5 (14.3)	46 (59.0)	NA	<0.001 <sup>a</sup>
N (%) with abnormal BRB-N				
Memory (immediate recall)	0 (0.0)	6 (7.7)	NA	n.s. <sup>a</sup>
Memory (delayed recall)	0 (0.0)	6 (7.7)	NA	n.s. <sup>a</sup>
Mental processing speed	5 (14.3)	12 (15.4)	NA	n.s. <sup>a</sup>
Executive functions	2 (5.7)	5 (6.4)	NA	n.s. <sup>a</sup>
Global cognitive index score	0 (0.0)	0 (0.0)	NA	n.s. <sup>a</sup>

N=number of patients/controls; y=years; BRB-N=Brief Repeatable Battery of Neuropsychological Tests; n.s.=not significant (p>0.05); NA=not applicable; values are given as frequency (percent), \*mean (SD) or as \*\*=median (interquartile range)

<sup>a</sup> Chi-square contingency Test, <sup>b</sup> 2-tailed T-Test, <sup>c</sup> Mann–Whitney U-Test

## **Standard protocol approvals, registrations, and patient consent.**

The study was approved by ethics committee of the Medical University of Graz. All participants gave written informed consent.

## **Neuropsychological testing**

Patients' neuropsychological assessment was based on the Brief Repeatable Battery of Neuropsychological Tests (BRB-N) as previously described (Khalil et al., 2011a). Briefly, the BRB-N consisted of the following subtests:

1. The Selective Reminding Test (SRT), which tests for verbal learning and memory, generating two measures of Immediate Recall (Long-Term Storage, Consistent Long Term Retrieval) plus a score for Delayed Recall (SRT-DR).
2. The 10/36-Spatial Recall Test (SPART), measuring visuospatial learning and delayed recall (SPART-DR).
3. The Symbol Digit Modalities Test (SDMT), measuring information processing speed, sustained attention, and concentration.
4. The Paced Auditory Serial Addition Test (3-second-version; PASAT3) which examines sustained attention and information-processing speed.
5. The Word List Generation (WLG) which measures semantic verbal fluency (WORD).

The BRB-N, translated and validated in German (Scherer, et al. 2004) was applied in a standardized, single test session by a trained clinical neuropsychologist in the following order: SRT, SPART, SDMT, PASAT3, SRT-DR, SPART-DR, WORD and lasted for approximately 30 minutes. To limit the number of comparisons we generated scores for the following domains by adding the z-values of respective subtests and adjustment for age, gender and education (Scherer et al., 2004): Memory (Immediate recall) (Consistent Long Term Retrieval, Long-Term Storage, SPART), memory (Delayed recall) (SRT-DR, SPART-DR), mental processing speed (PASAT, SDMT), and executive functions (WORD). Z-values below or equal -1.68 were considered as abnormal, which equates the performance of the lowest 5th percentile of healthy controls (Scherer et al., 2004).

## **Magnetic resonance imaging**

Patients and controls underwent quantitative MRI at 3 Tesla (Siemens Tim Trio, Siemens Healthcare, Erlangen, Germany) using a phased-array head coil with 12 receive elements and a consistent imaging protocol as described previously (Khalil et al., 2009). In brief, structural imaging included a FLAIR sequence (TR/TE/TI = 9000 ms/69 ms/2500 ms, in plane

resolution = 0.9x0.9 mm<sup>2</sup>, slice thickness = 3 mm, acquisition time = 4 minutes 22 seconds) and a T1-weighted 3D MPRAGE sequence with 1 mm isotropic resolution (TR/TE/TI/FA = 1900 ms/2.19 ms/900 ms/9°, acquisition time = 6 minutes 01 seconds). R2\* relaxation data were acquired with a spoiled 3D FLASH sequence with 12 equally spaced echoes (TR/TE1/FA = 68 ms/4.92 ms/20°; inter-echo spacing = 4.92 ms; in-plane resolution = 1x1 mm<sup>2</sup>; slice thickness = 4 mm, acquisition time = 4 minutes 51 seconds).

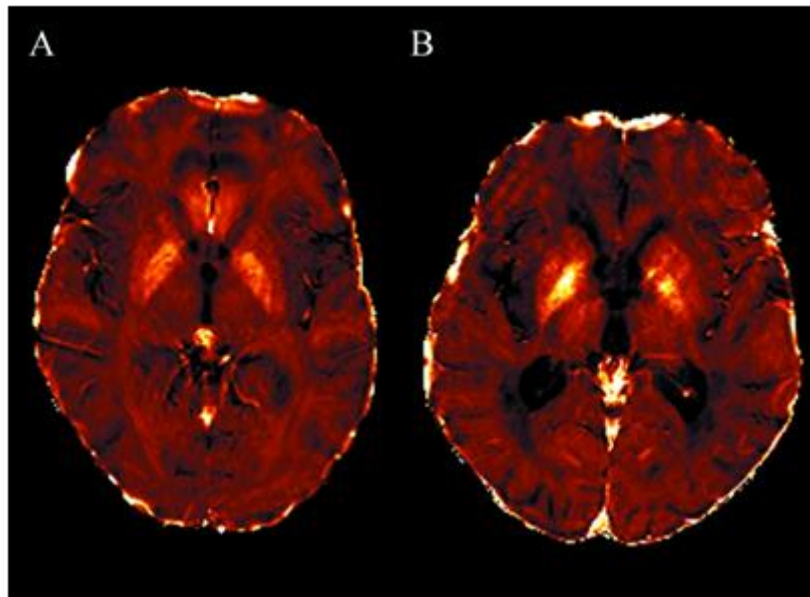
## **Image Analysis**

All image analyses were performed by trained and experienced technicians and MR readers, blinded to clinical information.

### **Regional R2\* mapping**

To eliminate image shifts caused by the bipolar data acquisition, all subsequent echoes provided by the FLASH sequence were registered to the first echo. Then, R2\* maps were calculated by monoexponential fitting using a least square approach and considering non-Gaussian distributed noise particularly impacting later echoes (He et al., 2008). On the basis of the high-resolution MPRAGE scan, bilateral deep gray matter structures (globus pallidus, putamen, caudate nucleus, thalamus and nucleus accumbens) were segmented automatically for all subjects using FIRST (Patenaude et al., 2011), which is a segmentation and registration algorithm based on deformable models from FSL (Smith et al., 2004). The resulting 3D models of these structures were eroded by one pixel to prevent partial volume effects and used to define above regions of interest in the R2\* maps. Subsequently, mean R2\* values and standard deviations were calculated for each structure (means from both hemispheres). Exemplary R2\* maps of two patients are presented in figures 1A and B.

Figure 1



R2\* maps of a 39 year old CIS patient (A) and a 42 year old MS patient (B). Both maps are scaled identically. Note increased mean R2\* rates in the globus pallidus: 33 s-1 vs. 44 s-1 and in the putamen 23 s-1 vs. 27 s-1, exemplarily reflecting increased iron deposition in MS.

### **Brain atrophy and T2 lesion load**

In patients, brain tissue volume and lesion load were measured as previously described (Enzinger et al., 2004; Khalil et al., 2011a; Khalil et al., 2009). In short, separate estimates of volumes of gray matter, white matter, cortical gray matter and ventricular CSF, normalized for subject head size, were estimated using SIENAX, which is part of FSL (Smith et al., 2004). For assessing T2 lesion load masks defining the lesions were created and the total lesion load was calculated by multiplying the area of all masks by the slice thickness.

### **Statistical analysis**

Statistical analyses were performed using SPSS 17.0 (SPSS Inc., Chicago, Illinois, USA). Statistical distribution of the data was tested by the Kolmogorov–Smirnov test. Groups were compared by Mann–Whitney U-Test or the 2-tailed t-Test, according to the statistical distribution of the data. Spearman and Pearson correlations served to calculate the correlation coefficients between imaging, clinical, and neuropsychological data. To reduce the number of correlations and given the fact that between group differences in R2\* relaxation rates emerged primarily for basal ganglia (BG) structures, we used the global BG region for these analyses. Thus, R2\* rates of the globus pallidus, putamen and caudate nuclei were averaged to obtain

whole BG R2\* values. Following univariate correlations we applied step-wise linear regression modeling to identify the factors independently predicting BG R2\* rates. In this model BG R2\* rates were added as the dependent variable. Variables showing the strongest correlation with BG R2\* rates in the Pearson or Spearman correlation analyses were then added as independent variables. Thus, this model was loaded with normalized gray matter volume, disease duration, age, T2-lesion load, EDSS and mental processing speed as independent variables. Other MRI variables did not enter this model due to multiple co-linearity, measured by the variation inflation factor.

## RESULTS

### Comparison of CIS, MS and controls

Clinical, demographic and neuropsychological data are presented in table 1. Median values (interquartile range) of automated measures of R2\* in the basal ganglia (BG), thalamus and nucleus accumbens are given in table 2. As can be seen significant between group differences emerged primarily for BG structures and also for the thalamus. Global BG R2\* rates were significantly higher in MS than in CIS and in controls. This difference was also apparent for each single BG structure in the globus pallidus, putamen and caudate nuclei (Table 2). In contrast, BG R2\* rates were even lower in CIS compared to HC. Compared to CIS, R2\* rates of MS patients were also significantly increased in the thalamus.

Table 2

Regional brain R2\* relaxation rates

	CIS	MS	HC	Significant differences
Basal ganglia	25.0 (23.7-26.7)	27.9 (25.8-29.4)	25.6 (24.6-28.5)	MS>CIS*** and HC**, CIS<HC* <sup>a</sup>
Putamen	22.6 (21.8-24.0)	25.3 (23.3-27.8)	23.7 (22.2-26.1)	MS>CIS*** and HC* <sup>a</sup>
Pallidum	31.7 (29.8-33.8)	35.3 (33.5-37.4)	33.0 (30.9-35.2)	MS>CIS*** and HC** <sup>a</sup>
Caudate	20.1 (19.1-21.4)	22.4 (20.7-24.0)	21.1 (20.0-22.9)	MS>CIS*** and HC*, CIS<HC* <sup>a</sup>
Thalamus	20.0 (19.6-20.7)	20.6 (19.9-21.3)	20.5 (19.9-21.0)	MS>CIS* <sup>b</sup>
Nucleus accumbens	31.7 (19.4-40.9)	28.3 (20.5-47.2)	36.5 (25.0-46.2)	n.s. <sup>b</sup>

R2\* rates [s<sup>-1</sup>] are given as median (interquartile range), n.s. = not significant (p>0.05), CIS = clinically isolated syndrome, MS = multiple sclerosis, HC=healthy controls, \*=p<0.05, \*\*=p<0.01, \*\*\*=p<0.001,

<sup>a</sup> 2-tailed T-Test, <sup>b</sup> Mann–Whitney U-Test

Table 3 shows the coexisting differences in T2 lesion load and compartmental volumes between investigated patient subgroups. As expected, T2 lesion load and signs of brain atrophy were more pronounced in MS compared to CIS patients (Table 3).

Table 3  
Morphological data

	CIS	MS	p-value
Brain volume	1655.3 (85.2)	1575.1 (95.2)	<0.001 <sup>a</sup>
Gray matter volume	897.0 (61.7)	839.8 (81.6)	<0.001 <sup>a</sup>
Cortex volume	725.8 (55.4)	676.1 (61.3)	<0.001 <sup>a</sup>
White matter volume	758.3 (58.8)	735.3 (54.1)	<0.05 <sup>a</sup>
Ventricular volume *	25.7 (18.9-31.2)	38.9 (25.9-50.3)	<0.001 <sup>b</sup>
T2 lesion load *	4.1 (1.8-11.5)	14.6 (4.5-25.2)	<0.005 <sup>b</sup>

Values [ccm] are given as mean (standard deviation) or as \*=median (interquartile range),

<sup>a</sup> 2-tailed T-Test, <sup>b</sup> Mann–Whitney U-Test

### **Univariate correlations of iron deposition with demographic, clinical and imaging variables**

Based on the finding of a significant increase of R2\* rates particularly in the basal ganglia of MS patients, we used primarily this variable for further analyses in relation to clinical, neuropsychological and conventional imaging parameters. As dysfunction in mental processing speed was most prevalent (Table 1) this variable was used to probe correlations between R2\* rates and neuropsychologic functioning.

For the entire cohort of patients with CIS or definite MS we found significant correlations of global BG R2\* rates with age ( $r=0.5$ ,  $p<0.001$ ; Pearson correlation), disease duration ( $r=0.5$ ,  $p<0.001$ ; Spearman correlation), the EDSS ( $r=0.3$ ,  $p<0.005$ ; Spearman correlation) and with z-values of mental processing speed ( $r=-0.3$ ;  $p<0.01$ ; Pearson correlation). Thalamic R2\* rates and z-values of mental processing speed showed no significant correlation. Focusing exclusively on patients with a diagnosis of MS, the correlation between BG R2\* rates and annualized relapse rate was also not significant.

Regarding imaging variables BG R2\* rates were correlated with T2 lesion load ( $r=0.4$ ,  $p<0.001$ ; Spearman correlation), normalized ventricular volume ( $r=0.5$ ,  $p<0.001$ ; Spearman correlation) and with volumes of whole brain, whole gray matter, and cortex ( $r=-0.5$ ,  $p<0.001$ ; Pearson correlation). There was no significant correlation between BG R2\* rates and white matter volume.

## Predictors of iron deposition in the basal ganglia

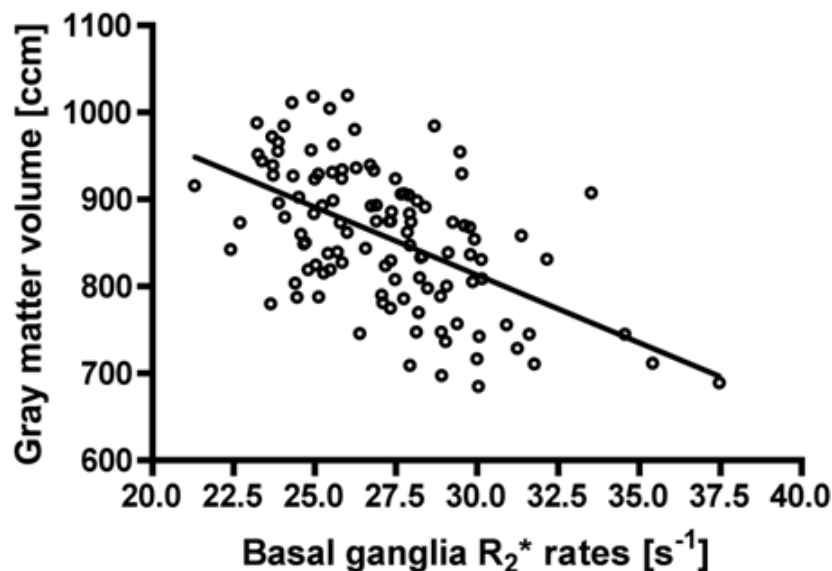
Using step-wise linear regression modeling on the entire patient cohort we identified gray matter atrophy ( $p < 0.001$ ) as the strongest independent predictor of BG  $R_2^*$  rates. This was followed by age ( $p < 0.001$ ) in the second step and by T2 lesion load ( $p < 0.005$ ) in the final step (Table 4). The model excluded the variables disease duration, EDSS and z-values of mental processing speed. The correlation of BG  $R_2^*$  rates with gray matter atrophy is shown in Figure 2.

Table 4

Stepwise linear regression model

Dependent variable	Step	Independent variables	Beta	p-value
Basal ganglia $R_2^*$ rates	1	Gray matter volume	-0.5	<0.001
	2	Gray matter volume	-0.4	<0.001
		Age	0.3	<0.001
	3	Gray matter volume	-0.2	<0.05
		Age	0.4	<0.001
		T2 lesion load	0.3	<0.005

Figure 2



Correlation of basal ganglia  $R_2^*$  relaxation rates with gray matter volume in multiple sclerosis. Reduced gray matter volumes are associated with higher basal ganglia iron levels measured by  $R_2^*$  relaxometry ( $r = -0.5$ ;  $p < 0.001$ ).



## DISCUSSION

Quantitative assessment of brain iron deposition by R2\* relaxometry in a large cohort of individuals with different stages of the disease confirmed markedly increased iron accumulation in the basal ganglia of patients with MS compared to healthy controls (Bakshi, et al. 2002; Bakshi, et al. 2000; Burgetova, et al. 2010; Ge, et al. 2007; Hammond, et al. 2008). In contrast, basal ganglia R2\* levels were even lower in our CIS subgroup than in controls. This clearly indicates that iron accumulation does not precede the development of MS but may occur as a byproduct of pathophysiologic processes of this disease.

So far, only few studies have investigated brain iron levels in CIS patients (Ceccarelli et al., 2010; Khalil et al., 2009). Similar to our results the only previous comparison of 47 CIS patients with 13 HC also found no differences in iron levels except for the left caudate nucleus in CIS patients with a more pronounced T2 hypointensity suggestive of greater iron accumulation (Ceccarelli, et al. 2010). In this study gray matter T2 hypointensity in CIS was not associated with an increased risk of developing clinically definite MS (Ceccarelli, et al. 2010). The finding of even lower R2\* rates in our CIS cohort than in controls may have been caused by a wider age range within the control group. In this context the high sensitivity and reliability of the R2\* technique for assessing gray matter iron concentrations should be noted as recently demonstrated in a post-mortem validation study (Langkammer et al., 2010). Although a variety of other MRI based techniques has been proposed for the assessment of brain iron concentration, the majority of these techniques has not been validated chemically so far. Additionally they usually require extensive post processing (e.g. of the gradient echo phase) which may affect the sensitivity for iron in an unpredictable manner (Ropele et al., 2011).

When investigating the association of basal ganglia R2\* rates as a measure of iron deposition with demographic and clinical variables several associations emerged. As expected, we found a correlation of BG R2\* rates with increasing age. The effect of age on non-haemin iron accumulation has been described already in 1958 and is especially pronounced in basal ganglia structures until the 4th decade of life (Hallgren and Sourander, 1958). Therefore it is essential to consider age as a covariate in analyses of brain iron levels and further to compare findings to age matched healthy controls. We also found BG R2\* rates to be correlated with disease duration. This is in line with other studies which have shown a positive association of this variable with measurements of increased brain iron content either based on high-resolution gradient-echo phase imaging (Hammond et al., 2008), susceptibility-weighted MRI

(Zivadinov, et al. 2010) or signal reduction on T2 weighted images (Bakshi et al., 2000). BG R2\* rates correlated with the EDSS. Increased brain iron deposition has been already linked to physical disability by others (Tjoa et al., 2005; Zhang et al., 2010; Zivadinov et al., 2010), although some studies could not confirm this correlation (Hammond et al., 2008). We found a significant correlation of BG R2\* rates with the z-values of mental processing speed but this correlation was not as close as previously reported (Brass et al., 2006). Such correlation has also been shown by a further study using magnetic field correlation but this finding was obtained in 17 patients only (Ge, et al. 2007). Importantly, we also did not find a correlation with mental processing speed in correlation to R2\* rates of the thalamus.

Regression analyses identified besides age only gray matter atrophy and T2 lesion load as independent predictors for BG R2\* rates. In this model, the EDSS, mental processing speed and disease duration did no longer have an independent impact on BG R2\* rates. The fact that disease duration did not independently predict BG R2\* rates is for several reasons not too surprising. Disease duration per se is not easy to define both because of the unknown period of asymptomatic disease evolution and the often oligosymptomatic first episode(s) of MS. Also disease duration does not contain information on disease severity while this compound information is well contained in morphologic markers of tissue destruction.

Earlier studies have also shown an association between increased brain iron load, reflected by T2 hypointensity, and signs of tissue destruction (Bakshi et al., 2001; Bermel et al., 2005). Although the exact mechanism is not yet clear these findings imply that increases in basal ganglia iron concentration are a consequence of MS related brain damage. The correlation of BG R2\* rates with gray matter atrophy could suggest that iron accumulates from dying neurons which traverse the basal ganglia. Axonal transection is a consistent feature of MS and related to the degree of inflammation (Trapp et al., 1998). The parallel correlation of BG R2\* rates with T2 lesion load, however, could also indicate that the basal ganglia constitute a sink for iron from macrophages in MS lesions. In MS brain tissue positive iron staining has been described in the surrounding of demyelinated plaques, myelinated white matter near lesions, within blood vessels of gray matter (Craelius et al., 1982) and in the putamen and thalamus (Drayer et al., 1987). Iron deposits have also been observed in macrophages and reactive microglia of MS brain sections (LeVine, 1997). Ferritin levels were elevated in lesions and normal appearing white matter of MS brain tissue (Petzold, et al. 2002) and proinflammatory cytokines as present in MS have been shown to increase the expression of hemoxygenase-1 and mitochondrial iron deposition (Mehindate, et al. 2001).

Altogether, our results indicate that increased brain iron levels are likely an epiphenomenon of MS pathology and not a cause of the disease. This does not preclude that once iron accumulates within the brain, subsequent oxidative stress induced tissue damage may enhance the extent of axonal damage and of neurodegeneration (Kell, 2010; Zecca et al., 2004). However, present findings do not support a strong role of such a mechanism. Nevertheless, it thus would be important to examine also more advanced stages of MS and to obtain longitudinal data. In this context investigated cohort had relatively low physical disability and therefore does not represent the full spectrum of the disease, which needs to be acknowledged as a limitation of this study.

**STUDY 6:**  
**QUANTITATIVE SUSCEPTIBILITY MAPPING**  
**IN MULTIPLE SCLEROSIS**

Christian Langkammer<sup>1\*</sup>, Tian Liu<sup>2\*</sup>, Michael Khalil<sup>1</sup>, Christian Enzinger<sup>1,3</sup>, Margit Jehna<sup>1</sup>,  
Siegfried Fuchs<sup>1</sup>, Franz Fazekas<sup>1</sup>, Yi Wang<sup>2</sup>, and Stefan Ropele<sup>1</sup>

(1) Department of Neurology, Medical University of Graz, Austria

(2) Department of Radiology, Cornell Medical College, New York City, NY, USA

(3) Department of Radiology, Medical University of Graz, Austria

\* Both authors contributed equally to this work

*Submitted*

## ABSTRACT

Quantitative susceptibility mapping (QSM) is a novel method that allows assessing magnetic susceptibility of tissues *in vivo*. We compared QSM and R2\* mapping findings in the basal ganglia (BG) of multiple sclerosis (MS) patients regarding their sensitivity to provide correlates of clinical and morphological measures of disease severity.

68 patients (26 with clinically isolated syndrome (CIS), 42 with relapsing-remitting MS) and 23 age-matched healthy controls (HC) underwent MRI at 3T. Susceptibility and R2\* maps were reconstructed from the same 3D multi-echo spoiled gradient echo sequence. Magnetic susceptibility and R2\* were measured in the BG and then related to clinical parameters and regional brain volumes.

The strongest predictor of magnetic susceptibility was age. Compared to HC, MS and CIS patients had increased (more paramagnetic) magnetic susceptibilities in the BG. R2\* mapping proved less sensitive than QSM regarding group differences. BG susceptibilities were higher with increasing neurologic deficits ( $r=0.32$ ,  $p<0.01$ ), and lower with normalized volumes of gray matter ( $r=-0.35$ ,  $p<0.001$ ) and cortex ( $r=-0.36$ ,  $p<0.001$ ).

QSM provided superior sensitivity of over R2\* mapping in the detection of clinically relevant tissue changes in the BG in MS, which are thought to reflect iron accumulation and demyelination. With QSM only, changes were already observed in CIS patients (also correlating with accrual of focal tissue damage) suggesting QSM can serve as a sensitive marker for important pathophysiological aspects of the disease already from its earliest stages.

## INTRODUCTION

Hypointensities in the basal ganglia of multiple sclerosis (MS) patients are a frequent finding on T2 weighted scans and have already been observed in the early days of clinical MRI scans (Bakshi et al., 2002; Drayer et al., 1987). While these T2 hypointensities can also be observed in normal aging subjects, they appear more pronounced in MS patients and are strongly associated with disease duration and severity (Neema et al., 2007). Histochemical analyses have identified increased iron levels as a source of microscopic field variations which in turn elicit T2 hyperintensities (Drayer et al., 1986).

With the availability of quantitative MRI techniques, assessment of iron levels became more accurate and sensitive compared to visual rating of the degree of hypointensities. Several MRI methods have been proposed to assess brain iron levels (Haacke et al., 2005; Ropele et al., 2011), but only few have been validated post-mortem so far. As such, a recent study validated both R2 and R2\* relaxation rates as linear measures for iron concentration in gray matter (GM) structures, with R2\* being more sensitive (Langkammer et al., 2010).

In fact, R2\* mapping in the BG of patients with clinically definite MS revealed significantly increased iron levels which were linked to disease duration and loss of cortical GM (Khalil et al., 2009). In contrast, there was no evidence for abnormal R2\* rates in the BG in patients with a clinically isolated syndrome (CIS) suggestive of MS, suggesting increased iron deposition to be a subsequent phenomenon in the evolution of MS. Consequently, R2\* relaxometry has been proposed as a potential marker secondary to inflammatory pathophysiological processes of the disease (Khalil et al., 2011b; Rovira and Montalban, 2011). However, depending on its distribution in brain tissue, iron not only causes microscopic field gradients, but also increases magnetic susceptibility of tissue, which can most accurately be assessed by quantitative susceptibility mapping (QSM). While the applicability of previous QSM methods in clinical cohorts was clearly hampered by e.g. the necessity of head tilting, recent developments now overcame these limitations, allowing determination of magnetic susceptibility from a single MRI scan (Bilgic et al., 2011; Li et al., 2011; Liu et al., 2011c; Liu et al., 2009; Schweser et al., 2011; Shmueli et al., 2009; Wharton and Bowtell, 2010; Wu et al., 2012b). This progress was achieved by solving the challenging inverse problem with regularized dipole inversion, and by the availability of sufficient computational power for image post processing.

In this context, it needs to be emphasized that the sources of the pathophysiological processes contributing to MRI measurable signal changes are complex. More specifically, the magnetic

bulk susceptibility of brain tissue is not only determined by the paramagnetic contribution of iron loaded ferritin, but also by the counteracting diamagnetic contribution of myelin, as it has only been noted most recently (He and Yablonskiy, 2009; Liu et al., 2011a).

We therefore here hypothesized QSM to be more sensitive to MS related tissue changes than R2\* mapping, as with this technique, the effect of iron accumulation and demyelination (both important pathophysiologic processes in MS) are additive (both cause a positive increase of the magnetic susceptibility), while in R2\* mapping, they exert opposing effects (demyelination reduces the R2\* rate while iron deposition increases R2\*).

Thus, this explorative study aimed at assessing changes of the magnetic susceptibility in the BG of MS and CIS patients and relating these findings to HC. First, we sought to compare the sensitivity of QSM and R2\* mapping for tissue changes in the BG. Second, we investigated how these changes in MRI measures related to clinical status, MS lesion load, and brain tissue loss which all are thought to vary between patients and with duration of the disease. Additionally, we also wanted to compare the sensitivity of QSM and R2\* mapping for tissue changes in the basal ganglia.

## MATERIALS AND METHODS

### Subjects

We prospectively enrolled 68 patients (mean age = 34.3 years, range from 19 to 59 years) from our MS outpatient clinic. Patients had a diagnosis of CIS suggestive of MS (n=26) or MS (n=42) (Polman et al., 2005) and underwent detailed neurological examination including the Expanded Disability Status Scale (EDSS) (Kurtzke, 1983).

Table 1  
Clinical and demographic data of the study cohort

	HC	CIS	MS	p-value
N	23	26	42	NA
N female (%)	12 (52.2)	19 (73.1)	28 (66.7)	n.s.
Age (years) *	32.7 (11.2)	35.4 (11.7)	34.6 (9.1)	n.s.
Disease duration (years) *	NA	0.77 (1.6)	7.3 (5.6)	<0.01 a
EDSS (expanded disability status scale)**	NA	1.2 (0 – 2)	1.0 (0 - 2)	n.s.

HC = healthy controls; N=number of patients/controls; n.s.= not significant (p>0.05); NA=not applicable; values are given as frequency (percent); \*mean ( $\pm$  standard deviation) or as \*\*=median (interquartile range); a Mann–Whitney U-Test.

Additionally, we recruited age matched healthy controls (HC, n=23) without known neuropsychiatric disorder. All participants underwent MRI of the brain at 3 Tesla (TimTrio, Siemens Healthcare, Erlangen, Germany) using a head coil array with 12 receiver channels using identical protocols. Characteristics of study participants are summarized in Table 1.

The local ethics committee approved this study and all subjects gave written informed consent.

## **MRI**

MRI gradient echo images for QSM reconstruction and calculation of R2\* rates were acquired with the identical spoiled 3D FLASH sequence, with 12 equally spaced echoes (TR/TE1/FA = 68 ms/4.92 ms/20°, inter-echo spacing = 4.92 ms, in-plane resolution = 1x1 mm<sup>2</sup>, slice thickness = 4 mm, number of slices = 32, acquisition time = 4 minutes 51 seconds).

The MRI protocol also included a FLAIR sequence (TR/TE/TI = 9000 ms/69 ms/2500 ms, in plane resolution = 0.9x0.9 mm<sup>2</sup>, slice thickness = 3 mm, acquisition time = 4 minutes 22 seconds) for assessment of MS lesions. A T1-weighted 3D MPRAGE sequence with 1 mm isotropic resolution was used (TR/TE/TI/FA = 1900 ms/2.19 ms/900 ms/9°, acquisition time = 6 minutes 1 second) for brain tissue segmentation.

## **Image processing and analysis**

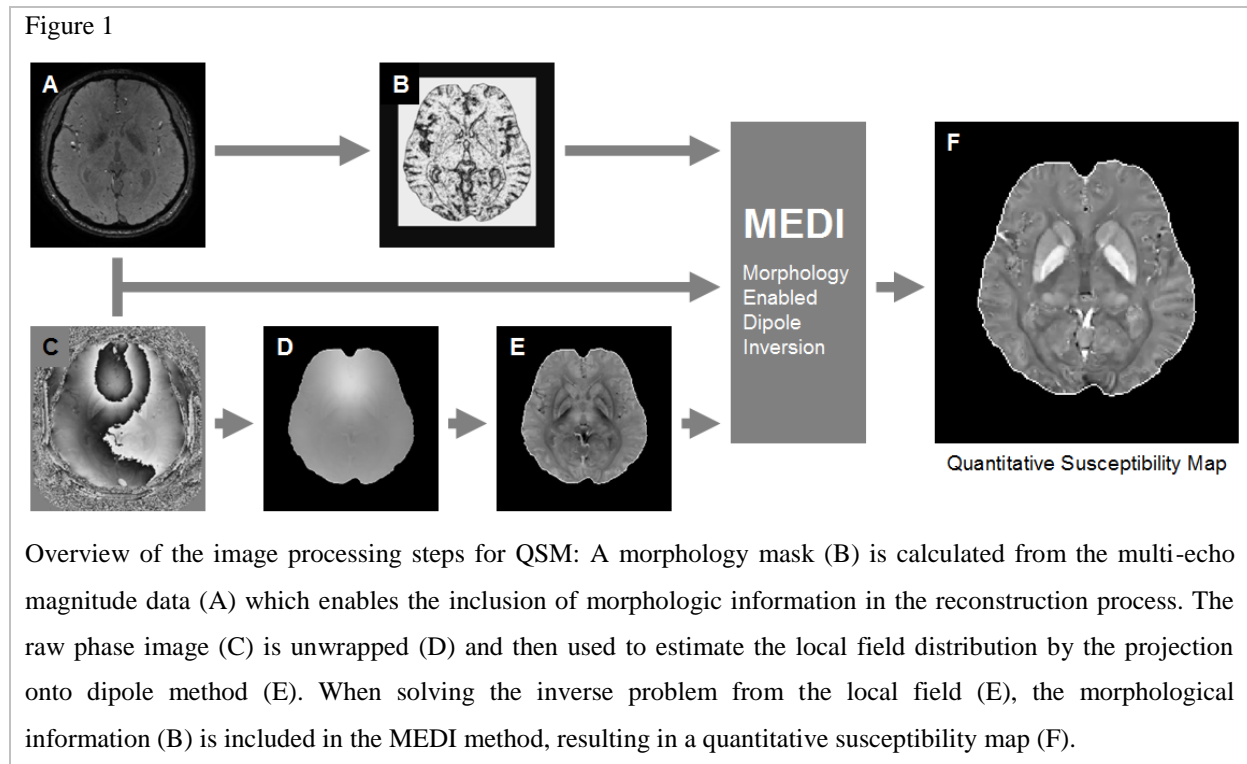
Trained and experienced technicians and MR readers blinded to clinical information performed all image analyses.

For R2\* mapping, all magnitude images of the gradient echo sequence were registered to the first echo to correct for image shifts induced by the bipolar readout gradient. Subsequently, R2\* was calculated pixel wise by fitting a mono-exponential decay function into the multi-echo data and by applying a truncation model to consider non-Gaussian noise at later echoes (He et al., 2008).

QSM images were reconstructed according to an algorithm described elsewhere in detail (Liu et al., 2012; Liu et al., 2011c). In short, QSM images were generated using a Morphology Enabled Dipole Inversion (MEDI) method, which inverts an estimated local magnetic field to generate a susceptibility distribution that is structurally consistent with an anatomical prior obtained in the same scan. The local magnetic field was calculated from a field map derived from MRI phase images, followed by a Projection onto Dipole Fields (PDF) method removing the background field induced by susceptibility sources outside the brain



parenchyma. Exemplarily, the process of QSM from raw gradient echo images (magnitude, wrapped phase), the generation of the morphology mask as well as the resulting reconstructed QSM images are shown in Figure 1.



On the basis of the high-resolution MPRAGE scan, bilateral deep GM structures (caudate nucleus, globus pallidus, and putamen) forming the BG were segmented automatically for all subjects using FIRST (Patenaude et al., 2011), a segmentation and registration algorithm based on deformable models, as part of FSL (Smith et al., 2004). The resulting 3D models of these structures were eroded by one pixel to reduce partial volume effects and then used to mask all regions of interest in the QSM images and R2\* maps. Subsequently, the mean magnetic susceptibility and standard deviations were calculated for each structure bilaterally. Additionally, a global measure for the BG was calculated by averaging either susceptibilities or R2\* rates of the caudate nucleus, the globus pallidus, and the putamen.

Normalized brain volume and regional volumes of white matter, and cortical and overall gray matter were measured using SIENAX, as part of FSL (Smith et al., 2004).

In patients, T2 lesion load was assessed on FLAIR scans by segmenting the lesions semi-automatically with a region-growing algorithm developed in-house. The total lesion load was then calculated by multiplying the area of all lesion masks with the slice thickness.

## **STATISTICAL METHODS**

All analyses were performed using STATISTICA 7.1 (StatSoft, Tulsa, USA). A p-value of  $p < 0.05$  was considered as statistically significant. Differences in clinical parameters, lesion and brain volumes,  $R2^*$ , and magnetic susceptibility between subgroups were tested by a 2-tailed t-test or Mann–Whitney U-test where appropriate. Normal distribution was tested with the Kolmogorov–Smirnov test. Group tests were carried out individually for the caudate, globus pallidus and the putamen, and also for the global BG.

Pearson and Spearman correlation analyses served to investigate the relation of clinical and demographic data (EDSS, disease duration, and age), T2 lesion load and brain volumes on BG susceptibility and  $R2^*$ . All tests were separately performed for CIS and MS, as well as for the entire patient group.

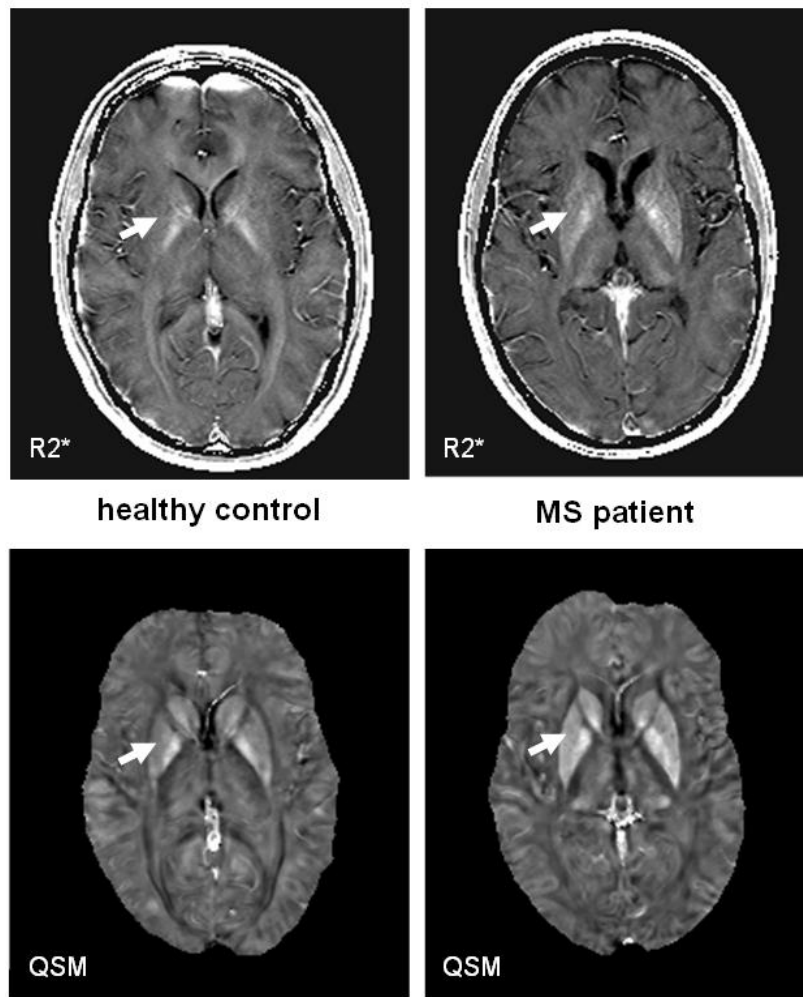
Stepwise forward multiple linear regression analysis served to identify independent predictors of magnetic tissue susceptibility and  $R2^*$  relaxation rate. Only the global BG susceptibility and global BG  $R2^*$  rate, were used as dependent variables for the multivariate analyses.

## **RESULTS**

### **Patient characteristics and morphology**

Characteristics of study participants are given in Table 1. Most notable, the mean age and EDSS did not vary significantly between the CIS and MS subgroup. For controls, age-matching was performed as brain iron is accumulating in the process of normal aging (Hallgren and Sourander, 1958). Morphological characteristics for patients and controls are given in Table 2. T2 lesion load was higher in MS compared to CIS patients. The normalized volumes of gray matter, cortex, white matter, and the entire brain were lower in MS patients compared to HC. MS patients also had significantly lower white matter volumes than CIS patients.

Figure 2



Representative R2\* rate (upper row) and quantitative susceptibility maps (lower row) of two 29-years individuals (left: healthy control, right: MS patient). Note increased (more paramagnetic) susceptibility in the basal ganglia in the MS patient. Differences are most evident in the putamen (arrow: 0.049 ppm vs. 0.092 ppm; images windowed identically: R2\* from 0 (black) to 40 s-1 (white) and QSM from -0.1 (black) to 0.25 ppm (white)).

### Group differences as assessed by QSM and R2\* mapping

Maps of magnetic susceptibility and R2\* were successfully obtained from all subjects. Figure 2 provides representative QSM and R2\* maps, where the MS patient demonstrates a higher (more paramagnetic) susceptibility in the basal ganglia (BG) than the age-matched HC.

Mean susceptibility values and R2\* rates in the caudate nucleus, globus pallidus, putamen and for the global BG are summarized in Table 3. A higher susceptibility (more paramagnetic) was found in all basal structures in the patients, when compared to HC. Magnetic susceptibilities were higher in the caudate nucleus and the putamen of CIS patients compared

to HC (Figure 3). No differences between CIS and MS patients were found regarding susceptibility.

Mean R2\* relaxation rates were increased in the caudate nucleus ( $p < 0.05$ ) and the putamen ( $p < 0.05$ ) of MS patients compared to HC. With respect to R2\* rates, no differences between CIS patients and HC nor CIS and MS patients were found.

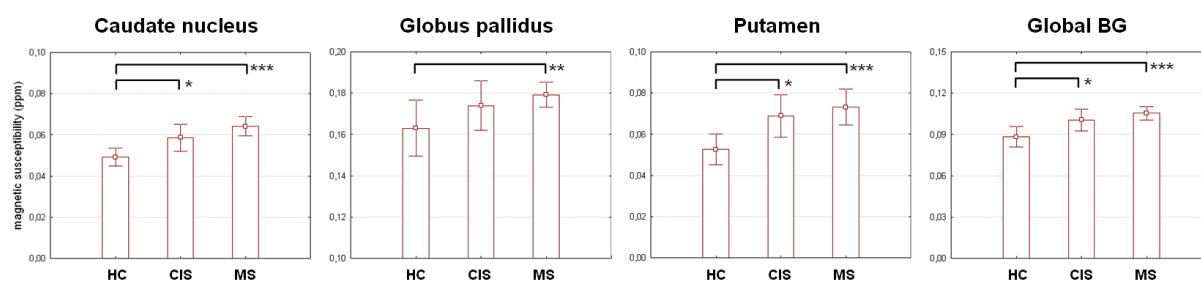
Table 2  
Morphological data

	HC	CIS	MS	p-value
Brain volume	1591.8 (77.1)	1547.9 (98.1)	1507.7 (96.1)	MS<HC ** b
Gray matter volume	811.8 (49.2)	787.5 (67.6)	771.7 (50.6)	MS<HC ** b
Cortical volume	665.7 (45.9)	650.2 (56.0)	631.1 (46.2)	MS<HC ** b
White matter volume	780.0 (35.8)	760.4 (42.1)	735.9 (51.6)	MS<CIS* a and MS<HC *** b
Ventricular volume	34.5 (13.2)	36.6 (16.7)	42.8 (19.9)	n.s.
T2 lesion load	NA	4.35 (5.3)	12.4 (13.0)	CIS<MS** b

Volumes [ml] are given as mean ( $\pm$ standard deviation) and have been normalized to the standard brain volume. a 2-tailed T-Test, b Mann–Whitney U-Test, n.s. = not significant ( $p > 0.05$ ); Significant differences are indicated by stars \*= $p < 0.05$ , \*\*= $p < 0.01$ , \*\*\*= $p < 0.001$ .

Figure 3

Box plots showing mean regional magnetic susceptibilities in components of the basal ganglia (BG) and their average in clinically isolated syndrome (CIS) and MS patients (MS) and healthy controls (HC).



Significant differences indicated by bars \*= $p < 0.05$ , \*\*= $p < 0.01$ , \*\*\*= $p < 0.001$ .

Table 3

Regional magnetic susceptibility and R2\* values

QSM	HC	CIS	MS	Significant differences
Caudate	0.049 (0.010)	0.059 (0.016)	0.064 (0.015)	MS>HC*** b and CIS>HC* a
Pallidum	0.163 (0.031)	0.174 (0.030)	0.179 (0.019)	MS>HC** b
Putamen	0.053 (0.017)	0.069 (0.025)	0.073 (0.028)	MS>HC** b and CIS>HC* a
Basal ganglia	0.088 (0.017)	0.101 (0.020)	0.106 (0.016)	MS>HC*** b and CIS>HC* b

R2*	HC	CIS	MS	Significant differences
Caudate	21.1 (1.7)	21.5 (2.7)	22.4 (2.7)	MS>HC* a
Pallidum	37.4 (4.1)	37.1 (3.9)	38.3 (2.8)	n.s.
Putamen	24.2 (2.3)	25.3 (3.4)	26.2 (4.0)	MS>HC* a
Basal ganglia	27.6 (2.4)	27.9 (2.9)	28.9 (2.5)	MS>HC* a

Magnetic tissue susceptibility – QSM [ppm] and R2\* rates [s<sup>-1</sup>] are given as mean (± standard deviation); n.s. = not significant (p>0.05); CIS = clinically isolated syndrome; MS = multiple sclerosis; HC=healthy controls; \*=p<0.05, \*\*=p<0.01, \*\*\*=p<0.001; a 2-tailed T-Test; b Mann–Whitney U-Test.

### Univariate correlations of BG magnetic susceptibility with demographic, clinical, and morphologic parameters

Table 4 shows results of univariate regression analyses in CIS, MS and both groups combined. The strongest correlation for global BG susceptibility was found for age (r=0.49, p<0.001, Pearson correlation). EDSS and BG susceptibility were also correlated (r=0.32, p<0.01, Spearman correlation) and this association was driven by the group of MS patients (Table 4). T2 lesion load correlated with BG susceptibilities only in CIS (r=0.48, p<0.05, Spearman correlation), but not in MS patients.

GM and whole brain volumes negatively correlated with BG susceptibility in the entire patient group. Analyzing patient groups separately, the significance of these correlations got lost in CIS while MS patients showed a correlation only between BG susceptibility and GM volume (r=-0.32, p=0.05, Pearson correlation), and a borderline correlation with cortical volume (r=-0.30, p=0.06, Pearson correlation).

Table 4

Uni-variate correlations of basal ganglia magnetic susceptibility and R2\* values with EDSS, T2 lesion load, age, and global and regional brain volumes for all patients and for CIS and MS patients separately

	Age	EDSS	T2 lesion load	Gray matter volume	Cortical volume	White matter volume	Whole brain volume
<b>QSM</b>							
CIS	0.43* a	n.s.	0.48* b	.n.s.	n.s.	n.s.	n.s.
MS	0.57*** a	0.35* b	n.s.	-0.32* a	n.s.	n.s.	n.s.
CIS+MS	0.49*** a	0.32* b	n.s.	-0.36** a	-0.35** a	n.s.	-0.28* a
<b>R2*</b>							
CIS	0.57** a	n.s.	n.s.	-0.53* a	-0.55** a	n.s.	-0.48* a
MS	0.49** a	n.s.	n.s.	n.s.	n.s.	n.s.	n.s.
CIS+MS	0.51*** a	n.s.	n.s.	-0.41*** a	-0.42*** a	n.s.	-0.36** a

Values denote correlation coefficient as obtained by a Pearson or b Spearman, respectively.

QSM = magnetic tissue susceptibility, EDSS = expanded disability status scale,

\*=p<0.05, \*\*=p<0.01, \*\*\*=p<0.001, n.s. = not significant (p>0.05).

### Univariate correlations of the BG R2\* rate with demographic, clinical, and morphologic parameters

The strongest association for global BG R2\* rate was found for age (r=0.51, p<0.001, Pearson correlation), and also in parallel to the observations with QSM, regional and global brain volumes negatively correlated with BG R2\* rates. However, BG R2\* did not show any association with EDSS, disease duration or T2 lesion load. Considering all patients, correlations were found for cortical GM and global brain volumes (see Table 4).

### Determinants of BG magnetic susceptibility and R2\* rate

All variables showing significant univariate correlations were considered in stepwise multiple regression models including CIS and MS patients. Considering R2\*, only age (beta=0.50, p<0.001) independently predicted changes in the BG. The magnetic susceptibility in the BG was independently predicted by age (beta=0.48, p<0.001) and T2 lesion load (beta=0.23, p<0.05).

## DISCUSSION

We here applied QSM, a novel technique for determination of the magnetic susceptibility of tissue, to assess tissue changes in CIS and MS patients. Unlike other susceptibility related MR parameters, e.g.  $R2^*$  and gradient echo phase, QSM directly reveals to which extent tissue is magnetized when it is exposed to a magnetic field. It therefore provides a true quantitative parameter with direct reflection of an intrinsic tissue property. As main finding, QSM demonstrated higher sensitivity in the assessment of MS-related tissue changes in the basal ganglia over  $R2^*$  relaxation rate mapping.

MS patients had increased (i.e., more paramagnetic) susceptibilities compared to HC which confirmed elevated iron levels in the basal ganglia. This observation was also made with other techniques including relaxometry, phase imaging and susceptibility weighted imaging (Bakshi et al., 2002; Burgetova et al., 2010; Ceccarelli et al., 2009; Khalil et al., 2011b; Lebel et al., 2011; Zivadinov et al., 2012).

Iron accumulation in CIS patients has been scarcely investigated so far. In a comparable previous study of our own (Khalil et al., 2011b), no differences in the BG between HC and CIS patients were observed using  $R2^*$  mapping. While this appears to contradict present findings at first glance it has to be highlighted, that also in the current study no differences between HC and CIS patients were observed using  $R2^*$  mapping (Table 3). Such differences were only found by using the putative more sensitive QSM approach and might be partly ascribed to demyelination (please refer to the discussion below). Supporting evidence for an involvement of the BG in CIS patients comes from the observation of T2 hypointensities, as in the left caudate nucleus, by others which were viewed as an indicator for progression to clinically definite MS (Ceccarelli et al., 2010). CIS patients were also noted to show BG atrophy (Audoin et al., 2010). However, our results reveal a widespread involvement of the BG, with significant changes in the caudate nucleus and the putamen. Clearly, the relevance of these findings needs to be shown in future longitudinal studies and covering a broader spectrum of the disease, but they strongly indicate a high sensitivity of QSM to capture early changes of MS.

Compared to  $R2^*$  relaxation rate mapping, QSM was more sensitive for discriminating CIS patients from HC. Notably, QSM allowed to identify the presence of tissue changes in the BG as early as in CIS patients when compared to HC via correlations with EDSS and T2 lesion load that were not seen with  $R2^*$  mapping. While these findings favor QSM as a more sensitive measure for such disease related susceptibility changes in MS, their origin is not

fully clear. Considering that  $R2^*$  and QSM were derived from the same data set, a possible explanation is the additive effect of demyelination. The proteins composing myelin have an overall diamagnetic susceptibility (in relation to water) and thus, are counteracting the paramagnetic contribution of iron. A reduction of the myelin content therefore has the same effect on susceptibility as an increased iron content (Langkammer et al., 2012). Recent histological work using proteolipid protein staining in tissue of 14 confirmed MS patients (mean age = 56.6 years, mean disease duration = 23.7 years) showed that overall 28.8% of the GM (including deep GM) compared to 15.6% of the WM was demyelinated, highlighting that the extent of GM damage in MS may be underestimated (Gilmore et al., 2009). Furthermore it is well known that subcortical nuclei are involved already at the earliest stages of the disease – in part probably via damage to traversing myelinated fiber tracts – and may contribute to subsequent disease evolution (Cifelli et al., 2002; Fernando et al., 2005; Miller et al., 2003). Given these observations, it seems plausible that demyelination in the BG contributed to the higher sensitivity of QSM. In contrast, both iron accumulation and demyelination exert a counteracting effect on  $R2^*$  which reduces the sensitivity of  $R2^*$  mapping to capture MS related tissue changes, and which may also explain why  $R2^*$  mapping did not reveal significant changes in the CIS cohort in this and previous work.

Another interesting finding is the observation that BG susceptibility is correlated with T2 lesion load in CIS but not MS patients. This might imply that tissue changes in the basal ganglia at earlier stages are more directly coupled to the extent of visible white matter damage than in more advanced MS. In this context it seems plausible, that demyelination increases the BG susceptibility in this early stage of MS in a more direct manner than later on, where excessive secondary iron deposition becomes the overwhelming effect and is obviously dominating the magnetic susceptibility independent of lesion load. However, given the limited number of patients included in our study, this will have to be elaborated further in bigger and more heterogeneous cohorts.

Although clinically not severely affected, brain atrophy was noted in MS patients and most pronounced in cortex and GM. GM volume of CIS patients lay between HC and MS patients, further supporting the notion that CIS patients may already show involvement of GM pathology (Calabrese et al., 2011). Interestingly, BG susceptibility negatively correlated with cortical and GM, but not with white matter volumes. This is in line with a similar observation using  $R2^*$  mapping that suggested tissue changes in the BG to mainly scale with disease progression (Khalil et al., 2011b). Whether possible neurodegenerative mechanisms triggered or promoted by the toxic effects of reactive oxygen in the BG also account for some loss of



GM volume remains unclear. There is some evidence that mitochondrial dysfunction or the accumulation of iron-related degradation products from neuronal loss in the BG may amplify neuronal damage (Nunez et al., 2012). Assessing the magnetic susceptibility also in cortical structures will help to clarify whether this mechanism is focally limited to deep gray matter nuclei or whether this occurs more globally in GM.

In the present study, atrophy did not maintain significant contribution in multiple regression models for  $R2^*$  in the BG, which might be explained by sample size, short disease duration and low disability levels. However, as  $R2^*$  and magnetic susceptibility were derived from the data acquired by the same gradient echo sequence, this underlines the higher sensitivity of QSM to assess disease related tissue changes.

## **CONCLUSION**

We here showed that QSM has superior sensitivity in the assessment of MS-related tissue changes in the basal ganglia over  $R2^*$  relaxation rate mapping. We interpret this increased susceptibility as primarily indicative of higher iron content, but demyelination might also play a role. Using QSM, susceptibility changes in the basal ganglia were observed already in CIS patients. Future longitudinal studies are mandatory to assess the prognostic value of QSM on the evolution of MS.

## SUMMARY AND OUTLOOK

### SUMMARY

This thesis covered the measurement of iron concentrations in the human brain by the use of MRI. After implementation on a clinical MR scanner, several quantitative MRI techniques including relaxation rate mapping, phase imaging, and quantitative susceptibility mapping, were first validated in postmortem measurements and then applied in a clinical setting. In this context, results from postmortem MRI and inductively coupled plasma mass spectroscopic form the essential basis of this thesis, as they provide insights into the association between MR contrast generation and the underlying biophysical properties.

In summary of the biophysical aspects, the following conclusions can be drawn from this work:

- Brain iron concentration in gray matter structures can be measured reliably using transverse MR relaxation rates and magnetic susceptibility.
- MR phase and QSM contrast between cortical gray and white matter can be mainly attributed to variations in myelin content, but not to iron concentration.
- The bulk susceptibility of white matter is diamagnetic while gray matter is paramagnetic (in respect to water).
- Gray-white matter contrast of T2\* weighted gradient echo sequences is based on the absolute effect of microscopic field variations, therefore it only reflects the extent but not the direction of susceptibility shifts.
- In white matter, the contributions of myelin and iron act additively on relaxation rates while they have a counteracting effect on MR phase and magnetic susceptibility.
- Given the previous observations, iron concentration in white matter cannot be assessed reliably using MR relaxation rate mapping, phase imaging or susceptibility mapping without correcting for the contribution of myelin.
- Thus, characterization of the diamagnetic contribution of myelin and the effect neuronal fiber orientation are essential for the assessment of iron in white matter.

Additionally to the underlying biophysical aspects, iron mapping was applied to assess disease related tissue changes in multiple sclerosis and amyotrophic lateral sclerosis and these findings can be summarized as follows:

### **Multiple sclerosis:**

- Iron concentrations in the basal ganglia, as assessed by R2\* mapping, were higher in MS patients than in age-matched healthy controls.
- Basal ganglia iron levels are correlated with disease duration, cognitive decline, atrophy, T2 lesion load and the Expanded Disability Status Scale (EDSS).
- Quantitative susceptibility mapping (QSM) confirmed the findings from R2\* mapping. However, QSM was even more sensitive for variations in the basal ganglia of MS patients than R2\* mapping.
- Using QSM, susceptibility changes in the basal ganglia were observed already at an early stage (clinically isolated syndrome) of the disease. We interpret this increased susceptibility as primarily indicative of higher iron content, but also as an additive contribution of demyelination in gray matter.
- R2\* relaxation rates were found to be lower in multiple sclerosis lesions than in white matter of normal controls (ISMRM 2011, abstract number 608). According to our model this can be either ascribed to changes in myelin content (demyelination or incomplete remyelination), to lower iron levels or to a combination of both.

### **Amyotrophic lateral sclerosis**

- R2\* relaxation rates of patients with amyotrophic lateral sclerosis were increased in the corticospinal tract. Interestingly, this region was closely localized to tissue with reduced fiber integrity, as assessed by diffusion tensor imaging. This indicates that neurodegenerative processes might be linked to abnormal iron metabolism.

## OUTLOOK

### **Iron mapping in white matter**

The magnetic susceptibility of iron is counteracted by the diamagnetic constituents of myelin. While the contribution of myelin is small in gray matter, in white matter structures this is affecting MRI measurements substantially. However, as many neurological diseases are considered mainly as white matter diseases, e.g. multiple sclerosis or amyotrophic lateral sclerosis, there is a need to reliably assess iron concentration also in white matter. Till now, it remains an open challenge to separate the susceptibility induced contributions of iron and myelin adequately. Several techniques for the quantification of the myelin content have been proposed including magnetization transfer imaging, mapping of the myelin water fraction, and mapping of the bound pool fraction. However, these techniques are not clinically applicable and still need validation. Therefore, the bulk susceptibility of the myelin compartment remains unknown and, thus, can hardly be corrected for the determination of white matter iron concentrations.

Additionally, it has been shown that the white matter fiber orientation plays a substantial role in contrast generation (Denk et al., 2011; He and Yablonskiy, 2009) and bulk susceptibility. Further work will also have to focus on the complementary contribution of the orientation of underlying white matter fibers with respect to the main magnetic field additionally to the separation of the contributions of iron and myelin.

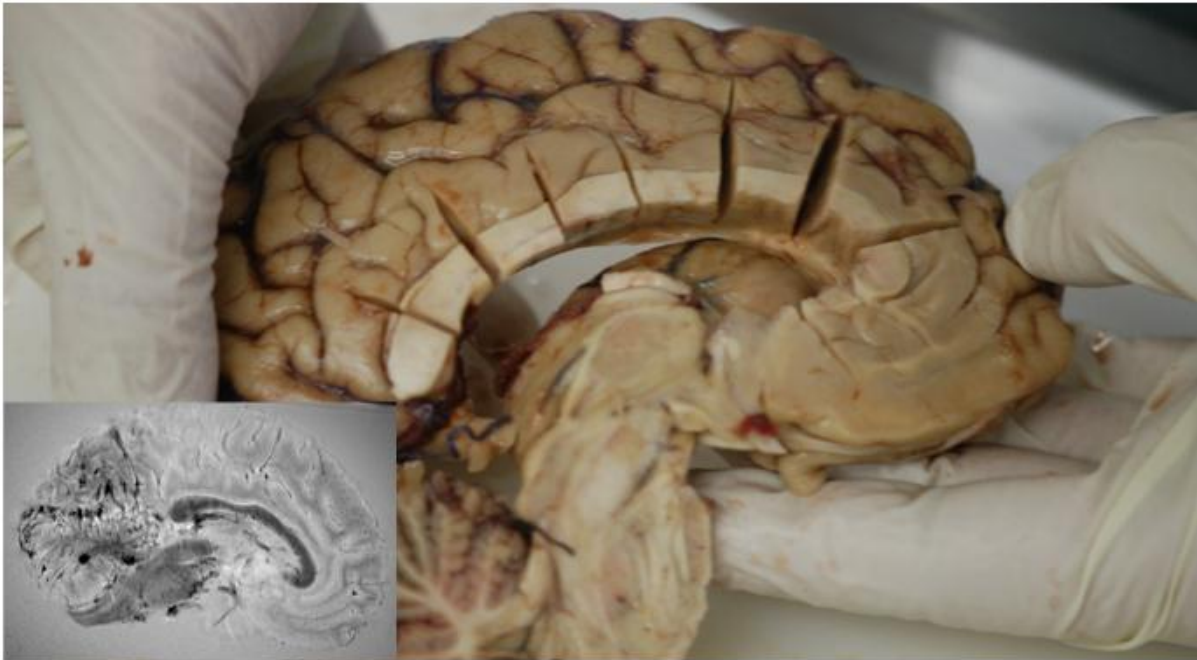
Disentangling the contribution of iron, myelin and fiber orientation to relaxation rates or susceptibility is not feasible when considering that only the iron concentration can be determined. To circumvent this problem, two approaches seem interesting in this context.

First, the brain can be rotated in the scanner with respect to the main magnetic field which has been entitled as “susceptibility tensor imaging”. Given that at least 6 independently orientated scans have been acquired, the anisotropy of the susceptibility can be described as a tensor (Li et al., 2012; Liu, 2010). The postmortem setup presented in this work offers the possibility to differently orientate formalin-fixed postmortem brains in the scanner. This will help to disentangle orientational effects in future work.

An alternative approach to account for the effect of fiber orientation is to select an anatomical structure where all fibers are aligned in a well defined way with respect to the magnetic field. The corpus callosum is ideally suited for this purpose as the fiber bundles connecting both hemispheres are virtually orientated orthogonal to the magnetic field. Moreover, the corpus

callosum is highly myelinated and exhibits a substantial variation in myelin density. Combining chemically determined iron concentrations and histology of sub regions might enlighten the knowledge about individual contributors to MRI contrast generation and subsequently to separate the additional contribution of fiber orientation (Figure 1).

Figure 1



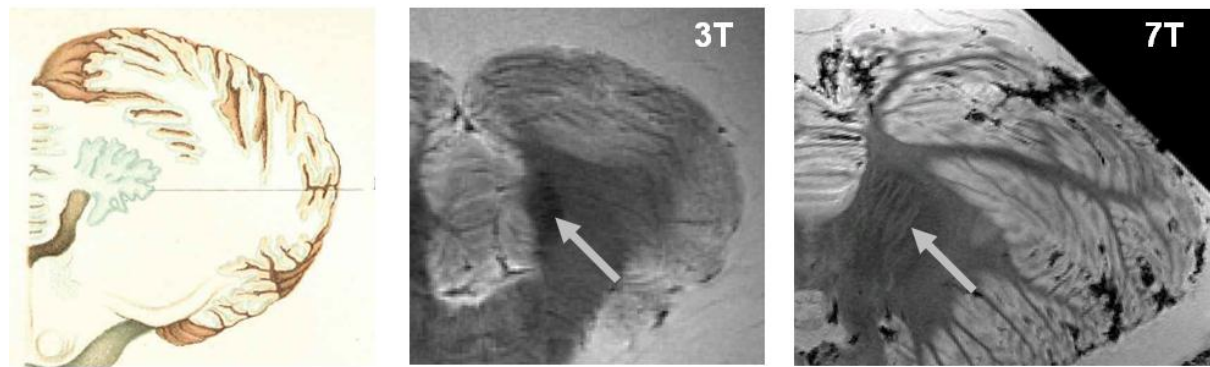
Dissection of the corpus callosum: Tissue specimens for the mass spectroscopic measurements are taken from a coronal brain slice. These iron concentrations combined with histological staining will serve to explain the generation of MR contrast as imaged before dissection (small inset).

### **Ultrahigh magnetic field MRI**

The advent of ultrahigh field MRI systems (7 Tesla and above) is especially beneficial for susceptibility effects as these scale with field strength and thus are more pronounced. Additionally, a the inherently better signal-to-noise ratio and a higher resolution offer a more detailed delineation of small folded structures as shown in Figure 4 and consequently a better regional assignment of brain iron..

Additionally, as efforts to reduce SAR levels include the increased usage of gradient echo sequences, susceptibility weighted contrast will be more a more prominent finding than at lower field strengths.

Figure 2



Cerebellar distribution of non-heme bound iron in the human brain visualized by Perls' staining (left). Non-hem bound iron is colored in blue and the brain was sliced in axial orientation. Left figure is taken from (Spatz 1922). The meandered form of the nucleus dentate becomes visible on high resolution 7 Tesla postmortem MRI (right), while structural details are not assessable on 3T (middle).

### **Longitudinal iron mapping in amyotrophic lateral sclerosis**

Abnormal iron levels were found in the corticospinal tract of patients with amyotrophic lateral sclerosis (ALS). These changes in iron concentration were closely localized to changes indicating reduced neuronal fiber integrity as investigated by diffusion tensor imaging. This is an interesting finding because the process of neurodegeneration has been linked with increased iron concentrations and it has been shown histologically in several diseases including Parkinson's and Alzheimer's that regional iron levels are increased when compared to normal controls. However, while this is an additional evidence for the important role of iron in neurodegenerative processes, it remains unclear whether iron accumulation is primary, or secondary.

Follow-up of ALS patients at an early stage of the disease will allow better determining the role of ironing in ALS and whether possible neurodegenerative mechanisms are triggered or promoted by the toxic effects of reactive oxygen.

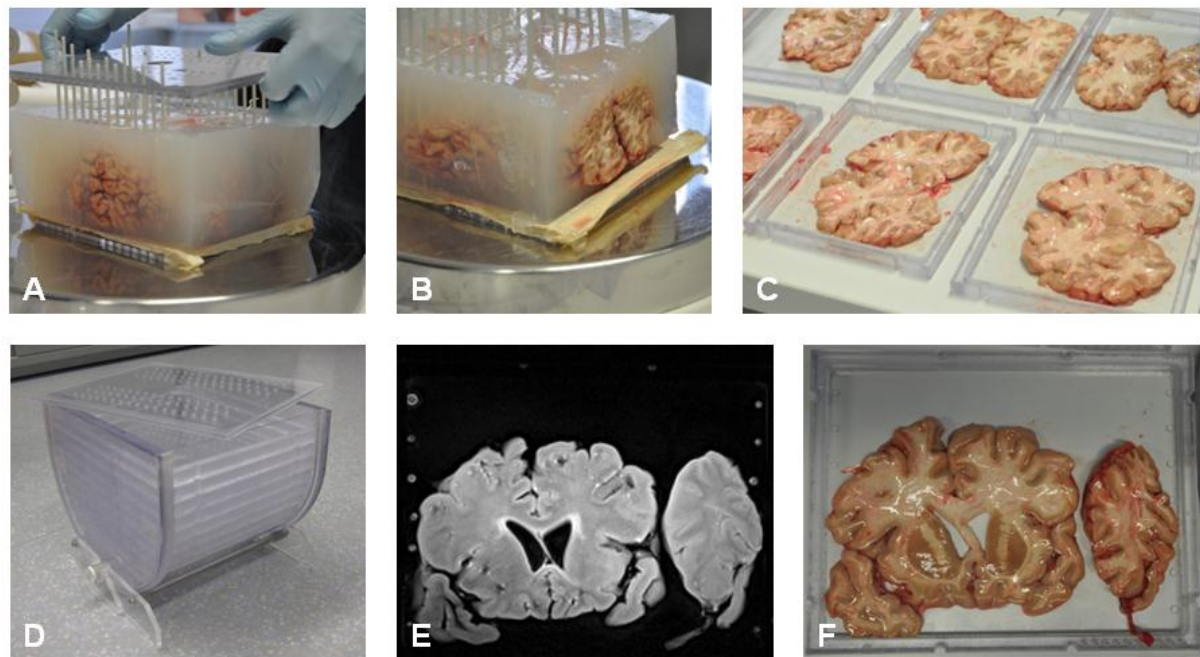
### **Fresh postmortem study**

The postmortem setup presented in this work served to investigate the contribution of iron to MR contrast generation as well as the validity of MR based measures for the assessment of iron concentrations in the brain. The corpses included in these studies were cooled and, depending on the postmortem interval, the body temperature at the start of the MRI varied between 4 and 24 °C.

Little is known about the temperature dependency of quantitative MR parameters and whether different brain structures exhibit different temperature coefficients. The bulk susceptibilities in the postmortem study included in this work have been corrected for effects of temperature by using the body temperature. However, while T1 can be corrected according to literature, the transverse relaxation rates have not been corrected because the influence of temperature remains largely unclear and is debated conversely in literature.

In an in-situ setting, the brain temperature cannot be determined, neither by MRI nor by the forensic pathologist. This would become possible after extraction of the brain but formalin fixation introduces water shifts and changes of the relaxation properties. Thus, the temperature dependence could be investigated only in the absence of brain fixation.

Figure 3



Workflow of the fresh postmortem study: The entire brain is embedded in agarose gel to maintain the structure and stiffness (A). Ceramic brads are arranged in 1cm spacing to enable precise cutting into 1 cm thick slices (B). Several plastic trays holding the brain slices (C) are positioned inside a plastic container which is filled with a buffer solution (D). The MRI (E) then is used as a reference to guide sample extraction for further histological and chemical analysis (F).

A study design using fresh, non formalin-fixed brains allows circumventing these problems (Figure 3). Brains extracted directly after death (<6 hours) will be included in this study and the temperature can be adjusted by changing the temperature of the surrounding buffer

solution. Additionally, when fixating the brains afterwards, this setup will allow studying the effect of formalin fixation on quantitative MRI parameters.



## REFERENCES

- Abrahams, S., Leigh, P.N., Goldstein, L.H., 2005. Cognitive change in ALS: a prospective study. *Neurology* 64, 1222-1226.
- Altamura, S., Muckenthaler, M.U., 2009. Iron toxicity in diseases of aging: Alzheimer's disease, Parkinson's disease and atherosclerosis. *J Alzheimers Dis* 16, 879-895.
- Andrews, N.C., 1999. Disorders of iron metabolism. *N Engl J Med* 341, 1986-1995.
- Audoin, B., Zaaraoui, W., Reuter, F., Rico, A., Malikova, I., Confort-Gouny, S., Cozzone, P.J., Pelletier, J., Ranjeva, J.P., 2010. Atrophy mainly affects the limbic system and the deep grey matter at the first stage of multiple sclerosis. *J Neurol Neurosurg Psychiatry* 81, 690-695.
- Axel, L., 1984. Relaxation times and NMR signals. *Magn Reson Imaging* 2, 121-130.
- Bakshi, R., Benedict, R.H., Bermel, R.A., Caruthers, S.D., Puli, S.R., Tjoa, C.W., Fabiano, A.J., Jacobs, L., 2002. T2 hypointensity in the deep gray matter of patients with multiple sclerosis: a quantitative magnetic resonance imaging study. *Arch Neurol* 59, 62-68.
- Bakshi, R., Dmochowski, J., Shaikh, Z.A., Jacobs, L., 2001. Gray matter T2 hypointensity is related to plaques and atrophy in the brains of multiple sclerosis patients. *J Neurol Sci* 185, 19-26.
- Bakshi, R., Shaikh, Z.A., Janardhan, V., 2000. MRI T2 shortening ('black T2') in multiple sclerosis: frequency, location, and clinical correlation. *Neuroreport* 11, 15-21.
- Bartzokis, G., Aravagiri, M., Oldendorf, W.H., Mintz, J., Marder, S.R., 1993. Field dependent transverse relaxation rate increase may be a specific measure of tissue iron stores. *Magn Reson Med* 29, 459-464.
- Behrens, T.E., Woolrich, M.W., Jenkinson, M., Johansen-Berg, H., Nunes, R.G., Clare, S., Matthews, P.M., Brady, J.M., Smith, S.M., 2003. Characterization and propagation of uncertainty in diffusion-weighted MR imaging. *Magn Reson Med* 50, 1077-1088.
- Berg, D., Youdim, M.B., 2006. Role of iron in neurodegenerative disorders. *Top Magn Reson Imaging* 17, 5-17.
- Bermel, R.A., Puli, S.R., Rudick, R.A., Weinstock-Guttman, B., Fisher, E., Munschauer, F.E., 3rd, Bakshi, R., 2005. Prediction of longitudinal brain atrophy in multiple sclerosis by gray matter magnetic resonance imaging T2 hypointensity. *Arch Neurol* 62, 1371-1376.

- Bieri, O., Scheffler, K., 2009. SSFP signal with finite RF pulses. *Magn Reson Med* 62, 1232-1241.
- Bilgic, B., Pfefferbaum, A., Rohlfing, T., Sullivan, E.V., Adalsteinsson, E., 2011. MRI estimates of brain iron concentration in normal aging using quantitative susceptibility mapping. *Neuroimage*.
- Bloch, F., 1946. Nuclear Induction. *Physical Review* 70, 460-474.
- Bluml, S., Schad, L.R., Stepanow, B., Lorenz, W.J., 1993. Spin-lattice relaxation time measurement by means of a TurboFLASH technique. *Magn Reson Med* 30, 289-295.
- Bothwell, T.H., 1995. Overview and mechanisms of iron regulation. *Nutr Rev* 53, 237-245.
- Bottomley, P.A., Foster, T.H., Argersinger, R.E., Pfeifer, L.M., 1984. A review of normal tissue hydrogen NMR relaxation times and relaxation mechanisms from 1-100 MHz: dependence on tissue type, NMR frequency, temperature, species, excision, and age. *Med Phys* 11, 425-448.
- Brass, S.D., Benedict, R.H., Weinstock-Guttman, B., Munschauer, F., Bakshi, R., 2006. Cognitive impairment is associated with subcortical magnetic resonance imaging grey matter T2 hypointensity in multiple sclerosis. *Mult Scler* 12, 437-444.
- Brooks, B.R., 1994. El Escorial World Federation of Neurology criteria for the diagnosis of amyotrophic lateral sclerosis. Subcommittee on Motor Neuron Diseases/Amyotrophic Lateral Sclerosis of the World Federation of Neurology Research Group on Neuromuscular Diseases and the El Escorial "Clinical limits of amyotrophic lateral sclerosis" workshop contributors. *J Neurol Sci* 124 Suppl, 96-107.
- Brooks, B.R., Miller, R.G., Swash, M., Munsat, T.L., 2000. El Escorial revisited: revised criteria for the diagnosis of amyotrophic lateral sclerosis. *Amyotroph Lateral Scler Other Motor Neuron Disord* 1, 293-299.
- Burgetova, A., Seidl, Z., Krasensky, J., Horakova, D., Vaneckova, M., 2010. Multiple sclerosis and the accumulation of iron in the Basal Ganglia: quantitative assessment of brain iron using MRI T2 relaxometry. *Eur Neurol* 63, 136-143.
- Calabrese, M., Rinaldi, F., Mattisi, I., Bernardi, V., Favaretto, A., Perini, P., Gallo, P., 2011. The predictive value of gray matter atrophy in clinically isolated syndromes. *Neurology* 77, 257-263.
- Campbell, A., Smith, M.A., Sayre, L.M., Bondy, S.C., Perry, G., 2001. Mechanisms by which metals promote events connected to neurodegenerative diseases. *Brain Res Bull* 55, 125-132.

- Carri, M.T., Ferri, A., Cozzolino, M., Calabrese, L., Rotilio, G., 2003. Neurodegeneration in amyotrophic lateral sclerosis: the role of oxidative stress and altered homeostasis of metals. *Brain Res Bull* 61, 365-374.
- Ceccarelli, A., Filippi, M., Neema, M., Arora, A., Valsasina, P., Rocca, M.A., Healy, B.C., Bakshi, R., 2009. T2 hypointensity in the deep gray matter of patients with benign multiple sclerosis. *Mult Scler* 15, 678-686.
- Ceccarelli, A., Rocca, M.A., Neema, M., Martinelli, V., Arora, A., Tauhid, S., Ghezzi, A., Comi, G., Bakshi, R., Filippi, M., 2010. Deep gray matter T2 hypointensity is present in patients with clinically isolated syndromes suggestive of multiple sclerosis. *Mult Scler* 16, 39-44.
- Cheng, Y.C., Neelavalli, J., Haacke, E.M., 2009. Limitations of calculating field distributions and magnetic susceptibilities in MRI using a Fourier based method. *Phys Med Biol* 54, 1169-1189.
- Ciccarelli, O., Behrens, T.E., Altmann, D.R., Orrell, R.W., Howard, R.S., Johansen-Berg, H., Miller, D.H., Matthews, P.M., Thompson, A.J., 2006. Probabilistic diffusion tractography: a potential tool to assess the rate of disease progression in amyotrophic lateral sclerosis. *Brain* 129, 1859-1871.
- Ciccarelli, O., Behrens, T.E., Johansen-Berg, H., Talbot, K., Orrell, R.W., Howard, R.S., Nunes, R.G., Miller, D.H., Matthews, P.M., Thompson, A.J., Smith, S.M., 2009. Investigation of white matter pathology in ALS and PLS using tract-based spatial statistics. *Hum Brain Mapp* 30, 615-624.
- Cifelli, A., Arridge, M., Jezzard, P., Esiri, M.M., Palace, J., Matthews, P.M., 2002. Thalamic neurodegeneration in multiple sclerosis. *Ann Neurol* 52, 650-653.
- Connor, J.R., Menzies, S.L., 1996. Relationship of iron to oligodendrocytes and myelination. *Glia* 17, 83-93.
- Craelius, W., Migdal, M.W., Luessenhop, C.P., Sugar, A., Mihalakis, I., 1982. Iron deposits surrounding multiple sclerosis plaques. *Arch Pathol Lab Med* 106, 397-399.
- Cusack, R., Papadakis, N., 2002. New robust 3-D phase unwrapping algorithms: application to magnetic field mapping and undistorting echoplanar images. *Neuroimage* 16, 754-764.
- Dahnke, H., Schaeffter, T., 2005. Limits of detection of SPIO at 3.0 T using T2 relaxometry. *Magn Reson Med* 53, 1202-1206.

- Dawe, R.J., Bennett, D.A., Schneider, J.A., Vasireddi, S.K., Arfanakis, K., 2009. Postmortem MRI of human brain hemispheres: T2 relaxation times during formaldehyde fixation. *Magn Reson Med* 61, 810-818.
- de Rochefort, L., Brown, R., Prince, M.R., Wang, Y., 2008. Quantitative MR susceptibility mapping using piece-wise constant regularized inversion of the magnetic field. *Magn Reson Med* 60, 1003-1009.
- de Rochefort, L., Liu, T., Kressler, B., Liu, J., Spincemaille, P., Lebon, V., Wu, J., Wang, Y., 2009. Quantitative susceptibility map reconstruction from MR phase data using bayesian regularization: validation and application to brain imaging. *Magn Reson Med* 63, 194-206.
- Deistung, A., Rauscher, A., Sedlacik, J., Stadler, J., Witoszynskyj, S., Reichenbach, J.R., 2008. Susceptibility weighted imaging at ultra high magnetic field strengths: theoretical considerations and experimental results. *Magn Reson Med* 60, 1155-1168.
- Denk, C., Torres, E.H., Mackay, A., Rauscher, A., 2011. The influence of white matter fibre orientation on MR signal phase and decay. *NMR Biomed*.
- Deoni, S.C., 2007. High-resolution T1 mapping of the brain at 3T with driven equilibrium single pulse observation of T1 with high-speed incorporation of RF field inhomogeneities (DESPOT1-HIFI). *J Magn Reson Imaging* 26, 1106-1111.
- Deoni, S.C., Peters, T.M., Rutt, B.K., 2005. High-resolution T1 and T2 mapping of the brain in a clinically acceptable time with DESPOT1 and DESPOT2. *Magn Reson Med* 53, 237-241.
- Deoni, S.C., Rutt, B.K., Peters, T.M., 2003. Rapid combined T1 and T2 mapping using gradient recalled acquisition in the steady state. *Magn Reson Med* 49, 515-526.
- Dexter, D.T., Carayon, A., Javoy-Agid, F., Agid, Y., Wells, F.R., Daniel, S.E., Lees, A.J., Jenner, P., Marsden, C.D., 1991. Alterations in the levels of iron, ferritin and other trace metals in Parkinson's disease and other neurodegenerative diseases affecting the basal ganglia. *Brain* 114 ( Pt 4), 1953-1975.
- Drayer, B., Burger, P., Darwin, R., Riederer, S., Herfkens, R., Johnson, G.A., 1986. MRI of brain iron. *AJR Am J Roentgenol* 147, 103-110.
- Drayer, B., Burger, P., Hurwitz, B., Dawson, D., Cain, J., 1987. Reduced signal intensity on MR images of thalamus and putamen in multiple sclerosis: increased iron content? *AJR Am J Roentgenol* 149, 357-363.

- Duyn, J.H., van Gelderen, P., Li, T.Q., de Zwart, J.A., Koretsky, A.P., Fukunaga, M., 2007. High-field MRI of brain cortical substructure based on signal phase. *Proc Natl Acad Sci U S A* 104, 11796-11801.
- Ellis, C.M., Simmons, A., Jones, D.K., Bland, J., Dawson, J.M., Horsfield, M.A., Williams, S.C., Leigh, P.N., 1999. Diffusion tensor MRI assesses corticospinal tract damage in ALS. *Neurology* 53, 1051-1058.
- Enzinger, C., Ropele, S., Smith, S., Strasser-Fuchs, S., Poltrum, B., Schmidt, H., Matthews, P.M., Fazekas, F., 2004. Accelerated evolution of brain atrophy and "black holes" in MS patients with APOE-epsilon 4. *Ann Neurol* 55, 563-569.
- Fatouros, P.P., Marmarou, A., Kraft, K.A., Inao, S., Schwarz, F.P., 1991. In vivo brain water determination by T1 measurements: effect of total water content, hydration fraction, and field strength. *Magn Reson Med* 17, 402-413.
- Fernando, K.T., Tozer, D.J., Miszkiel, K.A., Gordon, R.M., Swanton, J.K., Dalton, C.M., Barker, G.J., Plant, G.T., Thompson, A.J., Miller, D.H., 2005. Magnetization transfer histograms in clinically isolated syndromes suggestive of multiple sclerosis. *Brain* 128, 2911-2925.
- Fralix, T.A., Ceckler, T.L., Wolff, S.D., Simon, S.A., Balaban, R.S., 1991. Lipid bilayer and water proton magnetization transfer: effect of cholesterol. *Magn Reson Med* 18, 214-223.
- Fukunaga, M., Li, T.Q., van Gelderen, P., de Zwart, J.A., Shmueli, K., Yao, B., Lee, J., Maric, D., Aronova, M.A., Zhang, G., Leapman, R.D., Schenck, J.F., Merkle, H., Duyn, J.H., 2010. Layer-specific variation of iron content in cerebral cortex as a source of MRI contrast. *Proc Natl Acad Sci U S A* 107, 3834-3839.
- Gareau, P.J., Rutt, B.K., Karlik, S.J., Mitchell, J.R., 2000. Magnetization transfer and multicomponent T2 relaxation measurements with histopathologic correlation in an experimental model of MS. *J Magn Reson Imaging* 11, 586-595.
- Gelman, N., Ewing, J.R., Gorell, J.M., Spickler, E.M., Solomon, E.G., 2001. Interregional variation of longitudinal relaxation rates in human brain at 3.0 T: relation to estimated iron and water contents. *Magn Reson Med* 45, 71-79.
- Gelman, N., Gorell, J.M., Barker, P.B., Savage, R.M., Spickler, E.M., Windham, J.P., Knight, R.A., 1999. MR imaging of human brain at 3.0 T: preliminary report on transverse relaxation rates and relation to estimated iron content. *Radiology* 210, 759-767.
- Gilmore, C.P., Donaldson, I., Bo, L., Owens, T., Lowe, J., Evangelou, N., 2009. Regional variations in the extent and pattern of grey matter demyelination in multiple sclerosis: a

- comparison between the cerebral cortex, cerebellar cortex, deep grey matter nuclei and the spinal cord. *J Neurol Neurosurg Psychiatry* 80, 182-187.
- Gloor, M., Scheffler, K., Bieri, O., 2008. Quantitative magnetization transfer imaging using balanced SSFP. *Magn Reson Med* 60, 691-700.
- Goodall, E.F., Haque, M.S., Morrison, K.E., 2008. Increased serum ferritin levels in amyotrophic lateral sclerosis (ALS) patients. *J Neurol* 255, 1652-1656.
- Gotz, M.E., Double, K., Gerlach, M., Youdim, M.B., Riederer, P., 2004. The relevance of iron in the pathogenesis of Parkinson's disease. *Ann N Y Acad Sci* 1012, 193-208.
- Griffiths, P.D., Crossman, A.R., 1993. Distribution of iron in the basal ganglia and neocortex in postmortem tissue in Parkinson's disease and Alzheimer's disease. *Dementia* 4, 61-65.
- Grimaud, J., Millar, J., Thorpe, J.W., Moseley, I.F., McDonald, W.I., Miller, D.H., 1995. Signal intensity on MRI of basal ganglia in multiple sclerosis. *J Neurol Neurosurg Psychiatry* 59, 306-308.
- Grohn, H.I., Michaeli, S., Garwood, M., Kauppinen, R.A., Grohn, O.H., 2005. Quantitative T(1rho) and adiabatic Carr-Purcell T2 magnetic resonance imaging of human occipital lobe at 4 T. *Magn Reson Med* 54, 14-19.
- Gutteridge, J.M., 1992. Iron and oxygen radicals in brain. *Ann Neurol* 32 Suppl, S16-21.
- Haacke, E.M., Cheng, N.Y., House, M.J., Liu, Q., Neelavalli, J., Ogg, R.J., Khan, A., Ayaz, M., Kirsch, W., Obenaus, A., 2005. Imaging iron stores in the brain using magnetic resonance imaging. *Magn Reson Imaging* 23, 1-25.
- Haacke, E.M., Mittal, S., Wu, Z., Neelavalli, J., Cheng, Y.C., 2009. Susceptibility-weighted imaging: technical aspects and clinical applications, part 1. *AJNR Am J Neuroradiol* 30, 19-30.
- Haacke, E.M., Xu, Y., Cheng, Y.C., Reichenbach, J.R., 2004. Susceptibility weighted imaging (SWI). *Magn Reson Med* 52, 612-618.
- Hallgren, B., Sourander, P., 1958. The effect of age on the non-haemin iron in the human brain. *J Neurochem* 3, 41-51.
- Hammond, K.E., Metcalf, M., Carvajal, L., Okuda, D.T., Srinivasan, R., Vigneron, D., Nelson, S.J., Pelletier, D., 2008. Quantitative in vivo magnetic resonance imaging of multiple sclerosis at 7 Tesla with sensitivity to iron. *Ann Neurol* 64, 707-713.
- He, T., Gatehouse, P.D., Smith, G.C., Mohiaddin, R.H., Pennell, D.J., Firmin, D.N., 2008. Myocardial T2\* measurements in iron-overloaded thalassemia: An in vivo study to investigate optimal methods of quantification. *Magn Reson Med* 60, 1082-1089.

- He, X., Yablonskiy, D.A., 2009. Biophysical mechanisms of phase contrast in gradient echo MRI. *Proc Natl Acad Sci U S A* 106, 13558-13563.
- Henkelman, R.M., Stanisz, G.J., Graham, S.J., 2001. Magnetization transfer in MRI: a review. *NMR Biomed* 14, 57-64.
- Hocq, A., Brouette, N., Saussez, S., Luhmer, M., Gillis, P., Gossuin, Y., 2009. Variable-field relaxometry of iron-containing human tissues: a preliminary study. *Contrast Media Mol Imaging* 4, 157-164.
- Hopp, K., Popescu, B.F., McCrea, R.P., Harder, S.L., Robinson, C.A., Haacke, M.E., Rajput, A.H., Rajput, A., Nichol, H., 2010. Brain iron detected by SWI high pass filtered phase calibrated with synchrotron X-ray fluorescence. *J Magn Reson Imaging* 31, 1346-1354.
- House, M.J., St Pierre, T.G., Kowdley, K.V., Montine, T., Connor, J., Beard, J., Berger, J., Siddaiah, N., Shankland, E., Jin, L.W., 2007. Correlation of proton transverse relaxation rates (R2) with iron concentrations in postmortem brain tissue from alzheimer's disease patients. *Magn Reson Med* 57, 172-180.
- Imon, Y., Yamaguchi, S., Yamamura, Y., Tsuji, S., Kajima, T., Ito, K., Nakamura, S., 1995. Low intensity areas observed on T2-weighted magnetic resonance imaging of the cerebral cortex in various neurological diseases. *J Neurol Sci* 134 Suppl, 27-32.
- Jenkinson, M., Bannister, P., Brady, M., Smith, S., 2002. Improved optimization for the robust and accurate linear registration and motion correction of brain images. *Neuroimage* 17, 825-841.
- Jensen, J.H., Chandra, R., 2000a. NMR relaxation in tissues with weak magnetic inhomogeneities. *Magn Reson Med* 44, 144-156.
- Jensen, J.H., Chandra, R., 2000b. Strong field behavior of the NMR signal from magnetically heterogeneous tissues. *Magn Reson Med* 43, 226-236.
- Jensen, J.H., Chandra, R., Ramani, A., Lu, H., Johnson, G., Lee, S.P., Kaczynski, K., Helpert, J.A., 2006. Magnetic field correlation imaging. *Magn Reson Med* 55, 1350-1361.
- Jensen, J.H., Szulc, K., Hu, C., Ramani, A., Lu, H., Xuan, L., Falangola, M.F., Chandra, R., Knopp, E.A., Schenck, J., Zimmerman, E.A., Helpert, J.A., 2009. Magnetic field correlation as a measure of iron-generated magnetic field inhomogeneities in the brain. *Magn Reson Med* 61, 481-485.
- Kell, D.B., 2010. Towards a unifying, systems biology understanding of large-scale cellular death and destruction caused by poorly liganded iron: Parkinson's, Huntington's, Alzheimer's, prions, bactericides, chemical toxicology and others as examples. *Arch Toxicol* 84, 825-889.

- Khalil, M., Enzinger, C., Langkammer, C., Petrovic, K., Loitfelder, M., Tscherner, M., Jehna, M., Bachmaier, G., Wallner-Blazek, M., Ropele, S., Schmidt, R., Fuchs, S., Fazekas, F., 2011a. Cognitive impairment in relation to MRI metrics in patients with clinically isolated syndrome. *Mult Scler* 17, 173-180.
- Khalil, M., Enzinger, C., Langkammer, C., Tscherner, M., Wallner-Blazek, M., Jehna, M., Ropele, S., Fuchs, S., Fazekas, F., 2009. Quantitative assessment of brain iron by R(2)\* relaxometry in patients with clinically isolated syndrome and relapsing-remitting multiple sclerosis. *Mult Scler* 15, 1048-1054.
- Khalil, M., Langkammer, C., Ropele, S., Petrovic, K., Wallner-Blazek, M., Loitfelder, M., Jehna, M., Bachmaier, G., Schmidt, R., Enzinger, C., Fuchs, S., Fazekas, F., 2011b. Determinants of brain iron in multiple sclerosis: a quantitative 3T MRI study. *Neurology* 77, 1691-1697.
- Koenig, S.H., Brown, R.D., 3rd, Adams, D., Emerson, D., Harrison, C.G., 1984. Magnetic field dependence of 1/T1 of protons in tissue. *Invest Radiol* 19, 76-81.
- Koenig, S.H., Brown, R.D., 3rd, Spiller, M., Lundbom, N., 1990. Relaxometry of brain: why white matter appears bright in MRI. *Magn Reson Med* 14, 482-495.
- Koenig, S.H., Kellar, K.E., 1995. Theory of 1/T1 and 1/T2 NMRD profiles of solutions of magnetic nanoparticles. *Magn Reson Med* 34, 227-233.
- Koeppen, A.H., 2003. A brief history of brain iron research. *J Neurol Sci* 207, 95-97.
- Kurtzke, J.F., 1983. Rating neurologic impairment in multiple sclerosis: an expanded disability status scale (EDSS). *Neurology* 33, 1444-1452.
- Labadie C, O.D., Jarchow S et al., 2008. Detection of the Myelin Water Fraction in 4 Tesla Longitudinal Relaxation Data by Cross-Regularized Inverse Laplace Transform. *Proc. Intl. Soc. Mag. Reson. Med* 16, 2243.
- Labadie C, O.D., Jochimsen TH, Lee J, Möller HE, 2009. Comparison of Myelin Water Fraction in Cross-Regularized T1-Relaxograms of Normal White Matter at 3T and 7T and of Normal-Appearing White Matter at 3T *Proc. Intl. Soc. Mag. Reson. Med.* 17, 3210.
- Lacomis, D., Osbakken, M., Gross, G., 1986. Spin-lattice relaxation (T1) times of cerebral white matter in multiple sclerosis. *Magn Reson Med* 3, 194-202.
- Langkammer, C., Krebs, N., Goessler, W., Scheurer, E., Ebner, F., Yen, K., Fazekas, F., Ropele, S., 2010. Quantitative MR imaging of brain iron: a postmortem validation study. *Radiology* 257, 455-462.



- Langkammer, C., Krebs, N., Goessler, W., Scheurer, E., Yen, K., Fazekas, F., Ropele, S., 2012. Susceptibility induced gray-white matter MRI contrast in the human brain. *Neuroimage* 59, 1413-1419.
- Lebel, R.M., Eissa, A., Seres, P., Blevins, G., Wilman, A.H., 2011. Quantitative high field imaging of sub-cortical gray matter in multiple sclerosis. *Mult Scler.*
- Lee, J., Hirano, Y., Fukunaga, M., Silva, A.C., Duyn, J.H., 2010a. On the contribution of deoxy-hemoglobin to MRI gray-white matter phase contrast at high field. *Neuroimage* 49, 193-198.
- Lee, J., Shmueli, K., Fukunaga, M., van Gelderen, P., Merkle, H., Silva, A.C., Duyn, J.H., 2010b. Sensitivity of MRI resonance frequency to the orientation of brain tissue microstructure. *Proc Natl Acad Sci U S A* 107, 5130-5135.
- Lee, J., Shmueli, K., Kang, B.T., Yao, B., Fukunaga, M., van Gelderen, P., Palumbo, S., Bosetti, F., Silva, A.C., Duyn, J.H., 2011. The contribution of myelin to magnetic susceptibility-weighted contrasts in high-field MRI of the brain. *Neuroimage.*
- Lenz, C., Klarhofer, M., Scheffler, K., 2010. Limitations of rapid myelin water quantification using 3D bSSFP. *MAGMA* 23, 139-151.
- LeVine, S.M., 1997. Iron deposits in multiple sclerosis and Alzheimer's disease brains. *Brain Res* 760, 298-303.
- Li, T.Q., Yao, B., van Gelderen, P., Merkle, H., Dodd, S., Talagala, L., Koretsky, A.P., Duyn, J., 2009. Characterization of  $T(2)^*$  heterogeneity in human brain white matter. *Magn Reson Med* 62, 1652-1657.
- Li, W., Wu, B., Avram, A.V., Liu, C., 2012. Magnetic susceptibility anisotropy of human brain in vivo and its molecular underpinnings. *Neuroimage* 59, 2088-2097.
- Li, W., Wu, B., Liu, C., 2011. Quantitative susceptibility mapping of human brain reflects spatial variation in tissue composition. *Neuroimage.*
- Liu, C., 2010. Susceptibility tensor imaging. *Magn Reson Med* 63, 1471-1477.
- Liu, C., Li, W., Johnson, G.A., Wu, B., 2011a. High-field (9.4 T) MRI of brain dysmyelination by quantitative mapping of magnetic susceptibility. *Neuroimage* 56, 930-938.
- Liu, J., Liu, T., de Rochefort, L., Ledoux, J., Khalidov, I., Chen, W., Tsiouris, A.J., Wisnieff, C., Spincemille, P., Prince, M.R., Wang, Y., 2012. Morphology enabled dipole inversion for quantitative susceptibility mapping using structural consistency between the magnitude image and the susceptibility map. *Neuroimage* 59, 2560-2568.

- Liu, T., Khalidov, I., de Rochefort, L., Spincemaille, P., Liu, J., Tsiouris, A.J., Wang, Y., 2011b. A novel background field removal method for MRI using projection onto dipole fields (PDF). *NMR Biomed* 24, 1129-1136.
- Liu, T., Liu, J., de Rochefort, L., Spincemaille, P., Khalidov, I., Ledoux, J.R., Wang, Y., 2011c. Morphology enabled dipole inversion (MEDI) from a single-angle acquisition: comparison with COSMOS in human brain imaging. *Magn Reson Med* 66, 777-783.
- Liu, T., Spincemaille, P., de Rochefort, L., Kressler, B., Wang, Y., 2009. Calculation of susceptibility through multiple orientation sampling (COSMOS): a method for conditioning the inverse problem from measured magnetic field map to susceptibility source image in MRI. *Magn Reson Med* 61, 196-204.
- Luo, J., He, X., d'Avignon, D.A., Ackerman, J.J., Yablonskiy, D.A., 2010. Protein-induced water 1H MR frequency shifts: contributions from magnetic susceptibility and exchange effects. *J Magn Reson* 202, 102-108.
- Ma, J., Wehrli, F.W., 1996. Method for image-based measurement of the reversible and irreversible contribution to the transverse-relaxation rate. *J Magn Reson B* 111, 61-69.
- MacKay, A., Whittall, K., Adler, J., Li, D., Paty, D., Graeb, D., 1994. In vivo visualization of myelin water in brain by magnetic resonance. *Magn Reson Med* 31, 673-677.
- Marques, J.P., Maddage, R., Mlynarik, V., Gruetter, R., 2009. On the origin of the MR image phase contrast: an in vivo MR microscopy study of the rat brain at 14.1 T. *Neuroimage* 46, 345-352.
- Miller, D.H., Thompson, A.J., Filippi, M., 2003. Magnetic resonance studies of abnormalities in the normal appearing white matter and grey matter in multiple sclerosis. *J Neurol* 250, 1407-1419.
- Miller, D.H., Weinshenker, B.G., Filippi, M., Banwell, B.L., Cohen, J.A., Freedman, M.S., Galetta, S.L., Hutchinson, M., Johnson, R.T., Kappos, L., Kira, J., Lublin, F.D., McFarland, H.F., Montalban, X., Panitch, H., Richert, J.R., Reingold, S.C., Polman, C.H., 2008. Differential diagnosis of suspected multiple sclerosis: a consensus approach. *Mult Scler* 14, 1157-1174.
- Mitsumori, F., Watanabe, H., Takaya, N., 2009. Estimation of brain iron concentration in vivo using a linear relationship between regional iron and apparent transverse relaxation rate of the tissue water at 4.7T. *Magn Reson Med* 62, 1326-1330.
- Mittal, S., Wu, Z., Neelavalli, J., Haacke, E.M., 2009. Susceptibility-weighted imaging: technical aspects and clinical applications, part 2. *AJNR Am J Neuroradiol* 30, 232-252.

- Moore, G.R., Leung, E., MacKay, A.L., Vavasour, I.M., Whittall, K.P., Cover, K.S., Li, D.K., Hashimoto, S.A., Oger, J., Sprinkle, T.J., Paty, D.W., 2000. A pathology-MRI study of the short-T2 component in formalin-fixed multiple sclerosis brain. *Neurology* 55, 1506-1510.
- Morris, C.M., Candy, J.M., Oakley, A.E., Bloxham, C.A., Edwardson, J.A., 1992. Histochemical distribution of non-haem iron in the human brain. *Acta Anat (Basel)* 144, 235-257.
- Morrison, C., Henkelman, R.M., 1995. A model for magnetization transfer in tissues. *Magn Reson Med* 33, 475-482.
- Neema, M., Stankiewicz, J., Arora, A., Dandamudi, V.S., Batt, C.E., Guss, Z.D., Al-Sabbagh, A., Bakshi, R., 2007. T1- and T2-based MRI measures of diffuse gray matter and white matter damage in patients with multiple sclerosis. *J Neuroimaging* 17 Suppl 1, 16S-21S.
- Nunez, M.T., Urrutia, P., Mena, N., Aguirre, P., Tapia, V., Salazar, J., 2012. Iron toxicity in neurodegeneration. *Biometals*.
- Oba, H., Araki, T., Ohtomo, K., Monzawa, S., Uchiyama, G., Koizumi, K., Nogata, Y., Kachi, K., Shiozawa, Z., Kobayashi, M., 1993. Amyotrophic lateral sclerosis: T2 shortening in motor cortex at MR imaging. *Radiology* 189, 843-846.
- Ogg, R.J., Langston, J.W., Haacke, E.M., Steen, R.G., Taylor, J.S., 1999. The correlation between phase shifts in gradient-echo MR images and regional brain iron concentration. *Magn Reson Imaging* 17, 1141-1148.
- Ogg, R.J., Steen, R.G., 1998. Age-related changes in brain T1 are correlated with iron concentration. *Magn Reson Med* 40, 749-753.
- Oh, J., Han, E.T., Pelletier, D., Nelson, S.J., 2006. Measurement of in vivo multi-component T2 relaxation times for brain tissue using multi-slice T2 prep at 1.5 and 3 T. *Magn Reson Imaging* 24, 33-43.
- Orino, K., Lehman, L., Tsuji, Y., Ayaki, H., Torti, S.V., Torti, F.M., 2001. Ferritin and the response to oxidative stress. *Biochem J* 357, 241-247.
- Patenaude, B., Smith, S.M., Kennedy, D.N., Jenkinson, M., 2011. A Bayesian model of shape and appearance for subcortical brain segmentation. *Neuroimage* 56, 907-922.
- Peran, P., Hagberg, G., Luccichenti, G., Cherubini, A., Brainovich, V., Celsis, P., Caltagirone, C., Sabatini, U., 2007. Voxel-based analysis of R2\* maps in the healthy human brain. *J Magn Reson Imaging* 26, 1413-1420.
- Perls, M., 1867. Nachweis von Eisenoxyd in gewissen Pigmenten. *Virchows Arch. Pathol. Anat. Physiol. Klin. Med.* 39, 42-48.

- Petridou, N., Schafer, A., Gowland, P., Bowtell, R., 2009. Phase vs. magnitude information in functional magnetic resonance imaging time series: toward understanding the noise. *Magn Reson Imaging* 27, 1046-1057.
- Petridou, N., Wharton, S.J., Lotfipour, A., Gowland, P., Bowtell, R., 2010. Investigating the effect of blood susceptibility on phase contrast in the human brain. *Neuroimage* 50, 491-498.
- Phukan, J., Pender, N.P., Hardiman, O., 2007. Cognitive impairment in amyotrophic lateral sclerosis. *Lancet Neurol* 6, 994-1003.
- Polman, C.H., Reingold, S.C., Edan, G., Filippi, M., Hartung, H.P., Kappos, L., Lublin, F.D., Metz, L.M., McFarland, H.F., O'Connor, P.W., Sandberg-Wollheim, M., Thompson, A.J., Weinshenker, B.G., Wolinsky, J.S., 2005. Diagnostic criteria for multiple sclerosis: 2005 revisions to the "McDonald Criteria". *Ann Neurol* 58, 840-846.
- Pujol, J., Junque, C., Vendrell, P., Grau, J.M., Marti-Vilalta, J.L., Olive, C., Gili, J., 1992. Biological significance of iron-related magnetic resonance imaging changes in the brain. *Arch Neurol* 49, 711-717.
- Ramani, A., Dalton, C., Miller, D.H., Tofts, P.S., Barker, G.J., 2002. Precise estimate of fundamental in-vivo MT parameters in human brain in clinically feasible times. *Magn Reson Imaging* 20, 721-731.
- Rauscher, A., Barth, M., Reichenbach, J.R., Stollberger, R., Moser, E., 2003. Automated unwrapping of MR phase images applied to BOLD MR-venography at 3 Tesla. *J Magn Reson Imaging* 18, 175-180.
- Rauscher, A., Sedlacik, J., Barth, M., Mentzel, H.J., Reichenbach, J.R., 2005. Magnetic susceptibility-weighted MR phase imaging of the human brain. *AJNR Am J Neuroradiol* 26, 736-742.
- Reichenbach, J.R., 2012. The future of susceptibility contrast for assessment of anatomy and function. *Neuroimage*.
- Reichenbach, J.R., Haacke, E.M., 2001. High-resolution BOLD venographic imaging: a window into brain function. *NMR Biomed* 14, 453-467.
- Rinck, P.A., Meindl, S., Higer, H.P., Bieler, E.U., Pfannenstiel, P., 1985. Brain tumors: detection and typing by use of CPMG sequences and in vivo T2 measurements. *Radiology* 157, 103-106.
- Rippon, G.A., Scarneas, N., Gordon, P.H., Murphy, P.L., Albert, S.M., Mitsumoto, H., Marder, K., Rowland, L.P., Stern, Y., 2006. An observational study of cognitive impairment in amyotrophic lateral sclerosis. *Arch Neurol* 63, 345-352.

- Ropele, S., de Graaf, W., Khalil, M., Wattjes, M.P., Langkammer, C., Rocca, M.A., Rovira, A., Palace, J., Barkhof, F., Filippi, M., Fazekas, F., 2011. MRI assessment of iron deposition in multiple sclerosis. *J Magn Reson Imaging* 34, 13-21.
- Ropele, S., Fazekas, F., 2009. Magnetization transfer MR imaging in multiple sclerosis. *Neuroimaging Clin N Am* 19, 27-36.
- Ropele, S., Seifert, T., Enzinger, C., Fazekas, F., 2003. Method for quantitative imaging of the macromolecular 1H fraction in tissues. *Magn Reson Med* 49, 864-871.
- Rovira, A., Montalban, X., 2011. MR brain iron mapping in MS: a potential neurodegenerative marker or just another technique? *Neurology* 77, 1660-1661.
- Salat, D.H., Lee, S.Y., van der Kouwe, A.J., Greve, D.N., Fischl, B., Rosas, H.D., 2009. Age-associated alterations in cortical gray and white matter signal intensity and gray to white matter contrast. *Neuroimage* 48, 21-28.
- Salat, D.H., Tuch, D.S., Greve, D.N., van der Kouwe, A.J., Hevelone, N.D., Zaleta, A.K., Rosen, B.R., Fischl, B., Corkin, S., Rosas, H.D., Dale, A.M., 2005. Age-related alterations in white matter microstructure measured by diffusion tensor imaging. *Neurobiol Aging* 26, 1215-1227.
- Salomir, R., de Senneville, B.D., Moonen, C.T., 2003. A fast calculation method for magnetic field inhomogeneity due to an arbitrary distribution of bulk susceptibility. *Concepts in Magnetic Resonance Part B: Magnetic Resonance Engineering* 19B, 26–34.
- Schafer, A., Forstmann, B.U., Neumann, J., Wharton, S., Mietke, A., Bowtell, R., Turner, R., 2011. Direct visualization of the subthalamic nucleus and its iron distribution using high-resolution susceptibility mapping. *Hum Brain Mapp*.
- Schenck, J.F., 1992. Health and physiological effects of human exposure to whole-body four-tesla magnetic fields during MRI. *Ann N Y Acad Sci* 649, 285-301.
- Schenck, J.F., Dumoulin, C.L., Redington, R.W., Kressel, H.Y., Elliott, R.T., McDougall, I.L., 1992. Human exposure to 4.0-Tesla magnetic fields in a whole-body scanner. *Med Phys* 19, 1089-1098.
- Schenck, J.F., Zimmerman, E.A., 2004. High-field magnetic resonance imaging of brain iron: birth of a biomarker? *NMR Biomed* 17, 433-445.
- Scherer, P., Baum, K., Bauer, H., Gohler, H., Miltenburger, C., 2004. [Normalization of the Brief Repeatable Battery of Neuropsychological tests (BRB-N) for German-speaking regions. Application in relapsing-remitting and secondary progressive multiple sclerosis patients]. *Nervenarzt* 75, 984-990.

- Schmierer, K., Scaravilli, F., Altmann, D.R., Barker, G.J., Miller, D.H., 2004. Magnetization transfer ratio and myelin in postmortem multiple sclerosis brain. *Ann Neurol* 56, 407-415.
- Schmierer, K., Wheeler-Kingshott, C.A., Tozer, D.J., Boulby, P.A., Parkes, H.G., Yousry, T.A., Scaravilli, F., Barker, G.J., Tofts, P.S., Miller, D.H., 2008. Quantitative magnetic resonance of postmortem multiple sclerosis brain before and after fixation. *Magn Reson Med* 59, 268-277.
- Schneiders, N.J., Post, H., Brunner, P., Ford, J., Bryan, R.N., Willcott, M.R., 1983. Accurate T2 NMR images. *Med Phys* 10, 642-645.
- Schweser, F., Deistung, A., Lehr, B.W., Reichenbach, J.R., 2010. Differentiation between diamagnetic and paramagnetic cerebral lesions based on magnetic susceptibility mapping. *Med Phys* 37, 5165-5178.
- Schweser, F., Deistung, A., Lehr, B.W., Reichenbach, J.R., 2011. Quantitative imaging of intrinsic magnetic tissue properties using MRI signal phase: an approach to in vivo brain iron metabolism? *Neuroimage* 54, 2789-2807.
- Sedlacik, J., Kutschbach, C., Rauscher, A., Deistung, A., Reichenbach, J.R., 2008. Investigation of the influence of carbon dioxide concentrations on cerebral physiology by susceptibility-weighted magnetic resonance imaging (SWI). *Neuroimage* 43, 36-43.
- Sedlacik, J., Rauscher, A., Reichenbach, J.R., 2007. Obtaining blood oxygenation levels from MR signal behavior in the presence of single venous vessels. *Magn Reson Med* 58, 1035-1044.
- Shepherd, T.M., Flint, J.J., Thelwall, P.E., Stanisiz, G.J., Mareci, T.H., Yachnis, A.T., Blackband, S.J., 2009. Postmortem interval alters the water relaxation and diffusion properties of rat nervous tissue--implications for MRI studies of human autopsy samples. *Neuroimage* 44, 820-826.
- Shmueli, K., de Zwart, J.A., van Gelderen, P., Li, T.Q., Dodd, S.J., Duyn, J.H., 2009. Magnetic susceptibility mapping of brain tissue in vivo using MRI phase data. *Magn Reson Med* 62, 1510-1522.
- Shmueli, K., Dodd, S.J., Li, T.Q., Duyn, J.H., 2011. The contribution of chemical exchange to MRI frequency shifts in brain tissue. *Magn Reson Med* 65, 35-43.
- Sled, J.G., Pike, G.B., 2001. Quantitative imaging of magnetization transfer exchange and relaxation properties in vivo using MRI. *Magn Reson Med* 46, 923-931.
- Smith, S.A., Bulte, J.W., van Zijl, P.C., 2009. Direct saturation MRI: theory and application to imaging brain iron. *Magn Reson Med* 62, 384-393.

- Smith, S.M., Jenkinson, M., Johansen-Berg, H., Rueckert, D., Nichols, T.E., Mackay, C.E., Watkins, K.E., Ciccarelli, O., Cader, M.Z., Matthews, P.M., Behrens, T.E., 2006. Tract-based spatial statistics: voxelwise analysis of multi-subject diffusion data. *Neuroimage* 31, 1487-1505.
- Smith, S.M., Jenkinson, M., Woolrich, M.W., Beckmann, C.F., Behrens, T.E., Johansen-Berg, H., Bannister, P.R., De Luca, M., Drobnjak, I., Flitney, D.E., Niazy, R.K., Saunders, J., Vickers, J., Zhang, Y., De Stefano, N., Brady, J.M., Matthews, P.M., 2004. Advances in functional and structural MR image analysis and implementation as FSL. *Neuroimage* 23 Suppl 1, S208-219.
- Spatz, H., 1922. Über den Eisennachweis im Gehirn, besonders in Zentren des extrapyramidal-motorischen Systems. I. Teil. *Z. Ges. Neuro Psychiat.* 77, 261–390
- St Pierre, T.G., 2003. Deferiprone versus desferrioxamine in thalassaemia, and T2\* validation and utility. *Lancet* 361, 182; author reply 183-184.
- St Pierre, T.G., Clark, P.R., Chua-Anusorn, W., 2004. Single spin-echo proton transverse relaxometry of iron-loaded liver. *NMR Biomed* 17, 446-458.
- Stanisz, G.J., Henkelman, R.M., 1998. Diffusional anisotropy of T2 components in bovine optic nerve. *Magn Reson Med* 40, 405-410.
- Stanisz, G.J., Odrobina, E.E., Pun, J., Escaravage, M., Graham, S.J., Bronskill, M.J., Henkelman, R.M., 2005. T1, T2 relaxation and magnetization transfer in tissue at 3T. *Magn Reson Med* 54, 507-512.
- Stankiewicz, J., Panter, S.S., Neema, M., Arora, A., Batt, C.E., Bakshi, R., 2007. Iron in chronic brain disorders: imaging and neurotherapeutic implications. *Neurotherapeutics* 4, 371-386.
- Stein, F., 1923. Über den quantitativen Eisennachweis im extrapyramidalmotorischen Kernsystem beim Menschen. *Z. Ges. Neuro Psychiat.* 85, 614–621.
- Supprian, T., Hofmann, E., Warmuth-Metz, M., Franzek, E., Becker, T., 1997. MRI T2 relaxation times of brain regions in schizophrenic patients and control subjects. *Psychiatry Res* 75, 173-182.
- Tjoa, C.W., Benedict, R.H., Weinstock-Guttman, B., Fabiano, A.J., Bakshi, R., 2005. MRI T2 hypointensity of the dentate nucleus is related to ambulatory impairment in multiple sclerosis. *J Neurol Sci* 234, 17-24.
- Tofts, P.S., Jackson, J.S., Tozer, D.J., Cercignani, M., Keir, G., MacManus, D.G., Ridgway, G.R., Ridha, B.H., Schmierer, K., Siddique, D., Thornton, J.S., Wroe, S.J., Fox, N.C.,

2008. Imaging cadavers: cold FLAIR and noninvasive brain thermometry using CSF diffusion. *Magn Reson Med* 59, 190-195.
- Toosy, A.T., Werring, D.J., Orrell, R.W., Howard, R.S., King, M.D., Barker, G.J., Miller, D.H., Thompson, A.J., 2003. Diffusion tensor imaging detects corticospinal tract involvement at multiple levels in amyotrophic lateral sclerosis. *J Neurol Neurosurg Psychiatry* 74, 1250-1257.
- Torrey, H.C., 1956. Bloch Equations with Diffusion Terms. *Physical Review* 104, 563-565.
- Trapp, B.D., Peterson, J., Ransohoff, R.M., Rudick, R., Mork, S., Bo, L., 1998. Axonal transection in the lesions of multiple sclerosis. *N Engl J Med* 338, 278-285.
- Travis, A.R., Does, M.D., 2005. Selective excitation of myelin water using inversion-recovery-based preparations. *Magn Reson Med* 54, 743-747.
- van Walderveen, M.A., van Schijndel, R.A., Pouwels, P.J., Polman, C.H., Barkhof, F., 2003. Multislice T1 relaxation time measurements in the brain using IR-EPI: reproducibility, normal values, and histogram analysis in patients with multiple sclerosis. *J Magn Reson Imaging* 18, 656-664.
- Venkatesan, R., Lin, W., Haacke, E.M., 1998. Accurate determination of spin-density and T1 in the presence of RF-field inhomogeneities and flip-angle miscalibration. *Magn Reson Med* 40, 592-602.
- Vidarsson, L., Conolly, S.M., Lim, K.O., Gold, G.E., Pauly, J.M., 2005. Echo time optimization for linear combination myelin imaging. *Magn Reson Med* 53, 398-407.
- Vymazal, J., Brooks, R.A., Baumgarner, C., Tran, V., Katz, D., Bulte, J.W., Bauminger, R., Di Chiro, G., 1996. The relation between brain iron and NMR relaxation times: an in vitro study. *Magn Reson Med* 35, 56-61.
- Vymazal, J., Brooks, R.A., Zak, O., McRill, C., Shen, C., Di Chiro, G., 1992. T1 and T2 of ferritin at different field strengths: effect on MRI. *Magn Reson Med* 27, 368-374.
- Wang, S., Poptani, H., Woo, J.H., Desiderio, L.M., Elman, L.B., McCluskey, L.F., Krejza, J., Melhem, E.R., 2006. Amyotrophic lateral sclerosis: diffusion-tensor and chemical shift MR imaging at 3.0 T. *Radiology* 239, 831-838.
- Wengenack, T.M., Reyes, D.A., Curran, G.L., Borowski, B.J., Lin, J., Preboske, G.M., Holasek, S.S., Gilles, E.J., Chamberlain, R., Marjanska, M., Jack, C.R., Jr., Garwood, M., Poduslo, J.F., 2011. Regional differences in MRI detection of amyloid plaques in AD transgenic mouse brain. *Neuroimage* 54, 113-122.
- Wharton, S., Bowtell, R., 2010. Whole-brain susceptibility mapping at high field: a comparison of multiple- and single-orientation methods. *Neuroimage* 53, 515-525.



- Wharton, S., Schafer, A., Bowtell, R., 2010. Susceptibility mapping in the human brain using threshold-based k-space division. *Magn Reson Med* 63, 1292-1304.
- Wisner, G.L., Buxton, R.B., Rosen, B.R., Fisel, C.R., Oot, R.F., Brady, T.J., Davis, K.R., 1988. Susceptibility induced MR line broadening: applications to brain iron mapping. *J Comput Assist Tomogr* 12, 259-265.
- Wright, P.J., Mouglin, O.E., Totman, J.J., Peters, A.M., Brookes, M.J., Coxon, R., Morris, P.E., Clemence, M., Francis, S.T., Bowtell, R.W., Gowland, P.A., 2008. Water proton T1 measurements in brain tissue at 7, 3, and 1.5 T using IR-EPI, IR-TSE, and MPRAGE: results and optimization. *MAGMA* 21, 121-130.
- Wu, B., Li, W., Avram, A.V., Gho, S.M., Liu, C., 2012a. Fast and tissue-optimized mapping of magnetic susceptibility and T2\* with multi-echo and multi-shot spirals. *Neuroimage* 59, 297-305.
- Wu, B., Li, W., Guidon, A., Liu, C., 2012b. Whole brain susceptibility mapping using compressed sensing. *Magn Reson Med* 67, 137-147.
- Xu, X., Wang, Q., Zhang, M., 2008. Age, gender, and hemispheric differences in iron deposition in the human brain: an in vivo MRI study. *Neuroimage* 40, 35-42.
- Yablonskiy, D.A., Haacke, E.M., 1994. Theory of NMR signal behavior in magnetically inhomogeneous tissues: the static dephasing regime. *Magn Reson Med* 32, 749-763.
- Yamada, N., Imakita, S., Sakuma, T., Takamiya, M., 1996. Intracranial calcification on gradient-echo phase image: depiction of diamagnetic susceptibility. *Radiology* 198, 171-178.
- Yao, B., Li, T.Q., Gelderen, P., Shmueli, K., de Zwart, J.A., Duyn, J.H., 2009. Susceptibility contrast in high field MRI of human brain as a function of tissue iron content. *Neuroimage* 44, 1259-1266.
- Yarnykh, V.L., 2002. Pulsed Z-spectroscopic imaging of cross-relaxation parameters in tissues for human MRI: theory and clinical applications. *Magn Reson Med* 47, 929-939.
- Yong-Hing, C.J., Obenaus, A., Stryker, R., Tong, K., Sarty, G.E., 2005. Magnetic resonance imaging and mathematical modeling of progressive formalin fixation of the human brain. *Magn Reson Med* 54, 324-332.
- Zaleski, S.S., 1886. Das Eisen der Organe beim Morbus maculosus Werlhofii. *Arch. Exp. Pathol. Pharmacol.* 23, 77-90.
- Zecca, L., Youdim, M.B., Riederer, P., Connor, J.R., Crichton, R.R., 2004. Iron, brain ageing and neurodegenerative disorders. *Nat Rev Neurosci* 5, 863-873.

- Zhang, Y., Metz, L.M., Yong, V.W., Mitchell, J.R., 2010. 3T deep gray matter T2 hypointensity correlates with disability over time in stable relapsing-remitting multiple sclerosis: a 3-year pilot study. *J Neurol Sci* 297, 76-81.
- Zhong, K., Ernst, T., Buchthal, S., Speck, O., Anderson, L., Chang, L., 2011. Phase contrast imaging in neonates. *Neuroimage* 55, 1068-1072.
- Zhong, K., Leupold, J., von Elverfeldt, D., Speck, O., 2008. The molecular basis for gray and white matter contrast in phase imaging. *Neuroimage* 40, 1561-1566.
- Zhou, J., Golay, X., van Zijl, P.C., Silvennoinen, M.J., Kauppinen, R., Pekar, J., Kraut, M., 2001. Inverse T(2) contrast at 1.5 Tesla between gray matter and white matter in the occipital lobe of normal adult human brain. *Magn Reson Med* 46, 401-406.
- Zivadinov, R., Heininen-Brown, M., Schirda, C.V., Poloni, G.U., Bergsland, N., Magnano, C.R., Durfee, J., Kennedy, C., Carl, E., Hagemeyer, J., Benedict, R.H., Weinstock-Guttman, B., Dwyer, M.G., 2012. Abnormal subcortical deep-gray matter susceptibility-weighted imaging filtered phase measurements in patients with multiple sclerosis: a case-control study. *Neuroimage* 59, 331-339.
- Zivadinov, R., Schirda, C., Dwyer, M.G., Haacke, M.E., Weinstock-Guttman, B., Menegatti, E., Heininen-Brown, M., Magnano, C., Malagoni, A.M., Wack, D.S., Hojnacki, D., Kennedy, C., Carl, E., Bergsland, N., Hussein, S., Poloni, G., Bartolomei, I., Salvi, F., Zamboni, P., 2010. Chronic cerebrospinal venous insufficiency and iron deposition on susceptibility-weighted imaging in patients with multiple sclerosis: a pilot case-control study. *Int Angiol* 29, 158-175.

# CURRICULUM VITAE

## Personal details

Name Christian Langkammer  
Date of birth June 6<sup>th</sup>, 1982  
Citizenship Austrian

## Education

2008 – 2012 Graz University of Technology, Austria  
PhD studies in biomedical engineering  
2008 University of Oxford, Department of Clinical Neurology, UK  
Research stay at the *Centre for functional MRI of the brain*  
2007 Swiss Federal Institute of Technology, Zurich, Switzerland  
Interdisciplinary course in biomedical imaging  
2004 – 2005 University of Seville, Spain  
2001 – 2007 Graz University of Technology, Austria  
Master studies in biomedical engineering  
1996 – 2001 Federal Technical College, Klagenfurt, Austria

## Employment

2008 – present Department of Neurology, Medical University of Graz  
2009 – 2011 Ludwig Boltzmann Institute for Clinical Forensic Imaging  
2007 Siemens Corporate Research, Princeton, NJ

## LIST OF PUBLICATIONS

### PEER REVIEWED JOURNAL PAPERS

Determinants of brain iron in multiple sclerosis: A quantitative 3T MRI study.

Khalil M, Langkammer C, Ropele S, Petrovic K, Wallner-Blazek M, Loitfelder M, Jehna M, Bachmaier G, Schmidt R, Enzinger C, Fuchs S, Fazekas F.

Neurology. 2011 Nov 1;77(18):1691-7.

Susceptibility induced gray-white matter MRI contrast in the human brain.

Langkammer C, Krebs N, Goessler W, Scheurer E, Yen K, Fazekas F, Ropele S.

Neuroimage. 2012 Jan 16;59(2):1413-9.

MRI assessment of iron deposition in multiple sclerosis.

Ropele S, de Graaf W, Khalil M, Wattjes MP, Langkammer C, Rocca MA, Rovira A, Palace J, Barkhof F, Filippi M, Fazekas F.

J Magn Reson Imaging. 2011 Jul;34(1):13-21. doi: 10.1002/jmri.22590.

Cognitively preserved MS patients demonstrate functional differences in processing neutral and emotional faces.

Jehna M, Langkammer C, Wallner-Blazek M, Neuper C, Loitfelder M, Ropele S, Fuchs S, Khalil M, Pluta-Fuerst A, Fazekas F, Enzinger C.

Brain Imaging Behav. 2011 Jun 9.

The functional correlates of face perception and recognition of emotional facial expressions as evidenced by fMRI.

Jehna M, Neuper C, Ischebeck A, Loitfelder M, Ropele S, Langkammer C, Ebner F, Fuchs S, Schmidt R, Fazekas F, Enzinger C.

Brain Res. 2011 Jun 1;1393:73-83. Epub 2011 Apr 9.

Fast bound pool fraction mapping using stimulated echoes.

Soellinger M, Langkammer C, Seifert-Held T, Fazekas F, Ropele S.

Magn Reson Med. 2011 Sep;66(3):717-24. doi: 10.1002/mrm.22846. Epub 2011 Mar 24.

Relaxation time mapping in multiple sclerosis.

Ropele S, Langkammer C, Enzinger C, Fuchs S, Fazekas F.

Expert Rev Neurother. 2011 Mar;11(3):441-50. Review.

MRI-detected white matter lesions: do they really matter?

Schmidt R, Grazer A, Enzinger C, Ropele S, Homayoon N, Pluta-Fuerst A, Schwingenschuh P, Katschnig P, Cavalieri M, Schmidt H, Langkammer C, Ebner F, Fazekas F.

J Neural Transm. 2011 May;118(5):673-81. Epub 2011 Feb 22. Review.

Predicting the severity of relapsing-remitting MS: the contribution of cross-sectional and short-term follow-up MRI data.

Enzinger C, Fuchs S, Pichler A, Wallner-Blazek M, Khalil M, Langkammer C, Ropele S, Fazekas F.

Mult Scler. 2011 Jun;17(6):695-701. Epub 2011 Jan 12.

Lesion probability mapping to explain clinical deficits and cognitive performance in multiple sclerosis.

Kincses ZT, Ropele S, Jenkinson M, Khalil M, Petrovic K, Loitfelder M, Langkammer C, Aspeck E, Wallner-Blazek M, Fuchs S, Jehna M, Schmidt R, Vécsei L, Fazekas F, Enzinger C.

Mult Scler. 2011 Jun;17(6):681-9. Epub 2010 Dec 21.

Cognitive impairment in relation to MRI metrics in patients with clinically isolated syndrome.

Khalil M, Enzinger C, Langkammer C, Petrovic K, Loitfelder M, Tscherner M, Jehna M, Bachmaier G, Wallner-Blazek M, Ropele S, Schmidt R, Fuchs S, Fazekas F.

Mult Scler. 2011 Feb;17(2):173-80. Epub 2010 Oct 18.

Iron and Neurodegeneration in Multiple Sclerosis

Khalil M, Teunissen C, Langkammer C.

Mult Scler Int. 2011;2011:606807. Epub 2011 Feb 10.

High-grade internal carotid artery stenosis and chronic brain damage: a volumetric magnetic resonance imaging study.

Enzinger C, Ropele S, Gatttringer T, Langkammer C, Schmidt R, Fazekas F.

Cerebrovasc Dis. 2010;30(6):540-6. Epub 2010 Oct 15.

Quantitative MR imaging of brain iron: a postmortem validation study.

Langkammer C, Krebs N, Goessler W, Scheurer E, Ebner F, Yen K, Fazekas F, Ropele S.

Radiology. 2010 Nov;257(2):455-62. Epub 2010 Sep 15. Erratum in: Radiology. 2011 Mar;258(3):962.

Mapping of iron deposition in conjunction with assessment of nerve fiber tract integrity in amyotrophic lateral sclerosis.

Langkammer C, Enzinger C, Quasthoff S, Grafenauer P, Soellinger M, Fazekas F, Ropele S.

J Magn Reson Imaging. 2010 Jun;31(6):1339-45.

The impact of sex and vascular risk factors on brain tissue changes with aging: magnetization transfer imaging results of the Austrian stroke prevention study.

Ropele S, Enzinger C, Soellinger M, Langkammer C, Wallner-Blazek M, Schmidt R, Fazekas F.

AJNR Am J Neuroradiol. 2010 Aug;31(7):1297-301. Epub 2010 Mar 11.

Quantitative assessment of brain iron by R2\* relaxometry in patients with clinically isolated syndrome and relapsing-remitting multiple sclerosis.

Khalil M, Enzinger C, Langkammer C, Tscherner M, Wallner-Blazek M, Jehna M, Ropele S, Fuchs S, Fazekas F.

Mult Scler. 2009 Sep;15(9):1048-54. Epub 2009 Jun 25.